AD

USATRECOM TECHNICAL REPORT 65-4

INVESTIGATION OF METHODS FOR THE PREDICTION AND ALLEVIATION OF LIFT FAN NOISE

FINAL REPORT

By

Harry D. Sowers

April 1965

U. S. ARMY TRANSPORTATION RESEARCH COMMAND
FORT EUSTIS, VIRGINIA

CONTRACT DA 44-177-AMC-72(T)

GENERAL ELECTRIC COMPANY

DDC Availability Notice

Qualified requesters may obtain copies of this report from DDC.

This report has been furnished to the Department of Commerce for sale to the public.

Disclaimer

The findings in this report are not to be construed as an official Department of the Army position, unless so designated by other authorized documents.

When Government drawings, specifications, or other data are used for any purpose other than in connection with a definitely related Government procurement operation, the United States Government thereby incurs no responsibility nor any obligation whatsoever; and the fact that the Government may have formulated, furnished, or in any way supplied the said drawings, specifications, or other data is not to be regarded by implication or otherwise as in any manner licensing the holder or any other person or corporation, or conveying any rights or permission, to manufacture, use, or sell any patented invention that may in any way be related thereto.

Disposition Instructions

Destroy this report when it is no longer needed. Do not return it to the originator.

HEADQUARTERS
U S ARMY TRANSPORTATION RESEARCH COMMAND
FORT EUSTIS, VIRGINIA 23604

This report has been reviewed by the U. S. Army Transportation Research Command, and the results and conclusions drawn are considered to be technically sound. The report is published for the exchange of information and the stimulation of ideas.

Task 1D121401A142
Contract DA 44-177-AMC-72(T)

April 1965

INVESTIGATION OF METHODS FOR THE PREDICTION AND ALLEVIATION OF LIFT FAN NOISE

Final Report

Prepared by

General Electric Company
Advanced Engine and Technology Department
Cincinnati 15, Ohio

for

U. S. ARMY TRANSPORTATION RESEARCH COMMAND
FORT EUSTIS, VIRGINIA

Task 1D121401A142
Contract DA 44-177-AMC-72(T)

April 1965

INVESTIGATION OF METHODS FOR THE PREDICTION AND ALLEVIATION OF LIFT FAN NOISE

Final Report

Prepared by

General Electric Company
Advanced Engine and Technology Department
Cincinnati 15, Ohio

for

U. S. ARMY TRANSPORTATION RESEARCH COMMAND
FORT EUSTIS, VIRGINIA

ABSTRACT

A research investigation, both experimental and analytical, into the generation, suppression and prediction of fan noise has been completed. The technical effort of the program was divided into three major areas: theoretical investigations, acoustic normalizing techniques, and noise minimization and suppression design techniques. The three basic areas of investigation were supported by an extensive accumulation of scale model and full scale fan noise measurements, which have been presented in this report. Significant results have been obtained in each of the areas.

The theoretical investigations have provided insight into the basic noise generating mechanism of fan noise commonly called fan or compressor "whine". Analysis of the mechanism has included the classical theories of sound propagation as well as aerodynamic cascade theories and small perturbation concepts.

Acoustic normalizing techniques have resulted in a correlation curve of the overall sound power for 13 separate fan and compressor vehicles with each one being from a different design family. The curve covers designs from scale model to full scale and is useful in determining scaling effects as well as providing a basic guide to design engineers.

Investigation of noise minimization through design techniques incorporates the results of the analytical investigations and the normalized sound power relations. Results indicate the effect of rotor-stator spacing, blade number, RPM, inlet length and centerbody design.

Suppression techniques evaluated were wave cancellation, deflection, and absorptive suppressor designs. Test results of an absorptive type suppressor show up to 10.5 db maximum suppression as tested with a scale model fan configuration.

The noise data accumulated throughout the program are presented in table form for the sound pressure measurements made on each configuration.

PREFACE

This is the final report covering technical work performed under the U. S. Army Transportation Research Command (USATRECOM) Contract DA 44-177-AMC-72(T), "Fan Noise Research Investigation". The technical effort was initiated July 1963 and completed August 1964, with all technical requirements of the program having been fulfilled. The work was performed by the Advanced Engine and Technology Department (AETD) of the General Electric Company, Cincinnati, Ohio. Project Engineer for the program was H. D. Sowers, who authored this report with contributions by the following: G. M. Rentzipis, Advanced Technologies Laboratories, General Electric Company, Schenectady, N.Y., who wrote Appendix 1; D. C. Prince, Consulting Engineer, Analytical Investigations, who wrote Appendices 2, 3, 4, and 5; and T. J. Koenig, Noise Evaluation and Control, who wrote Appendix 6.

Acknowledgment is made to the following Noise Evaluation and Control, AETD, personnel: T. J. Koenig, Engineer, who was responsible for most of the tests conducted during the program; W. C. Sperry, Manager, who provided technical assistance throughout the program; R. G. Behrens, who assisted in data acquisition; E. O. McCann, who was responsible for magnetic tape data reduction and assisted in data acquisition; A. O. Price, who was responsible for reducing and preparing test results; and R. Lee, former Manager, who was fundamental in the conception and initiation of the program.

Technical effort was monitored by R. L. Brugh and J. E. Yeates, of the U. S. Army Transportation Research Command, Ft. Eustis, Virginia.

CONTENTS

ILLUSTRATIONS

TABLES

SYMBOLS

AR	aspect ratio, $\frac{\text{rotor blade height}}{\text{rotor blade chord}} = \frac{h}{c}$
A_a	rotor stage annulus area, ft^2
A_2	flow passage area between blades at stage exit, ft^2
c	speed of sound, ft/sec or m/sec; chord length of blade, in.
c/s	cycles per second
db	decibel
D_H	rotor hub diameter, ft
D_T	rotor tip diameter, ft
DI	directivity index, db
E	energy flux, btu/sec - ft^2
f	frequency
H_T	total enthalpy, Btu/lb
h	blade height, in.
IGV	inlet guide vane
kw	kilowatts
kc/s	kilocycles per second
L	length
l_x	passage open width, ft
l_y	passage length, ft
ΔL	difference in length
M	mach number
n	rotor speed, revolutions per minute

N_r	number of rotor blades
N_s	number of stator blades
OA	overall
P_r	pressure ratio
PWL	sound power level, db re 10^{-13} watts
RPS	revolutions per second
RPM	revolutions per minute
r	distance from sound source to receiver, ft
R_1	specific flow resistance, mks rayles/meter
S	blade circumferential spacing, in.
SPL	sound pressure level, db re .0002 microbar
T	temperature, °R
ΔT	temperature rise, °R
t	time, sec; material thickness of lined passage, in. or meter; blade thickness, in.
Δt	change in time, sec
V	local velocity, ft/sec
V_∞	free stream or undisturbed velocity, ft/sec
$\bar{V}_1$	average velocity of diffusing passage, ft/sec
$\bar{V}_2$	average velocity of converging passage, ft/sec
VTOL	vertical takeoff and land
W	weight flow, lb/sec
x	axial distance downstream or upstream from rotor blade, ft

y	circumferential distance, normal to x, ft
α	phase angle between two signals, degrees
β_1	angle of flow into rotor blade, degrees
β_2	angle of flow out of rotor blade, degrees
β_∞	flow angle at free stream, degrees
γ	arbitrary angle to indicate sinusodial wave signal, degrees
θ	angle from inlet axis of fan or compressor denoting position at which sound measurements were made, degrees
λ	wave length, ft
ρ	density, lb/ft^3 or kilograms/ m^3
σ	solidity, $\frac{\text{rotor blade chord}}{\text{rotor blade spacing}} = \frac{c}{s}$

INTRODUCTION

Recent developments in advanced propulsion system designs have utilized fan type configurations, such as the General Electric/Ryan XV5A aircraft, Figure 1 . The noise associated with a system of this type is generally less on a sound pressure level (SPL) basis than that associated with turbojet systems of the same thrust class due to the lower jet velocities. However, the fan noise or "whine" being generated by the rotor at the blade passing frequency is a very distinct sound that requires special consideration since standard jet noise suppression techniques are not applicable. This fan "whine" is the same noise generating mechanism as that associated with compressor noise. Some analysis of this type of discrete tone noise mechanism has been done previously, but only a limited amount of published data is available for evaluation of various analytical techniques. This effort and report provide extensive supporting data for analytical investigations, past and present, and a normalizing technique on a sound power level basis (PWL) for the performance of all the various design fans and compressors tested. In addition, suppression concepts have been investigated, and a 10.5-db reduction absorptive type suppressor that will provide a guide for future absorptive type suppressor applications has been designed and demonstrated.

This report is divided into sections corresponding to three major areas: analytical investigations, acoustic normalizing techniques, and noise minimization and suppression design techniques. A fourth section describes the vehicles tested and presents the basic data accumulated during the program.

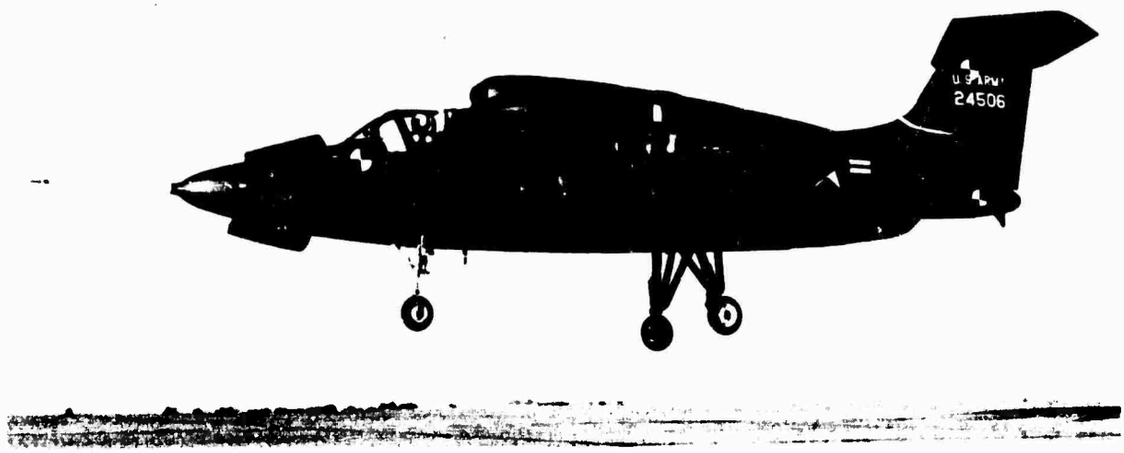

Figure 1. XV-5A Aircraft in Hover Mode

SECTION ONE - ANALYTICAL INVESTIGATIONS

Analysis of discrete tone noise from fans is made difficult by the many nonlinearties involved in the physical aspects of the problem. Previous investigations (references 15 and 18) obtained qualitative results by using the basic wave equation with appropriate boundary and initial conditions and making necessary assumptions such as rigid walls, small pressure fluctuations and homogeneous medium. These results defined the sound field both in the fan duct upstream and downstream of the rotor face and in the radiated field at a distance from the fan inlet or exhaust. The supporting data for these investigations, however, was sparse and did not adequately verify the results.

The problem of defining the discrete tone noise generating mechanism at the fan rotor is generally divided into two cases: rotor or rotational noise associated with the pressure field around the rotor blade, and rotor - stator interference noise resulting from the interaction of the viscous wake from a stator row upstream of the rotor with the rotor blades or the viscous wake from the rotor blade interacting with a downstream stator row. In all cases, the discrete tone fundamental frequency or first harmonic is defined by the product of the rotor speed, RPS, and the number of rotor blades, N_r. The analysis of this mechanism using the classical wave equation results in the definition of a "cutoff" frequency, which is the frequency above which the sound waves propagate from the rotor face and below which the sound is attenuated at a very fast rate. This cutoff frequency is defined for both the case of rotational noise and the case of rotor - stator interference noise. Appendix I is an analysis similar to that made by other investigators which shows the development of the cutoff frequency concept.

In the case of rotational noise, the cutoff frequency is not attained until rotor tip speeds approach Mach 1.0; thus, for the various scale model vehicles tested during this program, the necessary cutoff frequency was not reached. The rate of attenuation predicted for the sound field below the cutoff frequency is in the range of 55 db per blade space (reference 18, page 60), which would mean that the resultant sound pressure levels at distances of ten feet or more from the fan face would be insignificant. This same rate of attenuation was predicted using flat plate cascade theory as shown in Appendix II and Appendix III and Figures 2 and 3. Figure 2 shows the attenuation in velocity for the limiting case of no-flow velocity, while Figure 3 shows the effect due to Mach number, M, and flow angle, β. The test vehicles, Section Four, did not substantiate this theory, since all the vehicles tested with a lone rotor produced significant sound pressure levels at distances up to 50 feet.

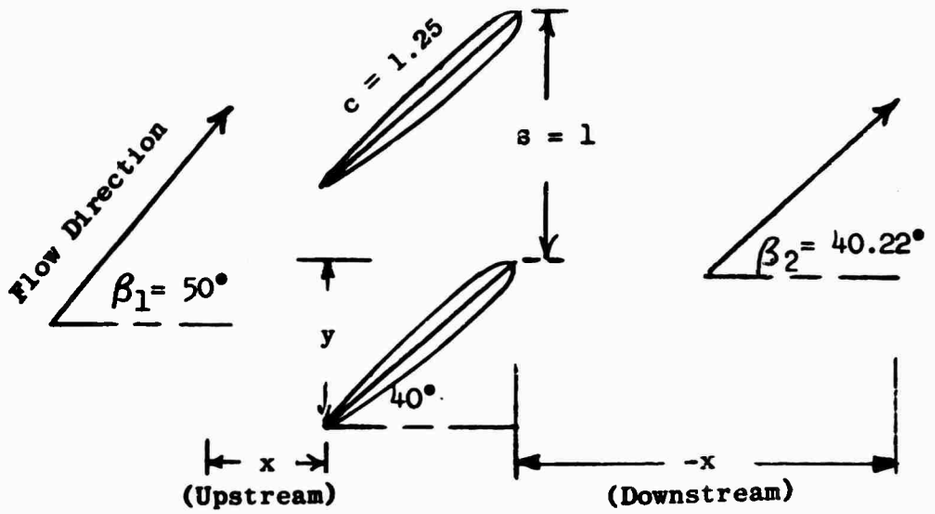

Figure 2.1. Velocity Field of a Flat Plate Cascade.

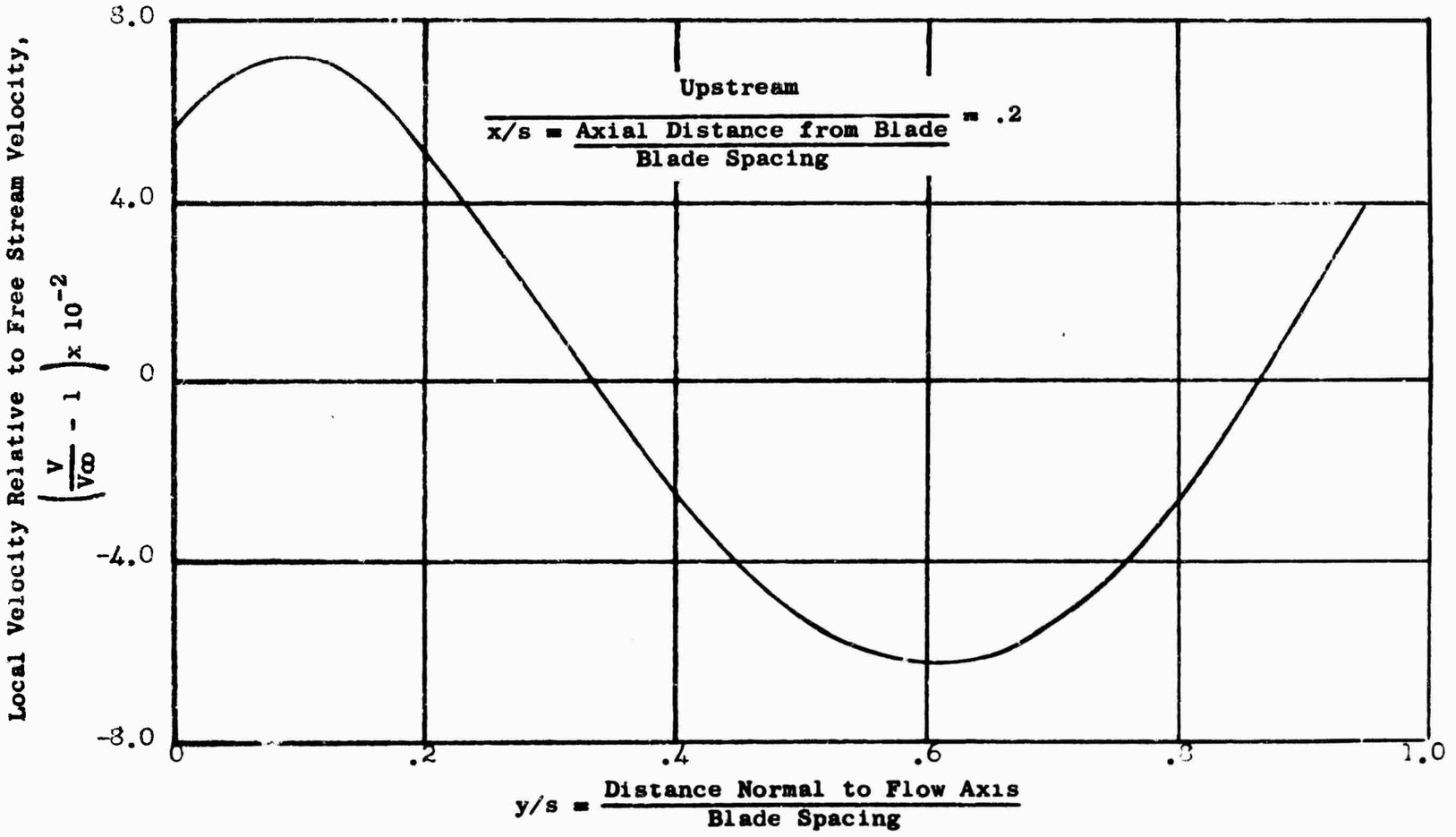

Figure 2.2 Velocity Field of a Flat Plate Cascade

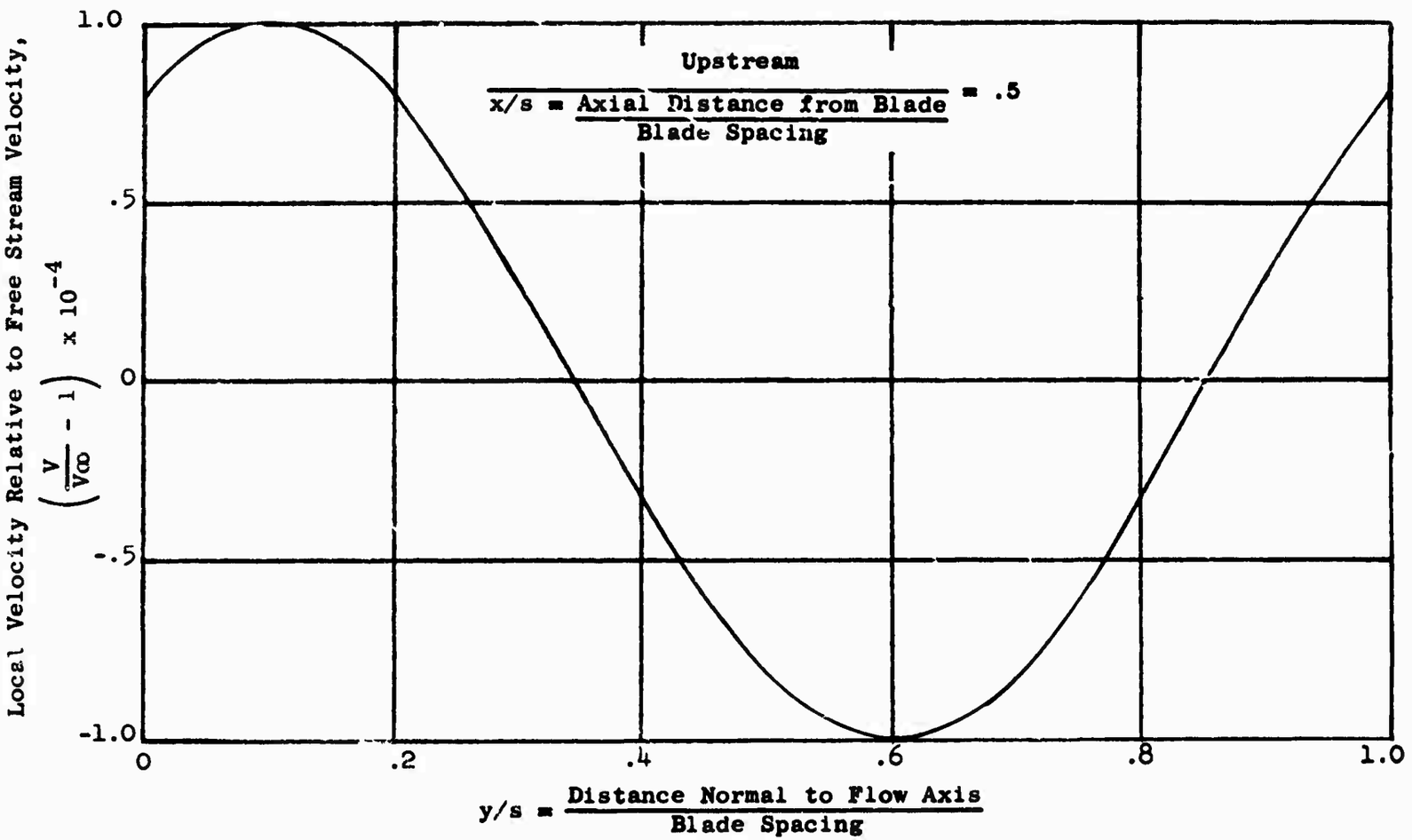

Figure 2.3. Velocity Field of a Flat Plate Cascade.

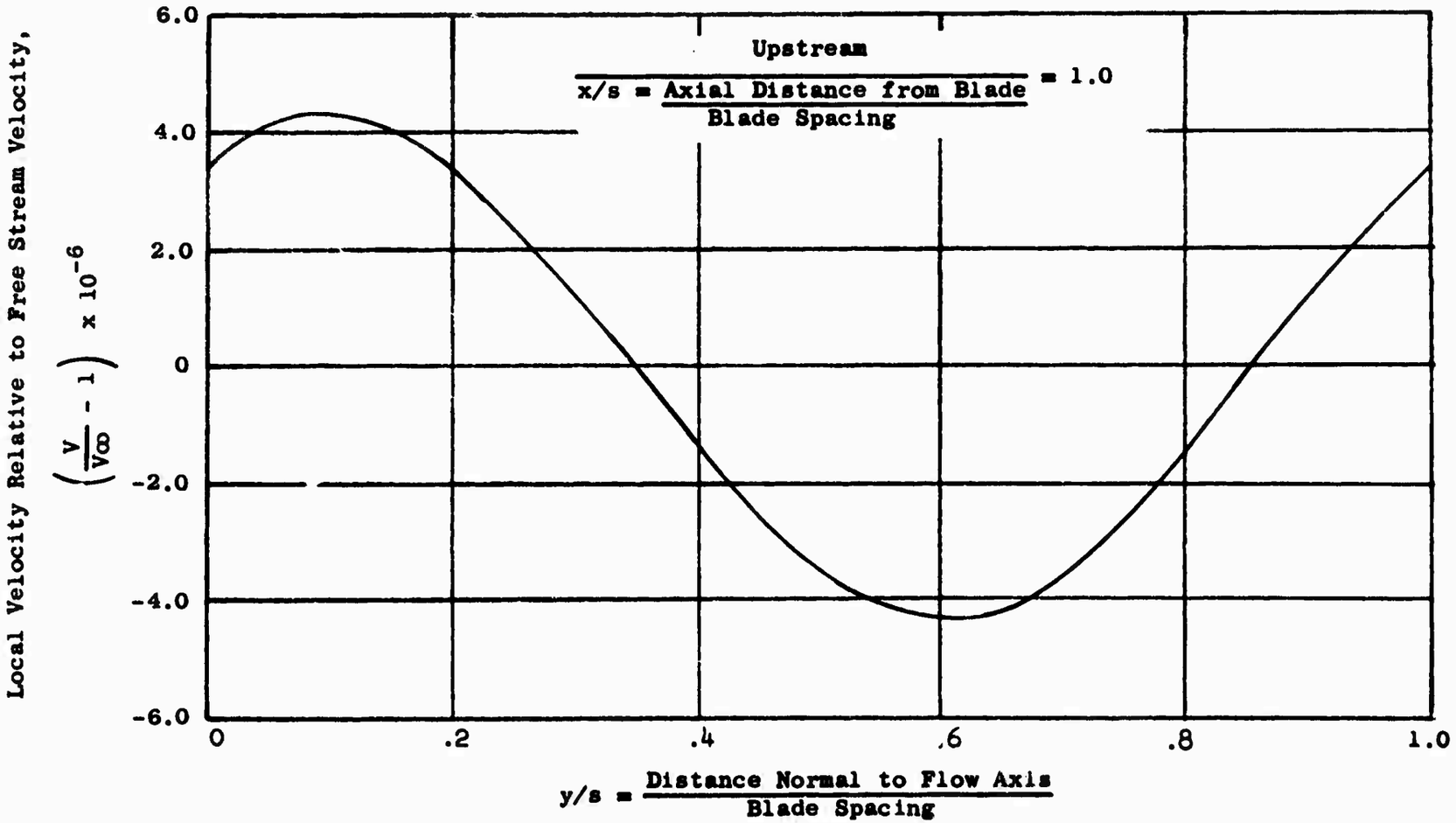

Figure 2.4. Velocity Field of a Flat Plate Cascade.

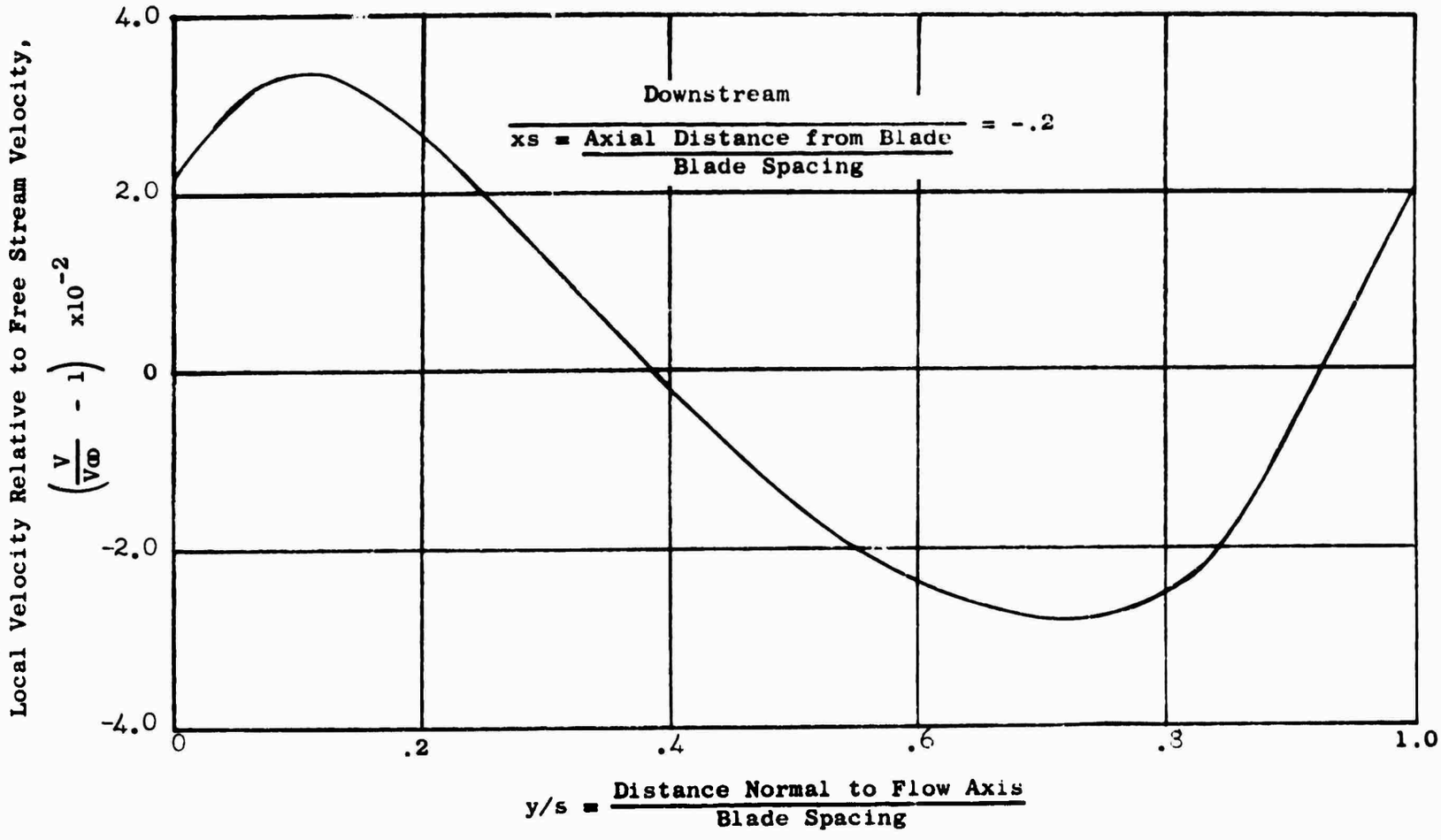

Figure 2.5. Velocity Field of a Flat Plate Cascade.

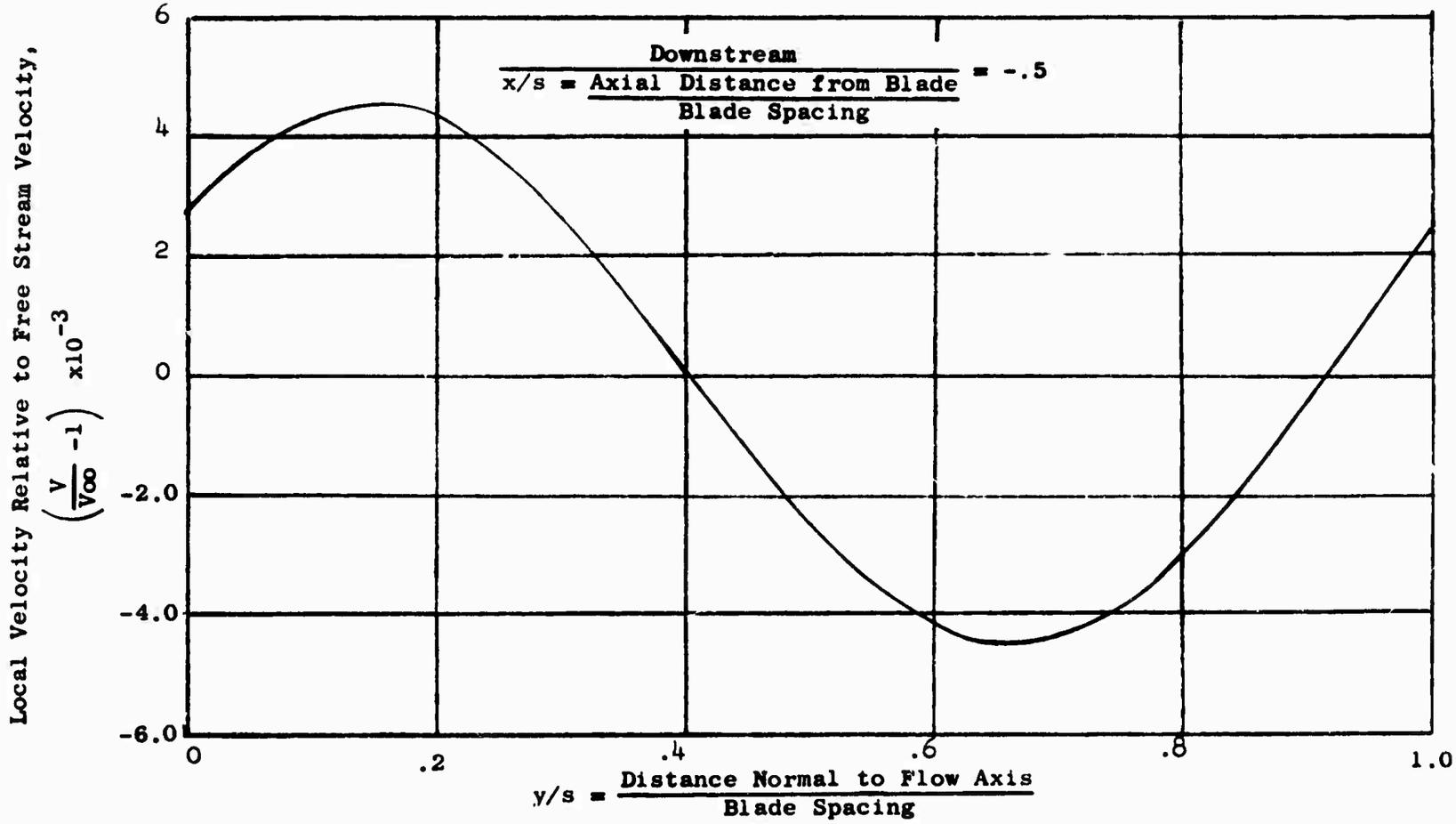

Figure 2.6. Velocity Field of a Flat Plate Cascade.

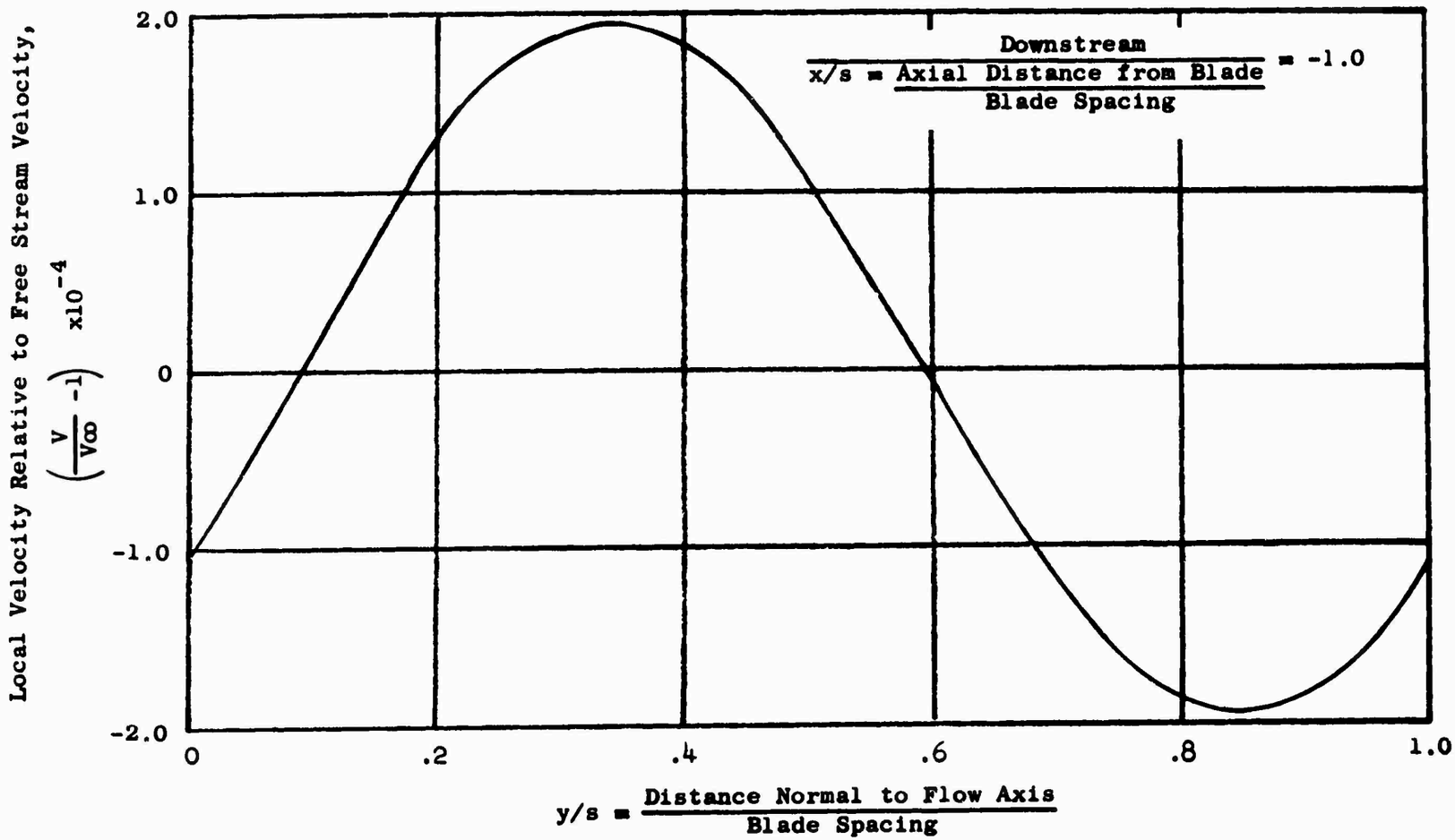

Figure 2.7. Velocity Field of a Flat Plate Cascade.

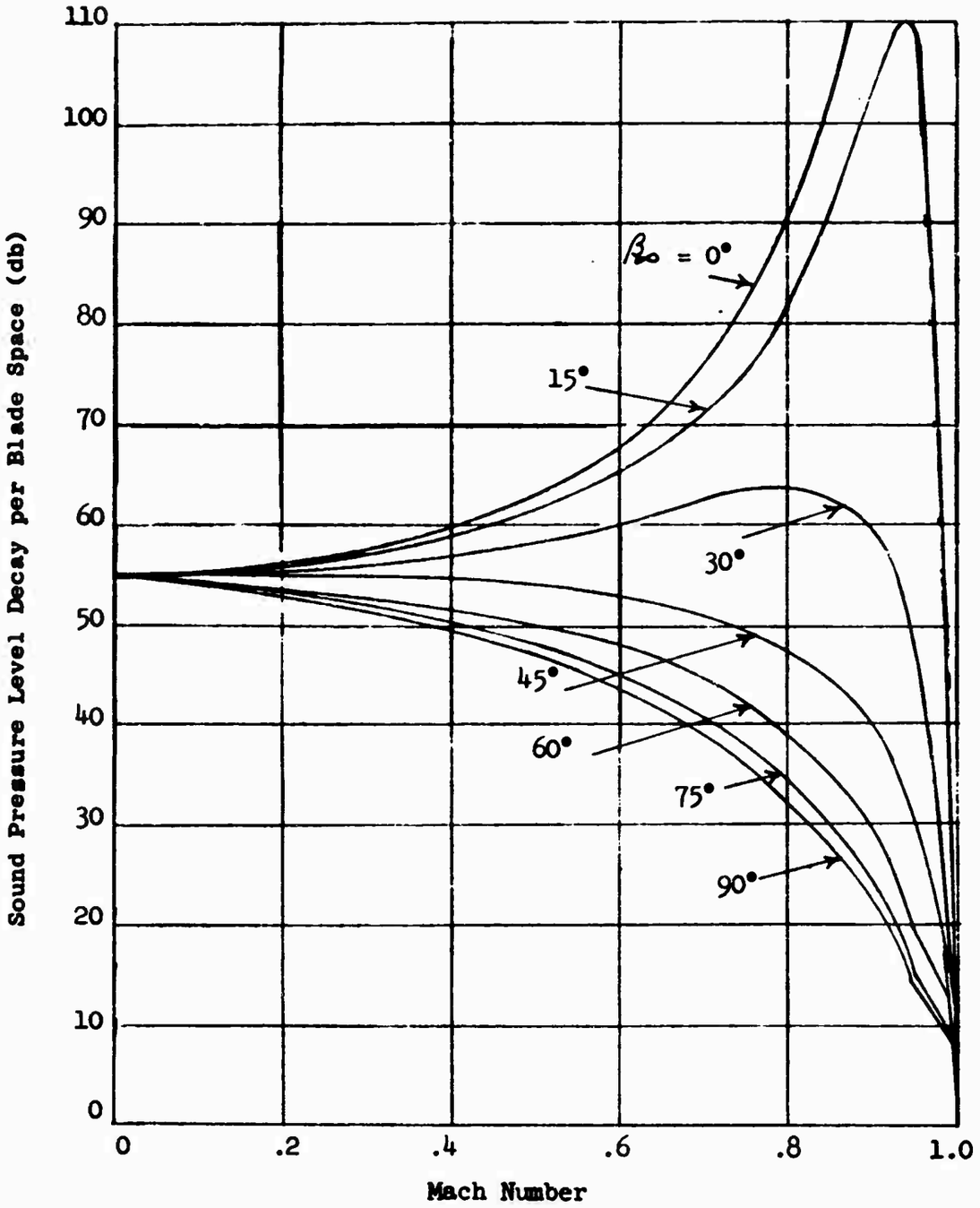

Figure 3. Sound Pressure Level Decay vs Tip Mach Number for Various Flow Angles.

The case of rotor - stator noise requires a variation in the cutoff frequency to account for the different pressure pattern at the rotor face due to the alignment of the rotor blades and stator blades. This is shown in detail in Appendix I. The conclusion drawn by this analysis and the previous analyses was that rotor - stator noise would be substantially more significant than the noise generated by a lone rotor. Test results of the rotor - stator fan and single-stage compressor test vehicles, Section Four, Table 1, with and without a stator row are shown in Figure 4. These test results show that the rotor only condition is still significant relative to the rotor - stator case and that a considerable variation is found in the db reduction obtained by removing the stator row. The rotor - stator fan attained only a 4-db reduction, while the single-stage compressor attained a 22-db reduction.

The above discussion for the rotational and rotor - stator noise generating mechanism indicates that further investigation is required to better define the amount of interference required to generate the high noise levels. For example, discontinuities on the fan inner surface or upstream and downstream support struts may be sufficient to interact with the rotor to produce discrete tones. Tests with no-lift devices, such as wires, placed near the rotor face would be an example of the type of investigation required.

Appendix IV is an analysis based on the interaction of cylindrical waves to define the sound field resulting from rotor - stator interference. The particular advantage of this type of analysis is the elimination of the cutoff frequency as it is presently defined and the relatively simple geometry of the analytical model. The cylindrical waves produced by each rotor - stator interaction are space and time sequenced so as to combine to produce plane wave fronts that propagate without attenuation. The disadvantage of this approach is the lack of a simple acoustic potential as is associated with plane or spherical waves, thus requiring the application of the unsteady flow method of characteristics. The results of the analysis were programmed for computer use as presented in Appendix IV, but further investigation is required to obtain realistic numerical results.

Having defined the noise mechanism at the rotor face and the propagation characteristic to the fan inlet or exhaust, the radiation pattern to space or directivity must be defined. This analysis is presented in Appendix V. The directivity patterns predicted by the analysis are a function of the number of rotor and stator blades, N_r and N_s respectively, RPM, and physical size of the radiating face. The analysis was programmed to utilize a computer in making the necessary calculations. Typical results from the program are shown in Figures 5.1 through 5.4. Note that the program predicts a considerable decrease in

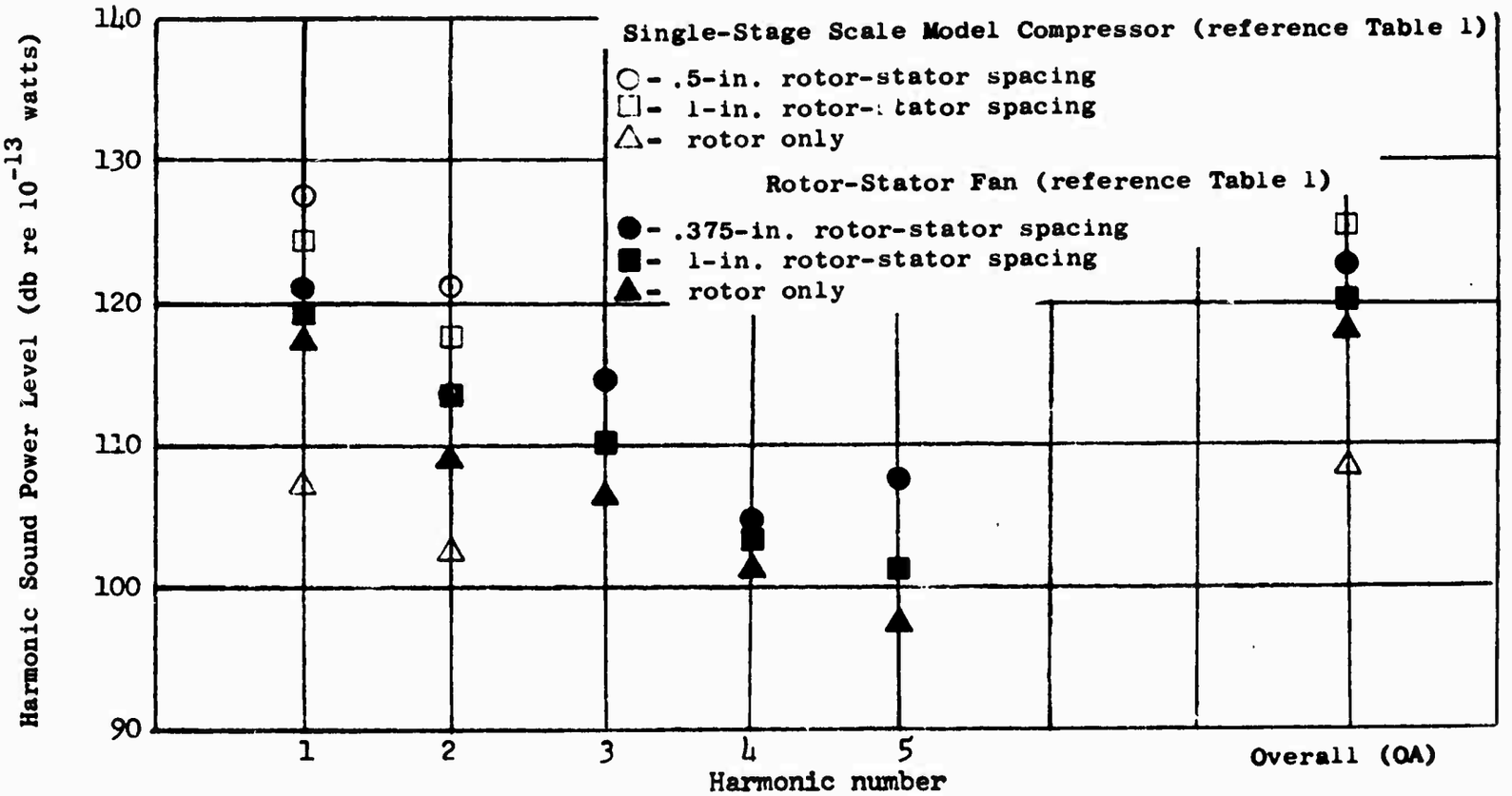

Figure 4. Variation in Rotor-Stator Interference Noise with Axial Spacing.

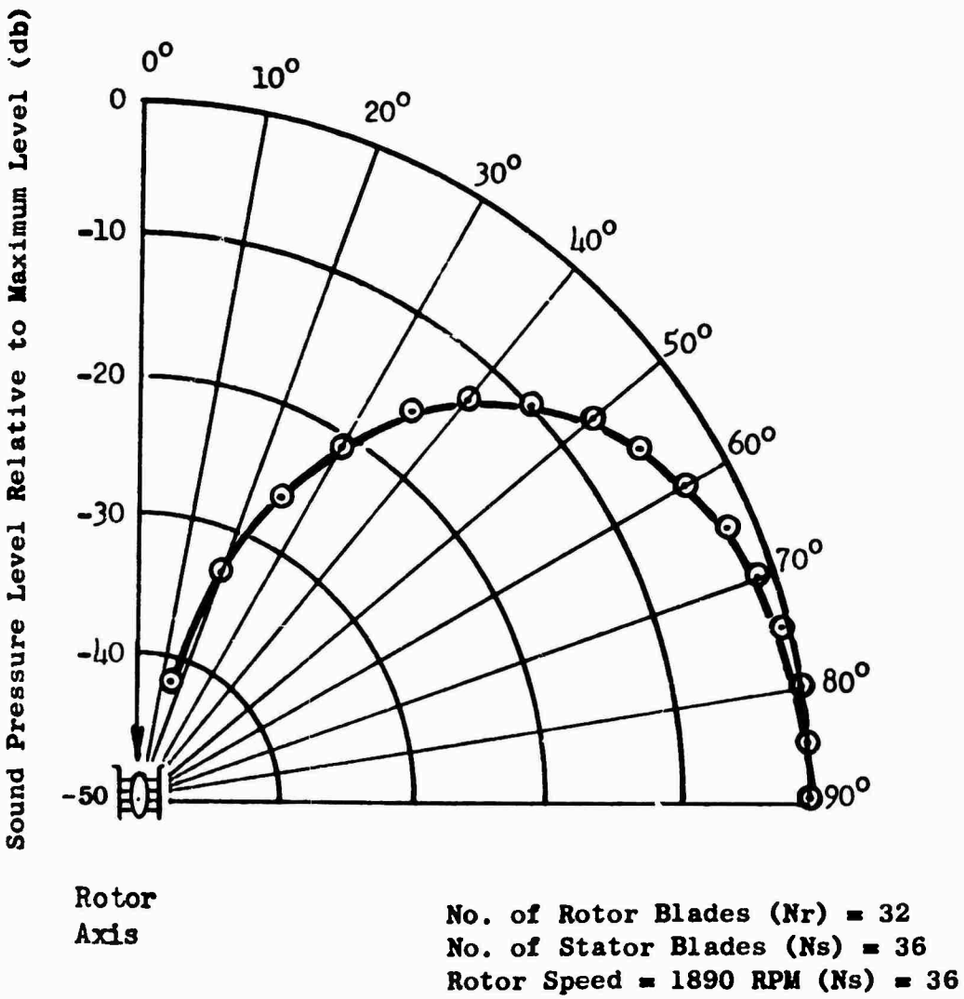

Figure 5.1. Predicted Directivity Pattern

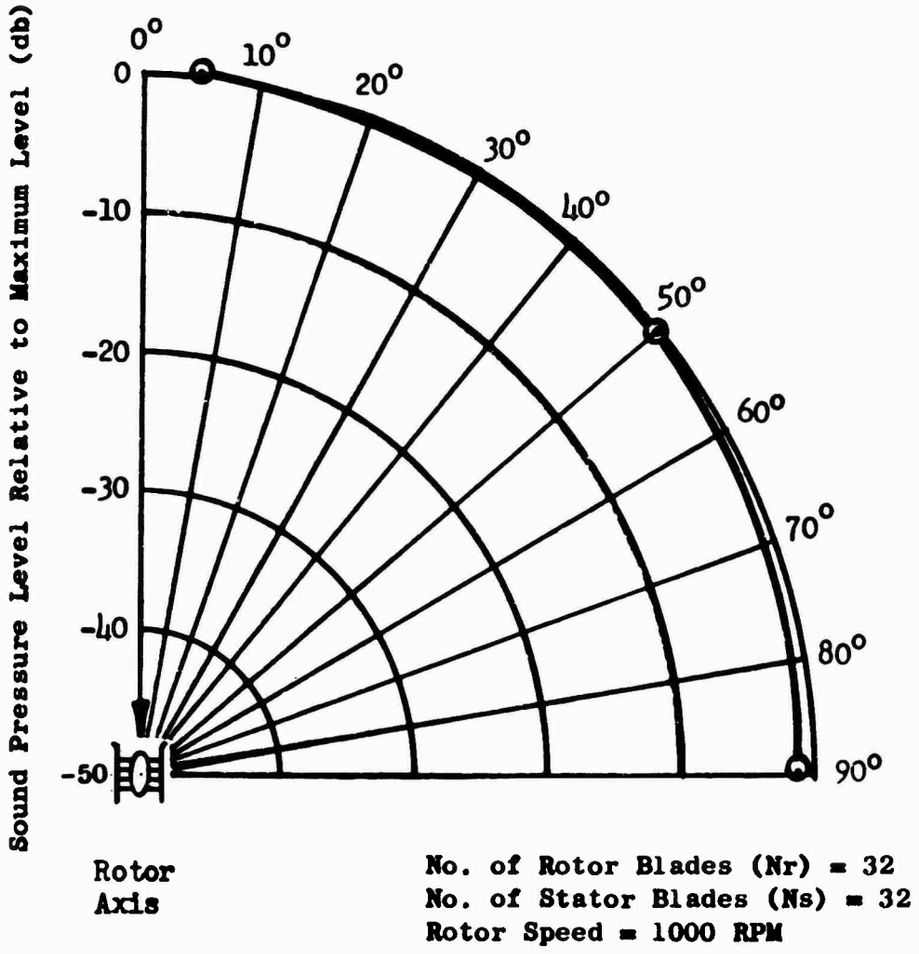

Figure 5.2. Predicted Directivity Pattern.

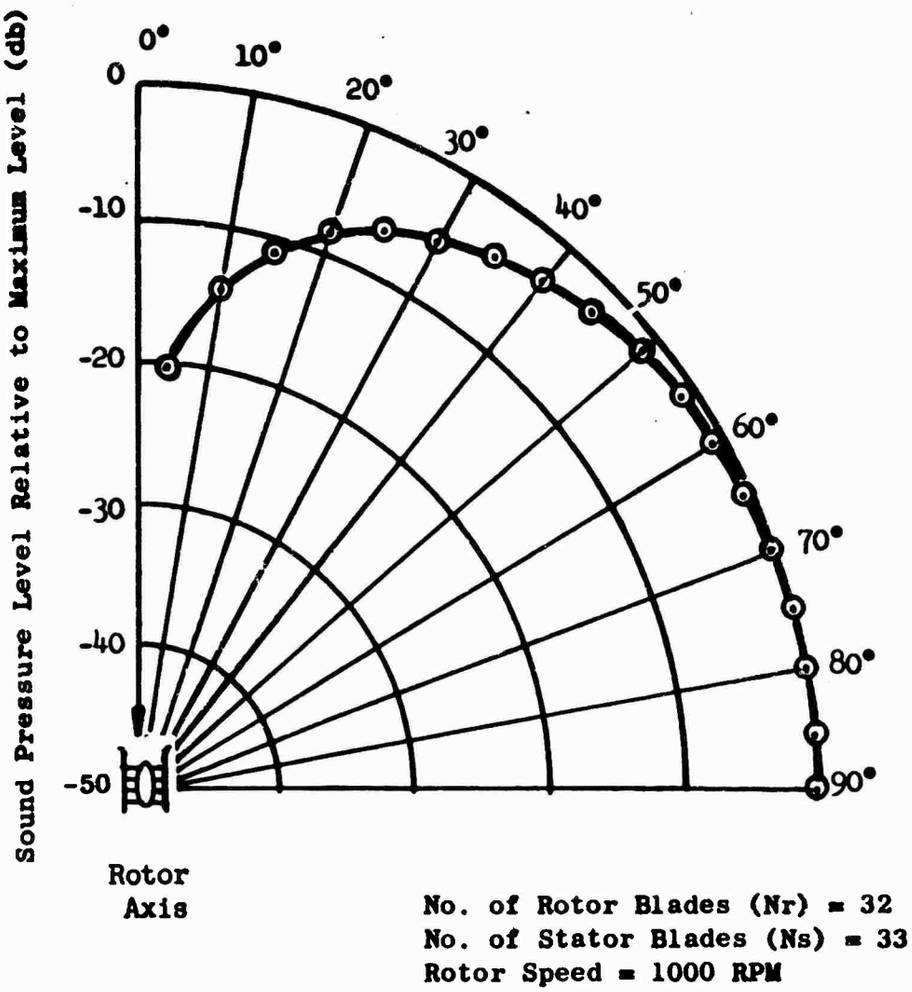

Figure 5.3. Predicted Directivity Pattern.

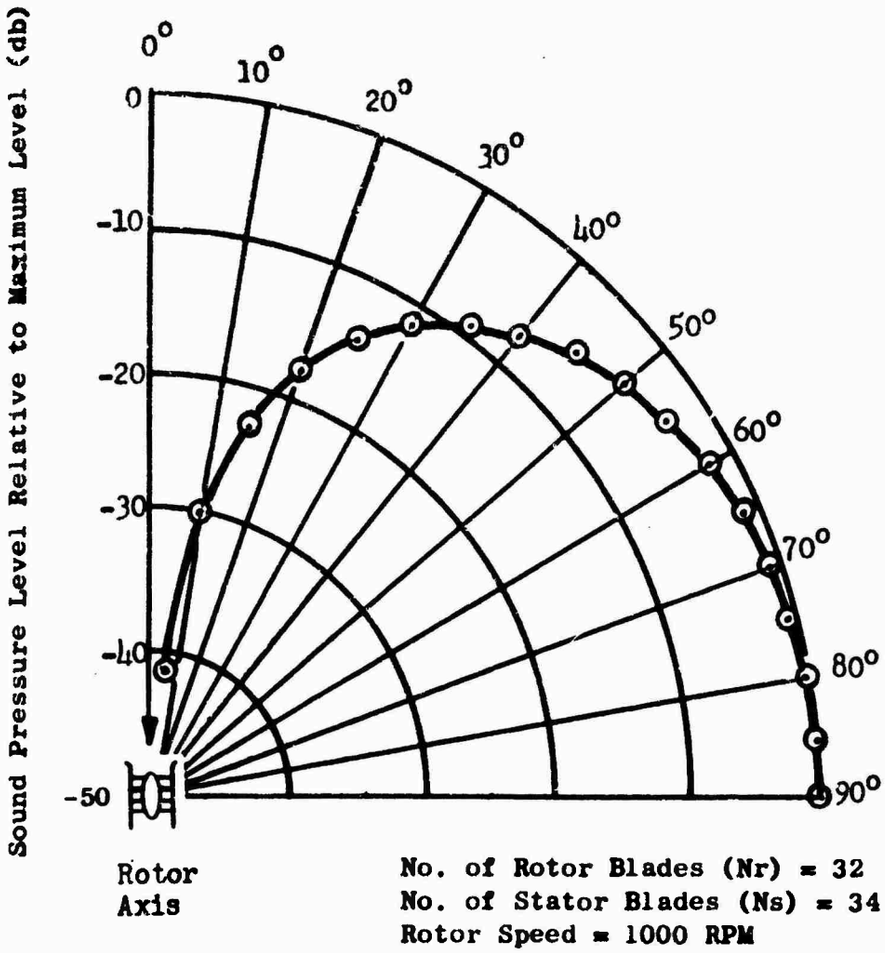

Figure 5.4 . Predicted Directivity Pattern

sound pressure level at some positions. This is the same type of directivity predicted in reference 18, page 35 . Variations in sound pressure level in the order of 15 db are not readily measured in actual cases, as evidenced by the data in Section Four and as shown in Figures 6 and 7. Further investigation of measured directivity patterns showed considerable variation in the patterns as a function of the distance from the fan face. Typical results are shown in Figures 8 and 9. The radial variations do not correspond to the spherical divergence relationship, as shown in Figure 9. In addition to the variations found in each test, considerable variation is found in measurements made on the same configuration but on different days. Figure 10 shows the variation for two runs made on different days with the development vehicle fan, Section 4, Table 1. These inconsistencies in measuring directivity patterns make correlation of analysis and test results unrealistic. In addition, they raise the question of the validity of attempting to predict directivity, since in practical applications the many variables encountered would make predictions unrealistic.

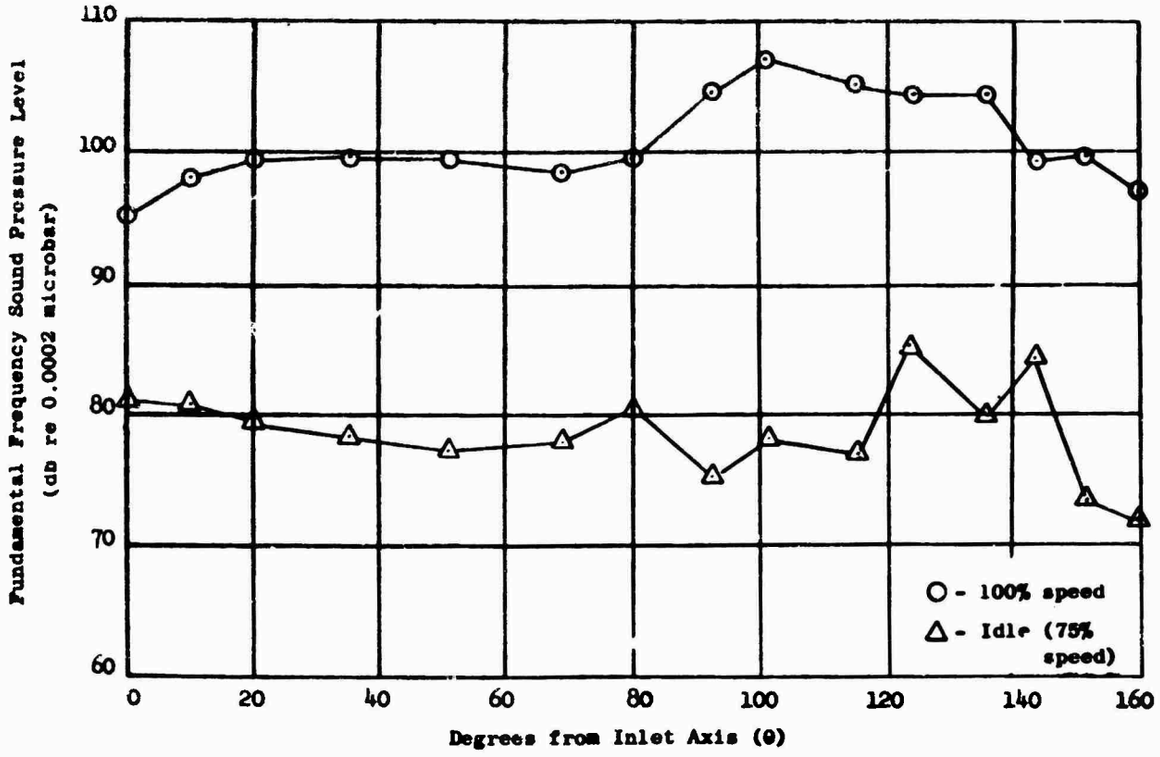

Figure 6. Sound Pressure Level Circumferential Survey of CJ805-23 Fan, 200-foot Radius (reference Table 1).

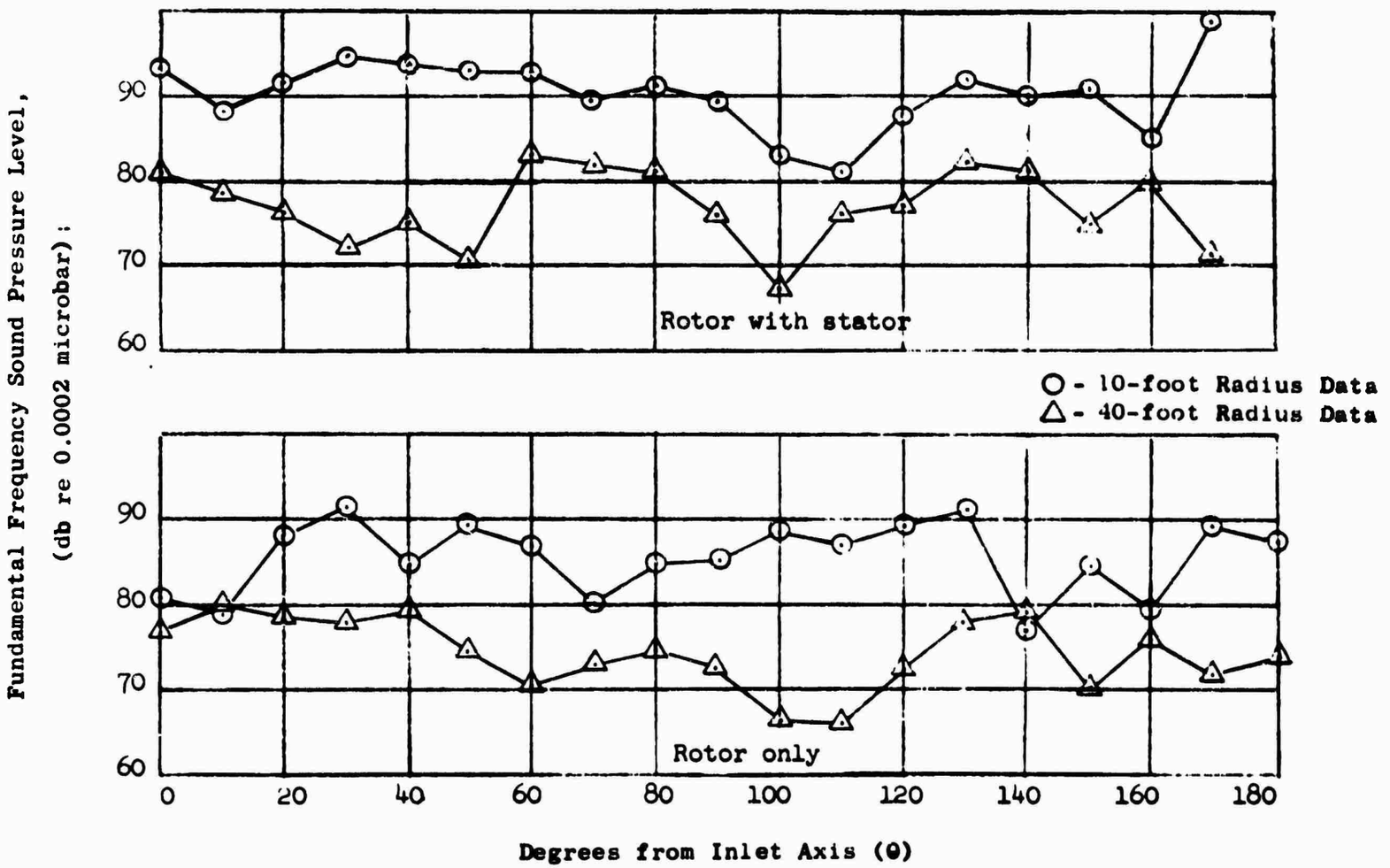

Figure 7 . Rotor-Stator Fan Circumferential Survey, (reference Table 1).

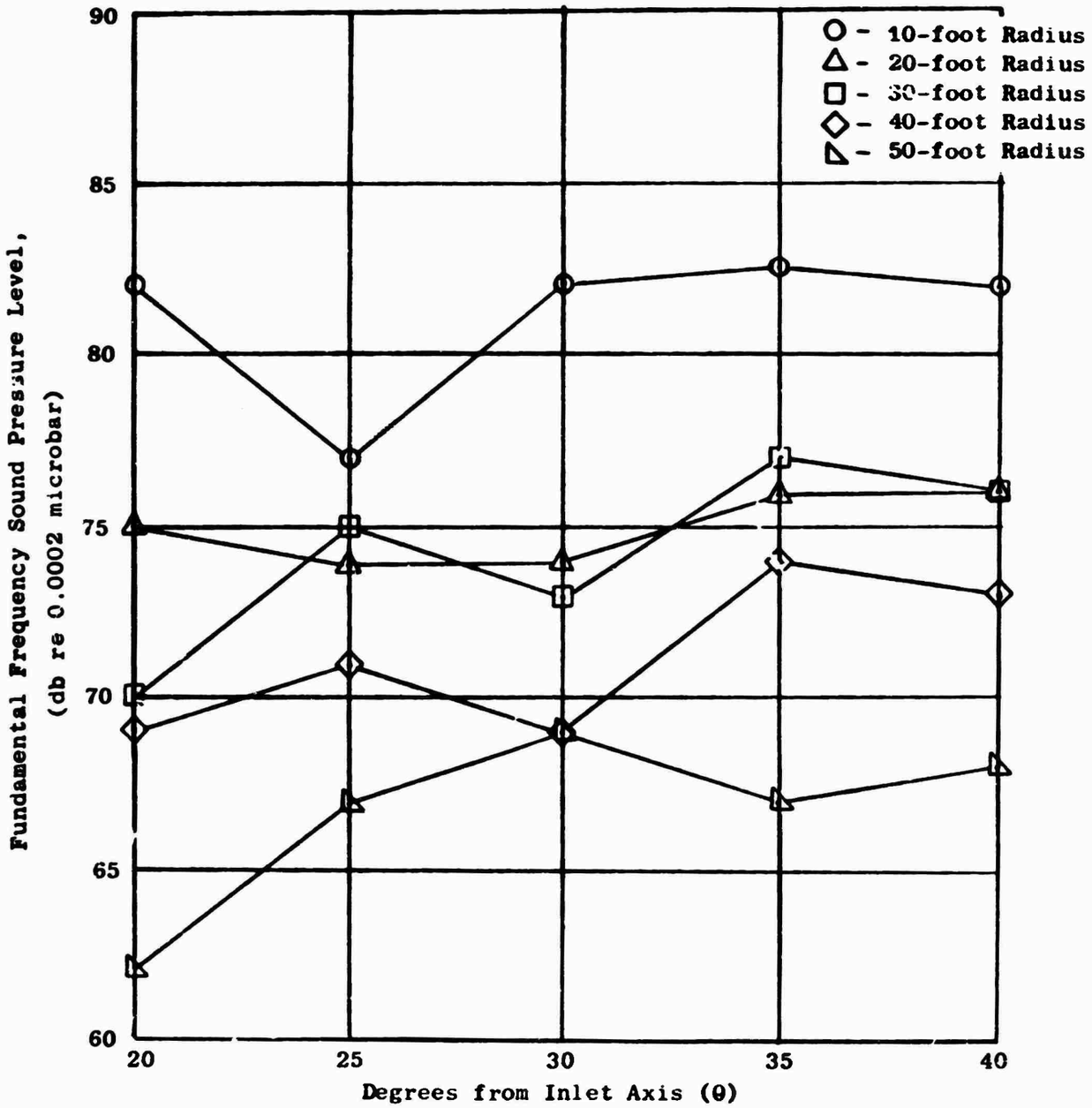

Figure 8. Radial Directivity Variation of Development Vehicle (reference Table 1).

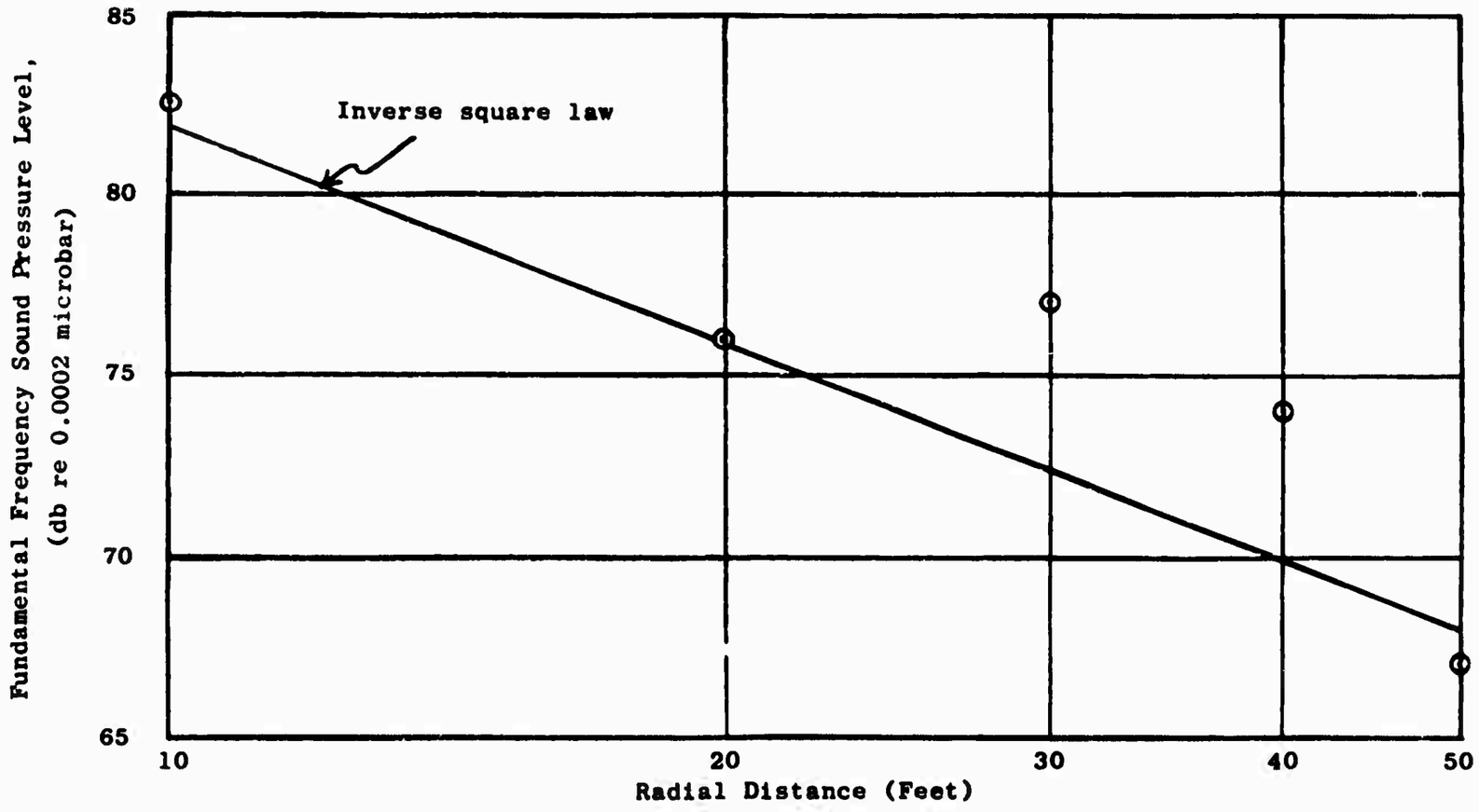

Figure 9. Sound Pressure Spherical Divergence of Development Vehicle (reference Table 1) at 35° from Inlet Axis.

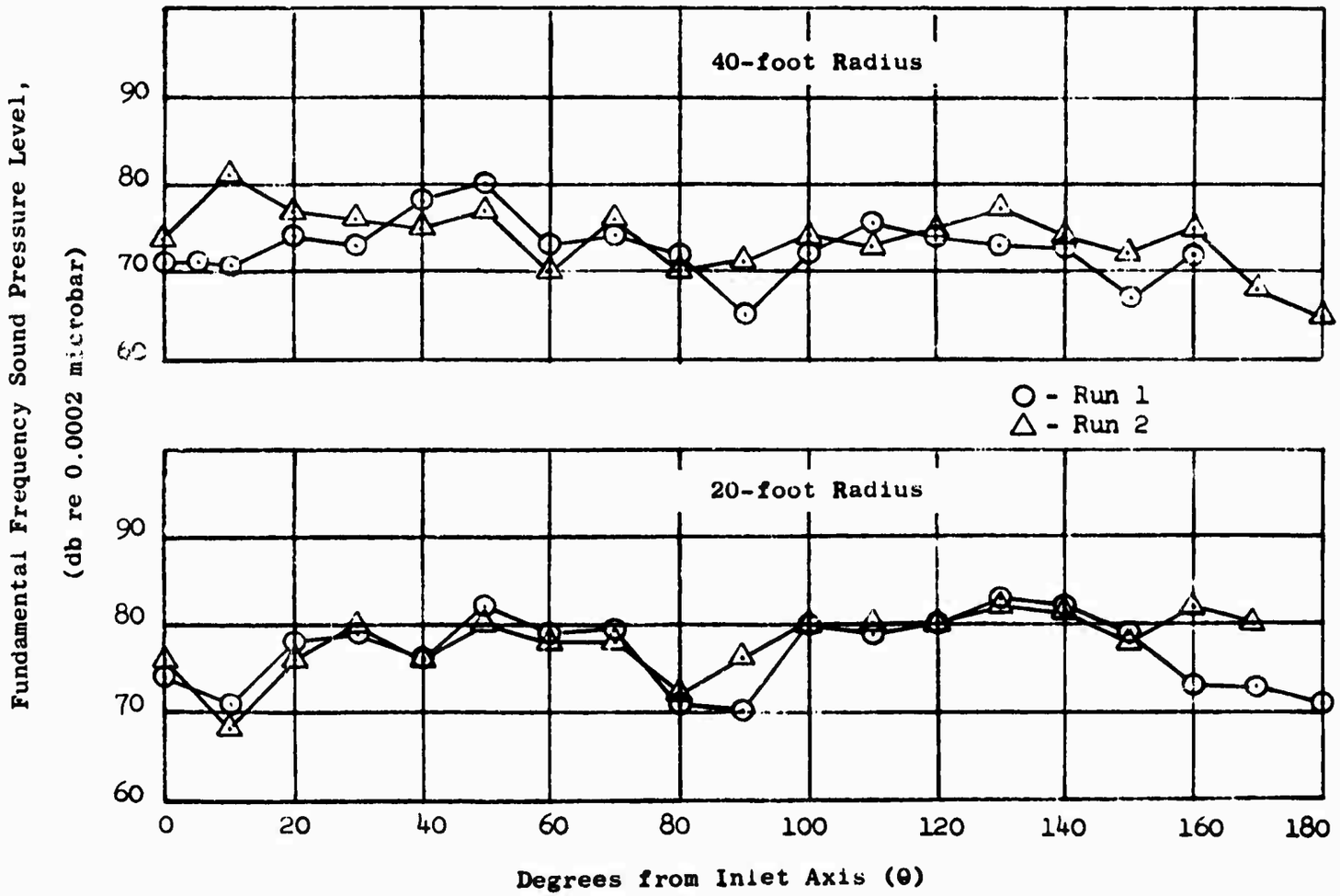

Figure 10. Sound Pressure Level Circumferential Survey of Development Vehicle (reference Table 1).

SECTION TWO - ACOUSTIC NORMALIZING TECHNIQUES

When a new fan design is in the development stage or when scale model fan test results are being extrapolated to predict full scale performance, applicable normalizing techniques are required. One of the methods used previously to determine acoustical performance of fans or compressors was a curve normalized on a shaft power basis and applicable to a particular design family. A typical prediction curve for various families is shown in Figure 11. This curve does not allow for new design analysis unless a similarity is maintained between the new design and one of the earlier families of designs. In addition, little or no data was available to substantiate the fact that the families of design lines were consistent from scale model to full scale. Utilizing the scale model and full scale data as presented in Section Four, shaft power was used to normalize the fan sound power, PWL, for the family of Vertical Takeoff and Land, VTOL, vehicles: inlet guide vane (IGV) - rotor fan, rotor - stator fan, lift fan, pitch fan, and cruise fan, all of which are described in Section 4, Table 1. This indicated, as shown in Figure 12, that the shaft power correlation did hold from scale model to full scale for predicting fan or compressor sound power, but the normalized relationship still did not allow evaluation of new designs.

The problem of normalizing the various design families onto one curve was solved by using an energy flux, E, concept and a design parameter

$$10 \log \frac{A_a \, n}{N_r} \quad (D_H/D_T)^2$$

with

A_a = Rotor annulus area, ft^2

n = Rotor speed, RPM

N_r = Number of rotor blades

D_H/D_T = ratio of rotor hub diameter to rotor tip diameter.

The normalized acoustic performance curve is shown in Figure 13. This empirical curve is based on scale model and full scale data and includes designs ranging from the 62-inch VTOL lift fan to scale model compressors. The solid symbols in Figure 13 represent data accumulated by the program, while the open symbols are measurements made prior to the program. The abscissa of the curve represents the total energy, E, of the air as it leaves the fan or compressor rotor stage on a per-unit time and area basis. The ordinate of the curve was determined by a parametric study of the various design parameters and the results of the noise data obtained on each vehicle.

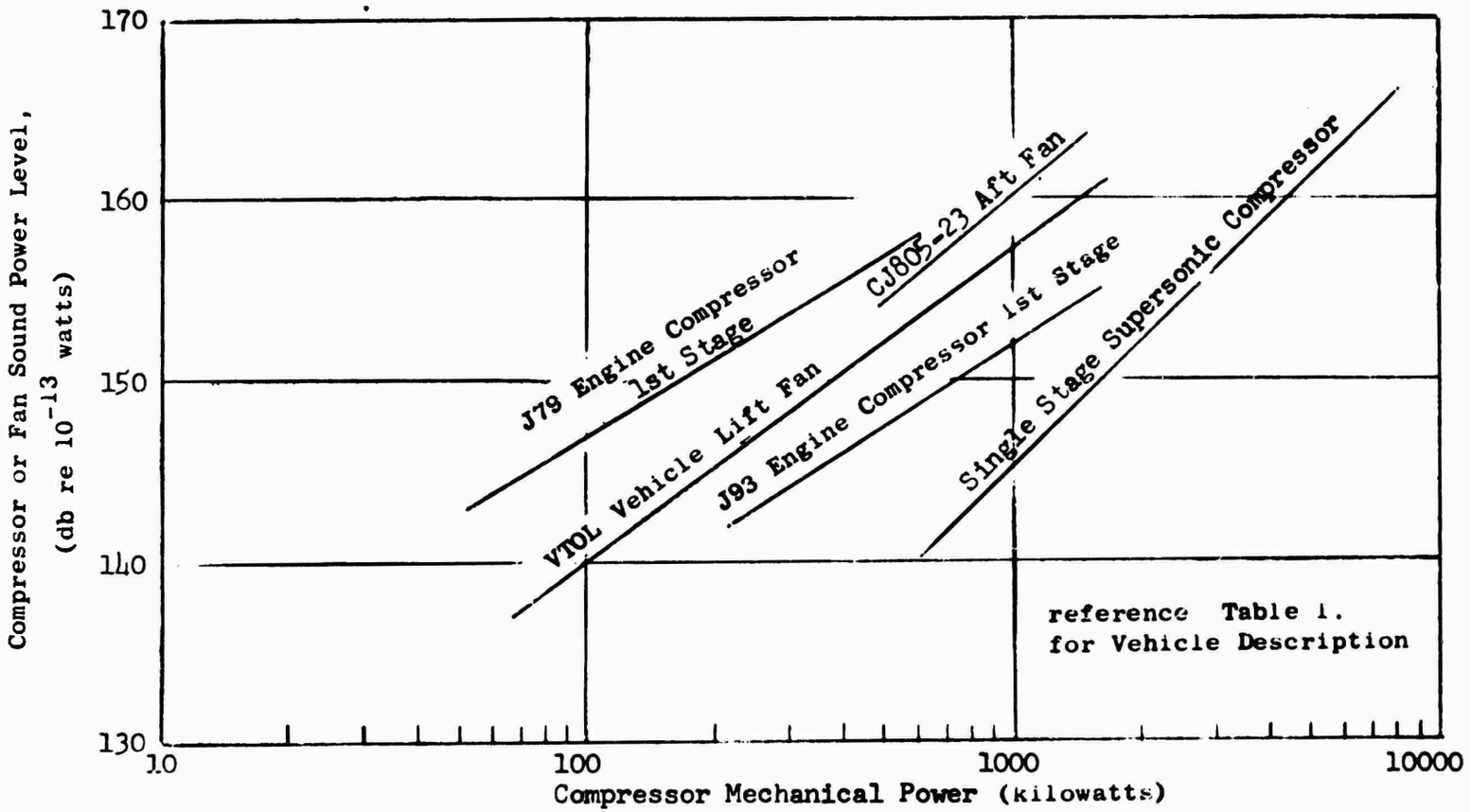

Figure 11. Compressor or Fan Mechanical Power vs Sound Power Generation.

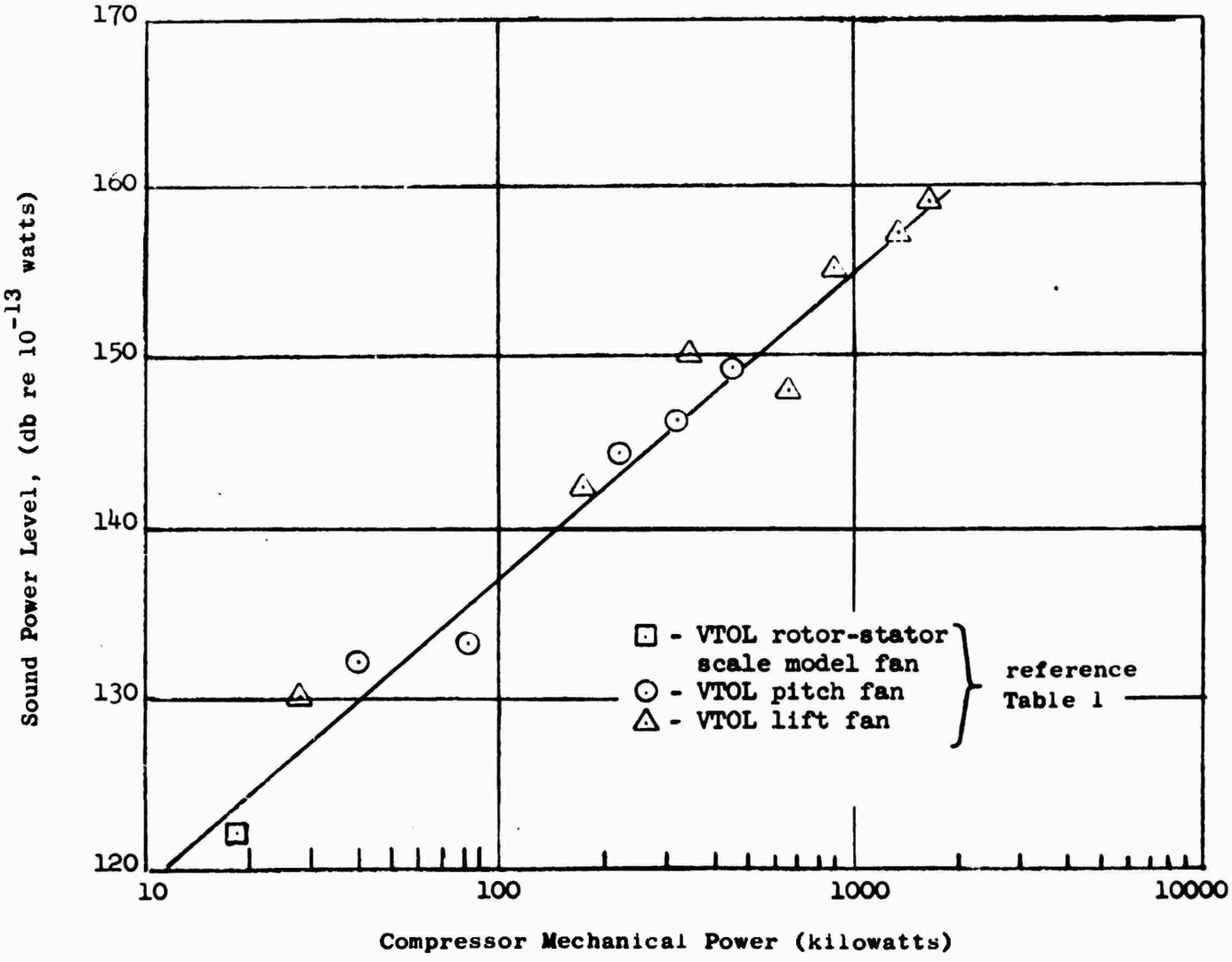

Figure 12 Mechanical Power of Various VTOL Fans vs Sound Power Generation.

Figure 13. Normalized Overall Power of Compressor and Fan Noise.

Since the curve is based on the fundamental acoustic parameter sound power, it allows the designs of various vehicles to be compared directly. This type of analogy is useful from both a research viewpoint and a design viewpoint. For research, the normalized curve eliminates many of the irregularities presently found in fan and compressor noise measurements. For the designer, the normalized curve provides a basis on which the various design parameters (rotor annulus area, A_a, rotor speed, n, rotor blade number, N_r, hub - tip ratio, D_H/D_T, fan air flow, W, and discharge total temperature, T_T) may be evaluated to determine the optimum combination for minimum noise generation. This is discussed further in Section Three.

The evaluation of advanced designs may be extended from the sound power level, determined by the normalized power curve, to a sound pressure level, SPL, by using additional normalized or average results from the test data. This is particularly important when the advanced design must conform to an SPL far field acoustic requirement. The overall power level may be reduced to a spectrum power level, SPWL, for each harmonic using Figure 14. This normalized power spectrum is the result of averaging the measurements taken on the various fan configurations, as shown in Figure 15. Note from Figure 15 that a considerable spread is found in the harmonic power spectrum data. Sound pressure level and power level are related to the directivity index, DI, and distance from the source, r, by the following equation:

$$SPL = PWL + DI - 20 \log r - 10.5$$

where the value of r is the radius at which the SPL is to be determined and the value of the directivity index, DI, is assumed to be 5. The value 5 corresponds to the average DI at the angle of maximum noise for the various vehicles tested. The angle of maximum noise or directivity was not normalized; thus, the SPL calculated can only be assumed to be in the vicinity of 30 to 60 degrees from the inlet or exhaust of the vehicle. This range for the angle of maximum noise is a reasonable value based on the data given in Section Four. If a design is to be considered that is similar to one of the test vehicle configurations, a more realistic value for the angle of maximum noise may be determined from Section Four.

As an illustration of the procedure discussed, assume the following fan design parameters:

Outer diameter	D_T	= 40 inches
Inner diameter	D_H	= 30 inches
Weight flow	W	= 150 lb/sec
Stage temperature rise	ΔT	= 15°R

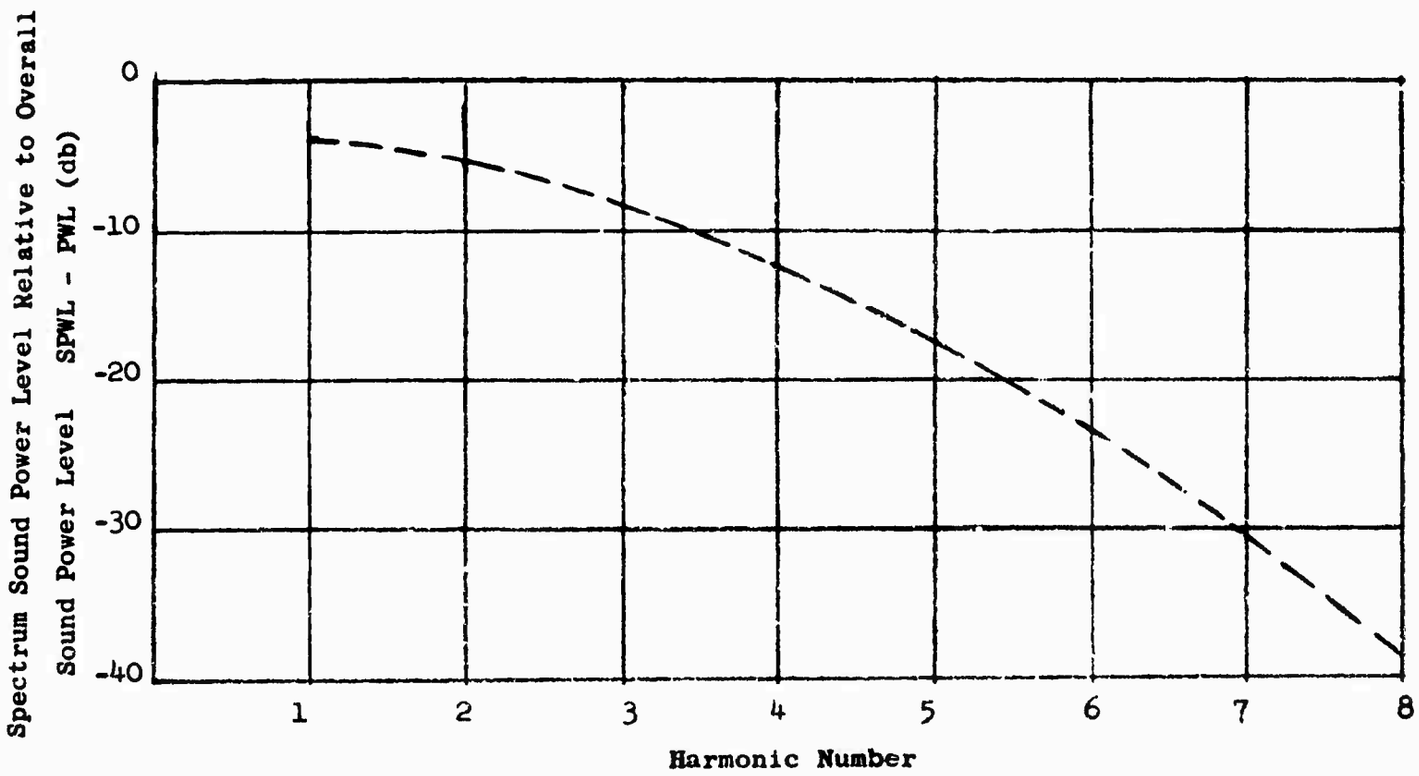

Figure 14 Normalized Power Spectrum of Compressor and Fan Noise.

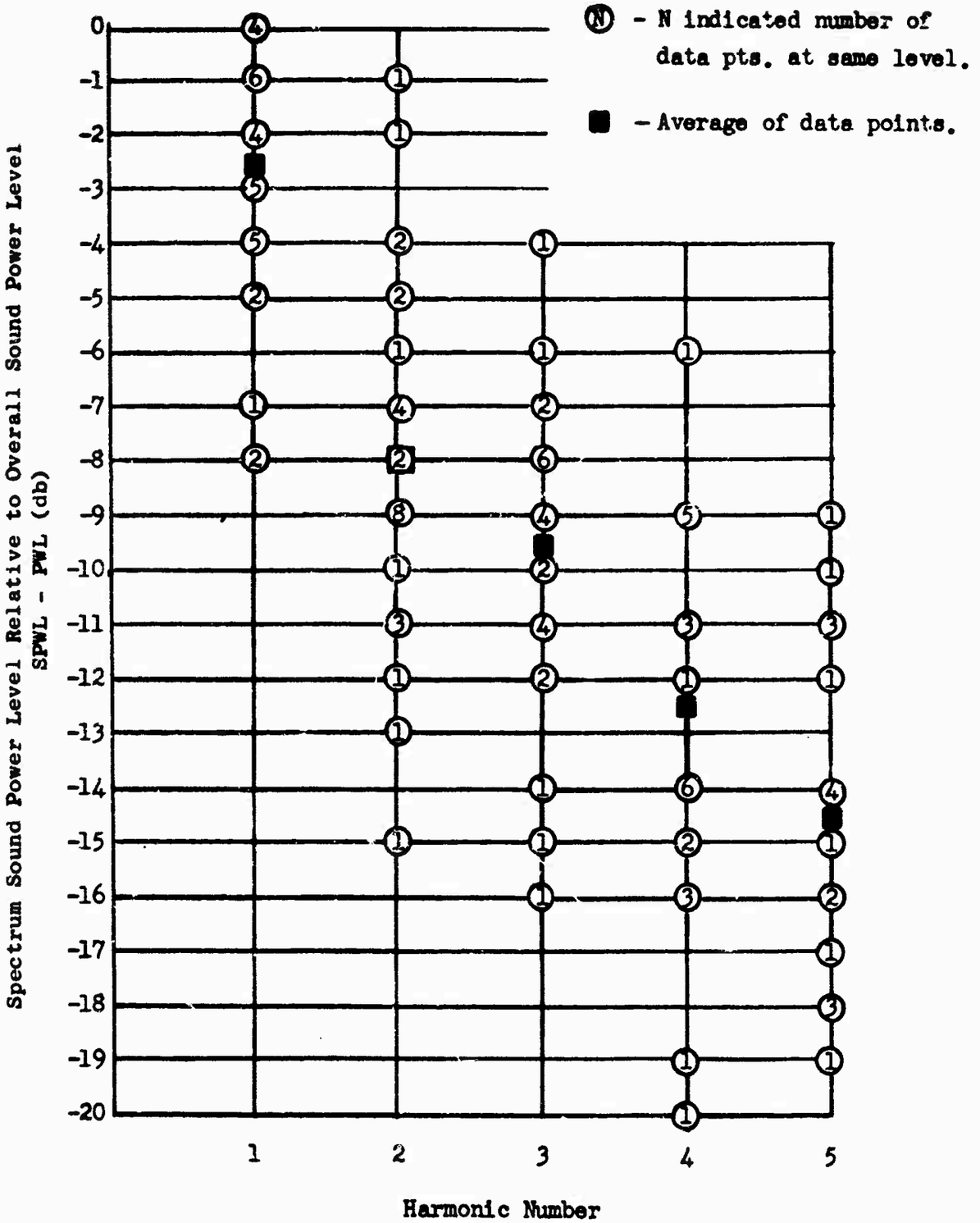

Figure 15. Accumulated Spectrum Sound Power Level Data

RPM	n = 5,000 RPM
Rotor blade no.	N = 54
Inlet temperature	T = 520°R

Calculate the following:

$$D_H/D_T = 30/40 = .75$$

$$(D_H/D_T)^2 = (.75)^2 = .562$$

$$A = \frac{\pi}{4} \times (D_T)^2 \left[1 - \frac{D_H^2}{D_T}\right] = \frac{\pi}{4} \times \left(\frac{40}{12}\right)^2 \left[1 - .562\right]$$

$$A_a = \frac{\pi}{4} \times 11.2 \times .438 = 3.86 \text{ ft}^2$$

$$T_T = T + \Delta T = 520°R + 15° = 535°R$$

H_T = Total Enthalpy = 128 $\frac{\text{Btu}}{\text{lb}}$ at 535°R (from gas tables)

$$E = \frac{H_T \times W}{A_a} = \frac{128 \times 150}{3.86} = 4.98 \times 10^3 \frac{\text{Btu}}{\text{sec-ft}^2}$$

From Figure 13, at $E = 4.98 \times 10^3 \frac{\text{Btu}}{\text{sec-ft}^2}$

$$PWL - 10 \log \frac{A_a n}{N_b} \left(\frac{D_H}{DT}\right)^2 = 133 \text{ db}$$

$$10 \log \frac{A_a n}{N_b} (D_H/D_T)^2 = 10 \log \frac{3.86 \times 8000}{54} \times .562 = 10 \log 322 = 10 \times 2.508 = 25$$

PWL = 133 + 25 = 158 db overall

Spectrum PWL, Figure 14:

First harmonic = PWL - 3.5 = 158 - 3.5 = 154.5 db

Second harmonic = PWL - 5.5 = 158 - 5.5 = 152.5 db

Sound pressure level at angle of maximum noise (assume a 100-foot radius):

$$SPL = PWL + DI - 20 \log r - 10.5$$

$$SPL = 158 + 5 - 20 \log 100 - 10.5$$

$$= 163 - 40 - 10.5 = 163 - 50.5$$

SPL = 112.5 db at 100 feet, angle of maximum noise

The above procedure allows a direct analysis of the acoustic performance of a development vehicle based on the fan design parameters. The question of installation effects, however, requires further analysis. Several installation parameters were investigated empirically: inlet length, exhaust duct length, centerbody shape, and exhaust louver vectoring.

The tests were made by varying the various parameters on the 26-inch-diameter VTOL scale model fans (reference Section Four, Table 1). Figures 16 through 19 show the results of these tests. The two centerbody configurations, Figure 16, showed no effect due to the throttling of the longer circular centerbody on the sound power distribution. If the circular centerbody was sufficiently large in diameter to block the flow, obviously a definite effect would be obtained. Three inlet lengths were tested: 4 inches, 9 inches, and 23.5 inches. Some data scatter is evident in Figure 17, but no definite trends are indicated to show an effect due to the varying inlet length. Figure 18 shows a comparison of two configurations with and without a 16-inch exit duct. The two configurations also vary in inlet length and centerbody, but the previous discussion allows a direct comparison. The data as shown on Figure 18 has some scatter, but no effect due to the long exit ducts may be concluded. Results of varying the exhaust louver angle with respect to the flow direction also showed data scatter, Figure 19, but again no definite trends were indicated. Thus, of all the parameters varied, it was generally concluded that no definite effect could be associated with installation characteristics excluding radical changes or those that varied the fan performance.

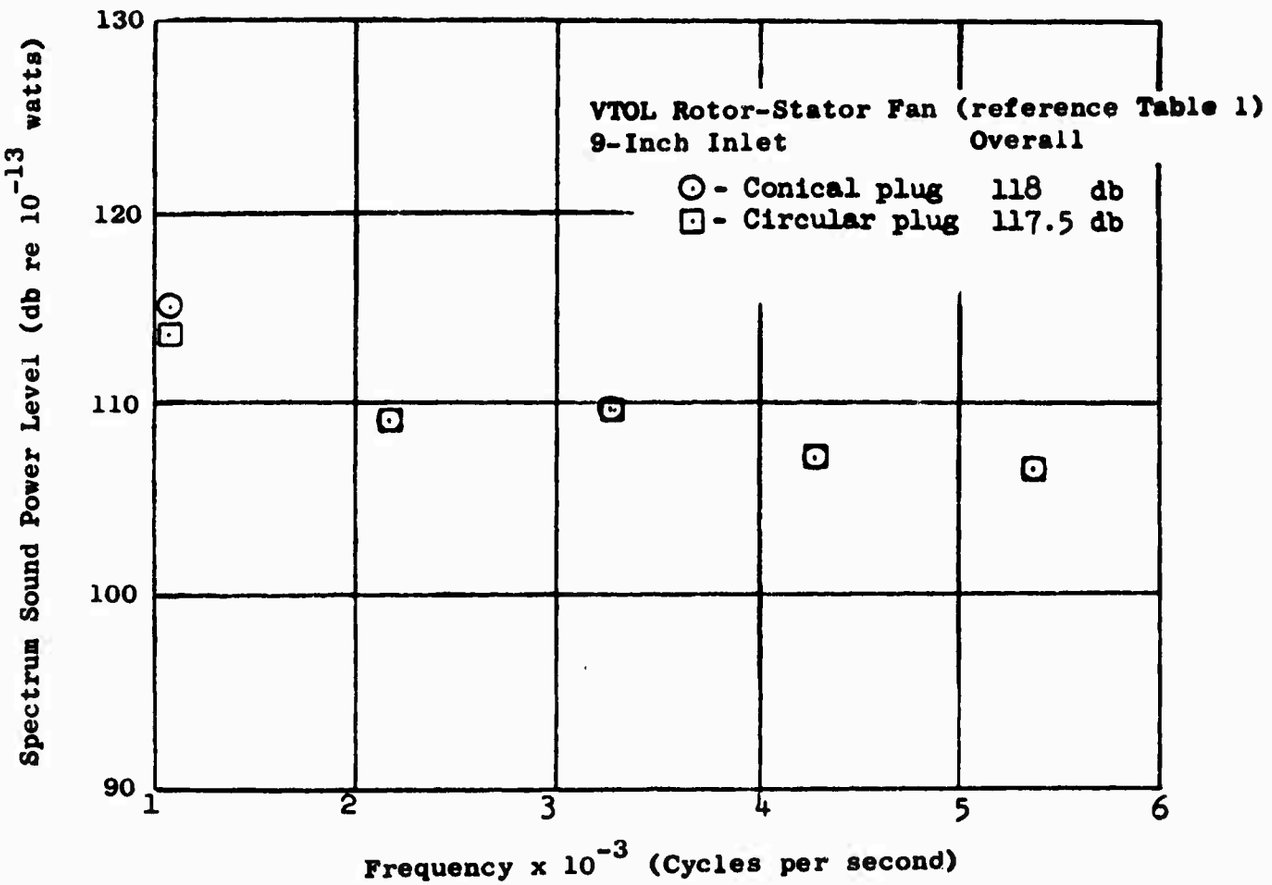

Figure 16. Spectrum Sound Power Level Variation with Exhaust Plug Design

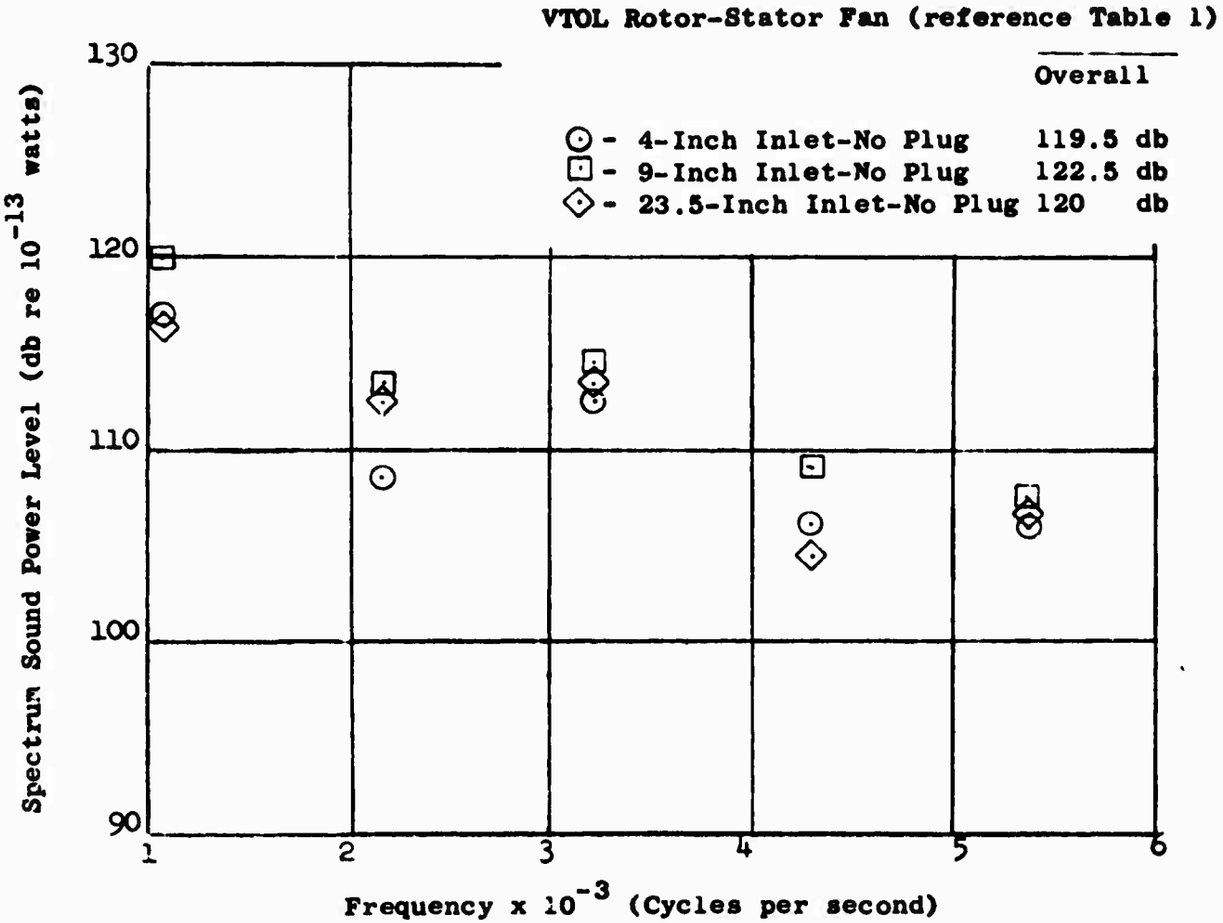

Figure 17. Spectrum Sound Power Level Variation with Inlet Duct Design.

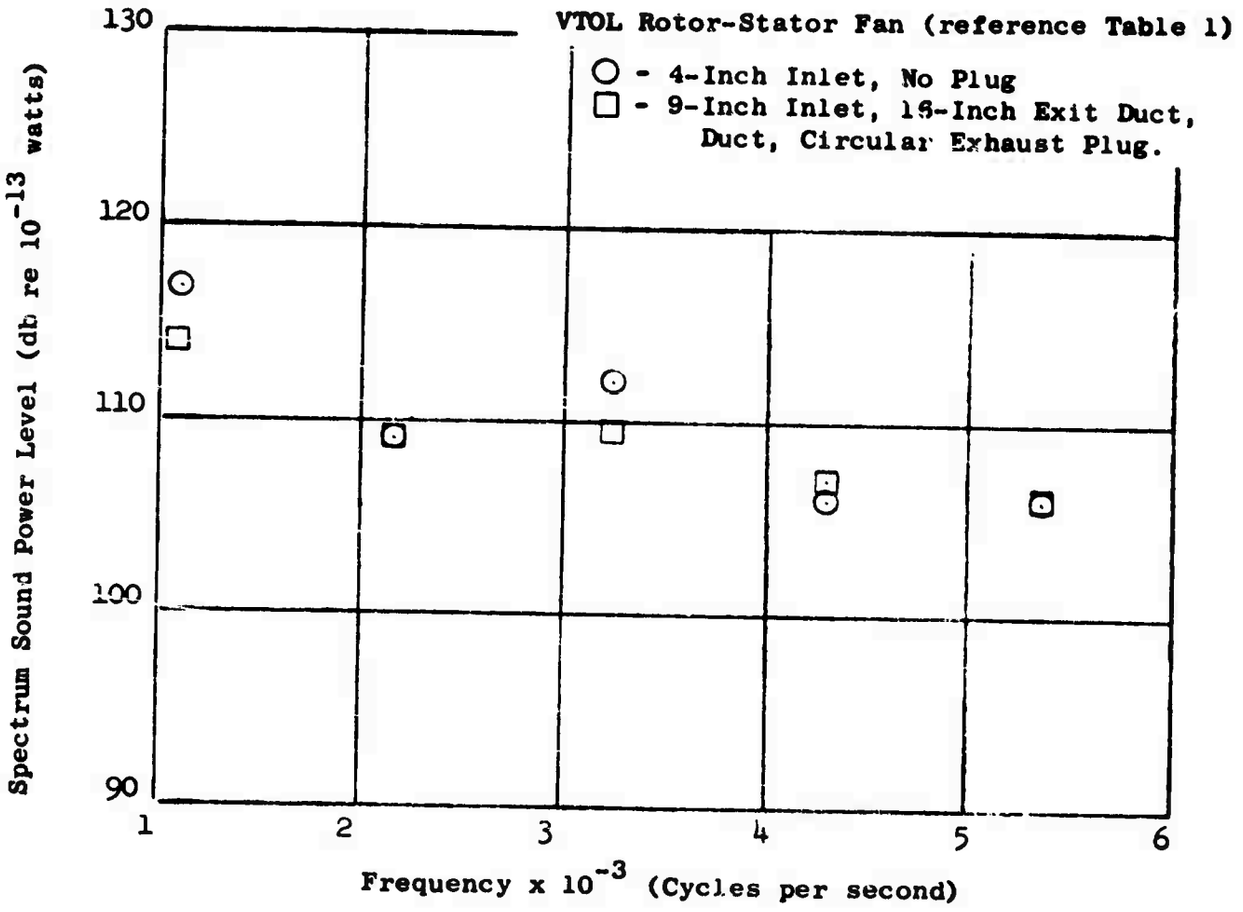

Figure 18. Spectrum Sound Power Level Variation with Exhaust Duct Design.

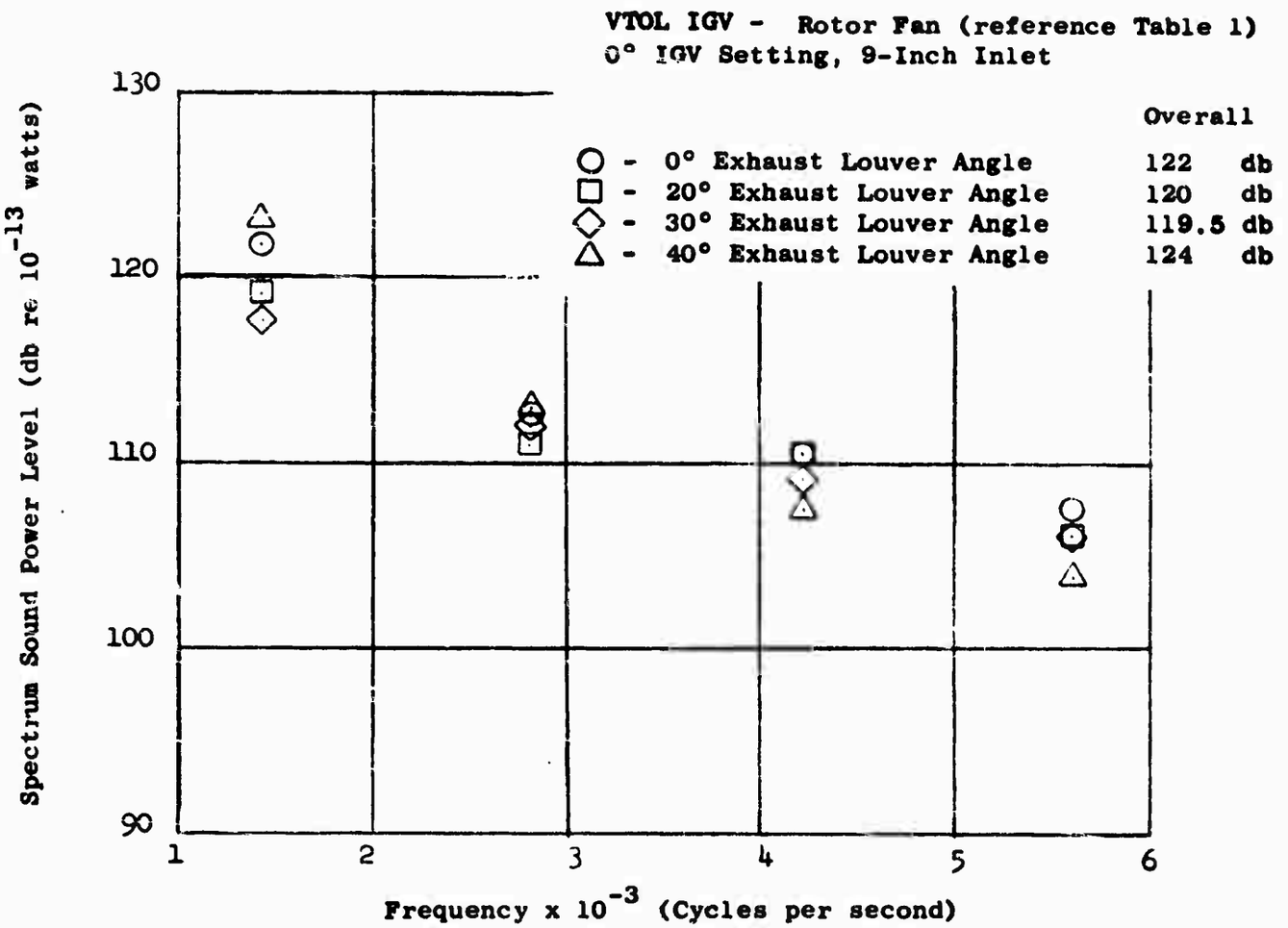

Figure 19. Spectrum Sound Power Level Variation with Exhaust Louver Vectoring Angle

SECTION THREE - NOISE MINIMIZATION AND SUPPRESSION

MINIMUM NOISE GENERATION PARAMETERS

Various design parameters are of particular interest when defining a new fan configuration for minimum noise generation. A basic design guide to be followed, at this point in the state of the art, is given by Figure 13, which was discussed in Section Two. This normalized power level curve shows that a large fan doing the same work as a smaller fan should be inherently quieter on an energy flux basis, but a small fan doing proportionally the same work as a large fan may generate nearly the same amount of noise. For fans of a given power requirement, the parameter

$$10 \log \frac{A_a \; n \; (D_H/D_T)^2}{N_r}$$

may be evaluated to determine qualitatively the proper design approach. Factors in the numerator of the normalizing function, A_a, n, and $(D_H/D_T)^2$, should be minimized. The area, A_a, also appears in the energy flux term, the abscissa of the curve. Thus, if the area is varied, the amount of work done by the fan must be varied to maintain constant energy flux; but this requires that the fan performance requirement be redefined. The factor n, or RPM, shows that the work, if done at a slower speed, will generate less noise, which is consistent with propellor theory. The term $(D_H/D_T)^2$, hub-tip ratio squared, is a measure of the radial distribution of the blade loading. The higher D_H/D_T terms are representative of a short blade; thus, for the same number of blades and the same work, they have a higher blade loading. With the lower D_H/D_T terms is associated a smaller blade loading on the same basis. The denominator, N_r, blade number, has the same correlation as D_H/D_T, in that the higher blade number for the same fan power indicates a lower blade loading and obviously the smaller blade number indicates a higher blade loading. This, too, is consistent with propellor theory. Utilization of the normalized power curve in the above manner could provide at least a guide in defining the most optimum configuration acoustically. In particular, designs that are near the knee of the curve, energy flux values up to

$$3 \times 10^3 \; \frac{\text{Btu}}{\text{sec - ft}^2}$$

could benefit appreciably from proper design.

One of the common characteristics of all the various fan and compressor designs shown on Figure 13 is the relatively close rotor - stator spacing. This spacing has a definite effect on the noise generated by the fan, as discussed in Section One. Several tests were made on the scale model fan configurations to define the amount of noise reduction obtained by increasing the rotor - stator gap. Obviously the case of a lone rotor is the maximum amount of noise reduction that can be obtained through this particular design parameter variation. Figure 20 shows the results of these tests in terms of power level variation with axial rotor - stator spacing. The extreme variation in maximum reduction obtained without a stator row indicates that more data must be obtained to determine how much interference is required to produce the high sound pressure levels. For instance, even with the stators removed, there may be a disturbance between the rotor and some discontinuity in the surface of the stator row or perhaps a disturbance between a downstream or upstream strut that is significant.

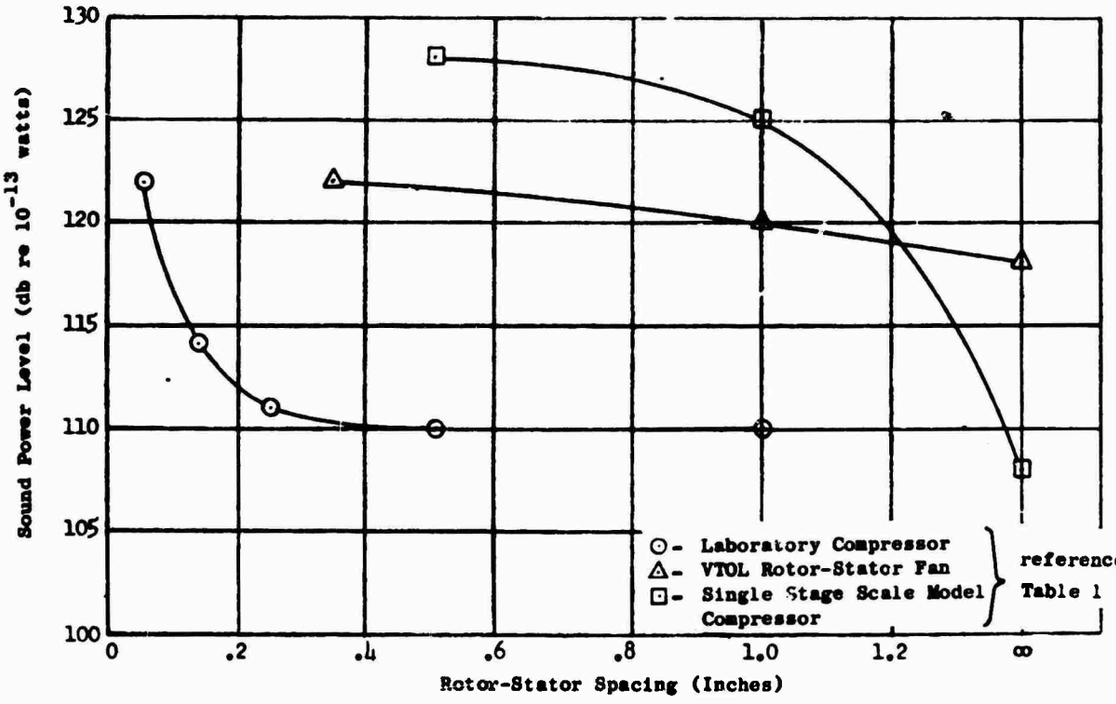

Figure 20. Variation in Sound Power Level with Rotor-Stator Axial Spacing.

A design parameter of considerable interest is the blade passing frequency of the fan, the product of the number of rotor blades and the RPM. If this frequency is put beyond the audible range through high blade numbers and/or high RPM, obviously the result would be a quiet fan. Investigation of this approach was beyond the scope of the research investigation, but should be kept in mind as a possible means of eliminating noise.

NOISE SUPPRESSION SCHEMES

Three suppression schemes were evaluated on an engineering assessment basis: deflection methods, wave cancellation, and absorptive suppression. Of the three methods assessed, one, absorptive suppression, was selected for further evaluation and was demonstrated on a scale model fan configuration.

DEFLECTION METHODS

The concept of altering the directivity pattern of a particular fan configuration to minimize noise in specified areas was assessed qualitatively as being unrealistic under actual operating conditions.

The tests described in Section Two, in which various installation characteristics were investigated, showed no consistent effect on the directivity patterns, while results of Section One point out the irregularity of directivity patterns for the same design and the difficulty in prediction of directivity. The control of these directivity patterns would require a major effort in acoustical design for each operating condition and fan configuration. As additional information is obtained with regard to the basic noise generating mechanism of fans and as an accurate representation of the sound field being produced by the rotor is defined, control or prediction of the directivity patterns will become more realistic.

WAVE CANCELLATION

The pure-tone characteristics of the fan noise allows an analysis to be made, assuming a sinusoidal wave shape, that shows considerable reduction in level obtained by varying the phase of two signals being radiated from adjacent sources. Figure 21 shows the relative amplitude of the addition of two signals as a function of the phase shift between them. Obviously, a 180-degree phase shift produces total cancellation; however, with a shift of approximately 115 degrees, a reduction in amplitude of 50 percent is obtained that would provide a notable reduction in noise level. The phase shift obtained between two signals

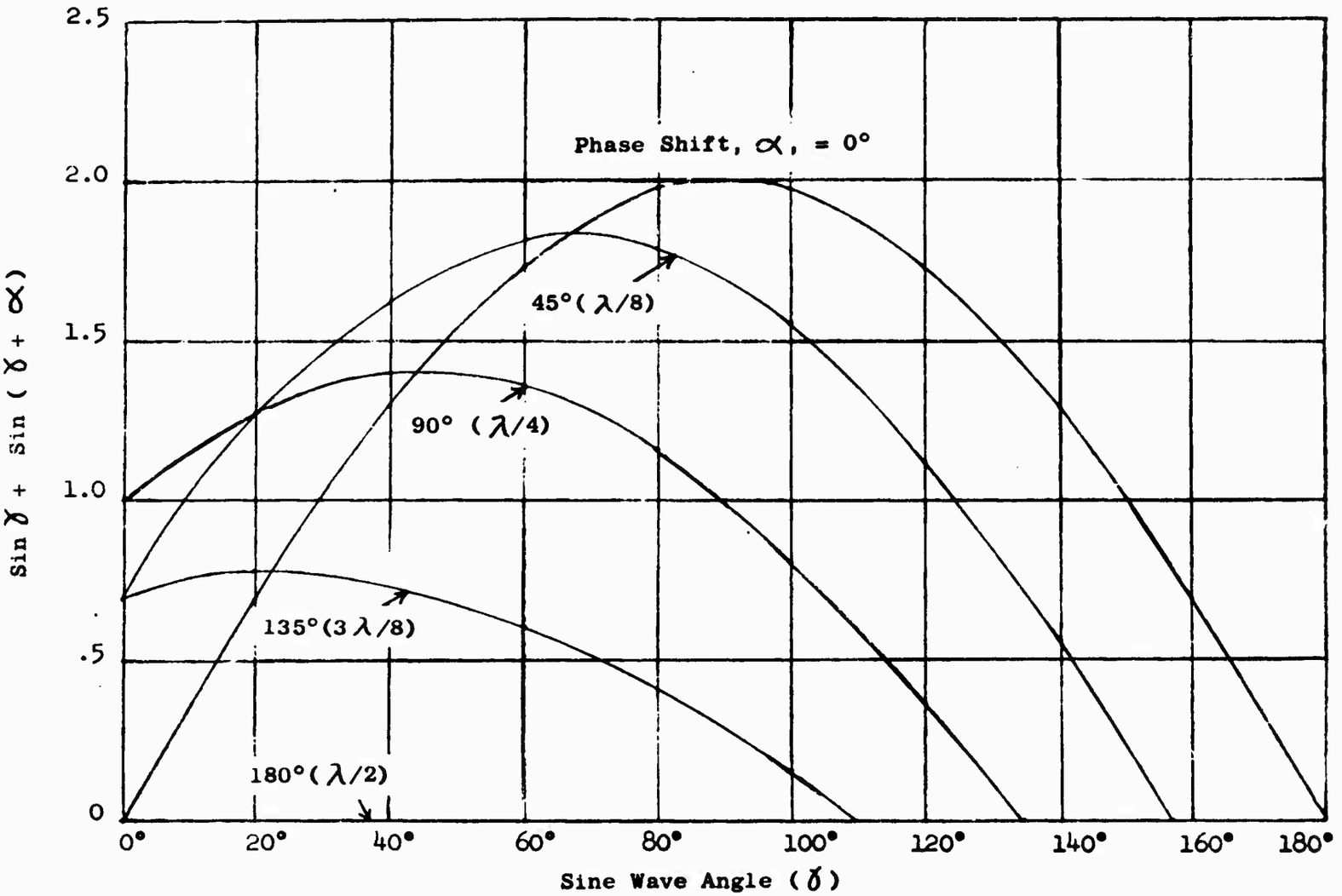

Figure 21. Relative Amplitude vs. Angle for Various Phase Shifts. Variation in Wave Amplitude vs Phase Shift for the Addition of Two Sine Waves.

may be analyzed as a function of the distance ,L, traveled by the two waves to the point at which they interact. Figure 22 is a resultant plot of this type of analysis showing the difference in distance, Δ L, versus frequency for various degrees of phase shift.

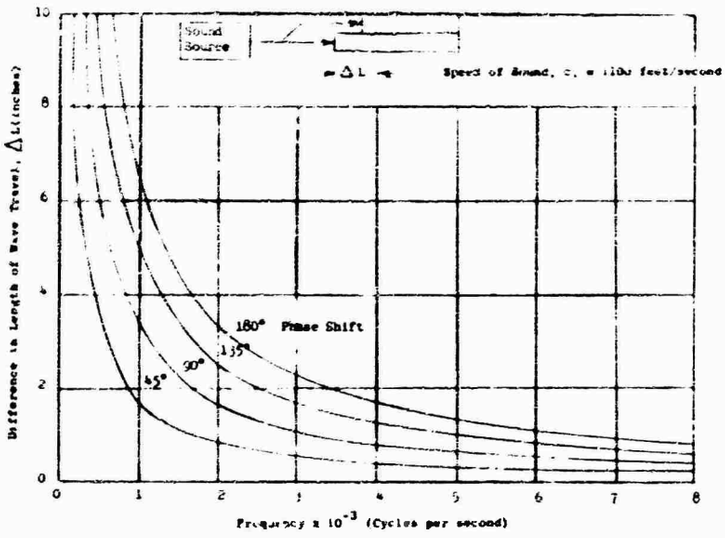

Figure 22. Correlation of Length of Wave Travel, Frequency, and Phase Shift for Sine Wave Interaction.

Tests were conducted on a system of this type, as shown in Figures 23 and 24. Microphones 1 and 2 were used to determine phase shift, while microphone 3 was used to determine the db reduction. The results are shown in Figure 25 in terms of the Δ db obtained and phase shift as compared to the theoretical reduction. The data were consistent and showed that reduction could be obtained over the local area of interference between the microphones; however, measurements made at various distances from 10 feet to 1 foot away from the tubes did not show reduction. In these laboratory tests, the phase shift was obtained by varying the distance of the source from the plane of emission, but in an actual application this is not practical; thus, the phase shift must be obtained aerodynamically. This may be done by designing alternate diffusing and converging passages for the flow, thus varying the velocity at which the signal passes through each section. At the same frequency and a different velocity, the wave length varies; thus, a phase shift is obtained. The system used for demonstration is shown in Figures 26 and 27. This flow passage was designed for a 180-degree phase shift at an inlet Mach number of .30 and a source of .1670 cycle per second, c/s.

These figures were based on the following relationships for the two passages:

$$f = \frac{1}{2\Delta t} \qquad \text{at 180 degrees phase shift}$$

and

$$t = \frac{L}{\bar{V}_1} - \frac{L}{\bar{V}_2}$$

where

f = frequency, c/s

Δt = time difference, sec

t = time, sec

L = length of travel, ft

$\bar{V}_1$ = average velocity through diffusing passage, ft/sec

$\bar{V}_2$ = average velocity through converging passage, ft/sec

No substantial data was obtained with this system due to instability of the air flow through the passages, the difficulties in maintaining a signal that could be effectively changed in wave length, and reflections of the signal from the walls of the flow passage sufficient to affect the wave length variations.

The conclusion drawn from the tests was that the wave cancellation technique would require excessive aerodynamic design and alteration of the fan design, such as "egg-crating" the exhaust to provide significant noise reduction.

ABSORPTIVE SUPPRESSION

The use of acoustical material to suppress fan whine had been demonstrated previously in the development of an absorptive suppressor for the CJ805-23 aft fan engine, reference Table 1. This suppressor consisted of a fiberglass-type material covered with a fine mesh screen and perforated metal and located on the inner diameter of the fan exhaust passage. The suppression obtained was quite significant, particularly on a Δ db per linear length of suppressor basis, being approximately 1 db suppression per inch. This type of design is applicable to inlet and outlet guide vane modification as well as flow passage applications, assuming that this same suppression rate may be maintained or improved. This method of suppression was chosen for further investigation and for demonstration on a scale model fan configuration.

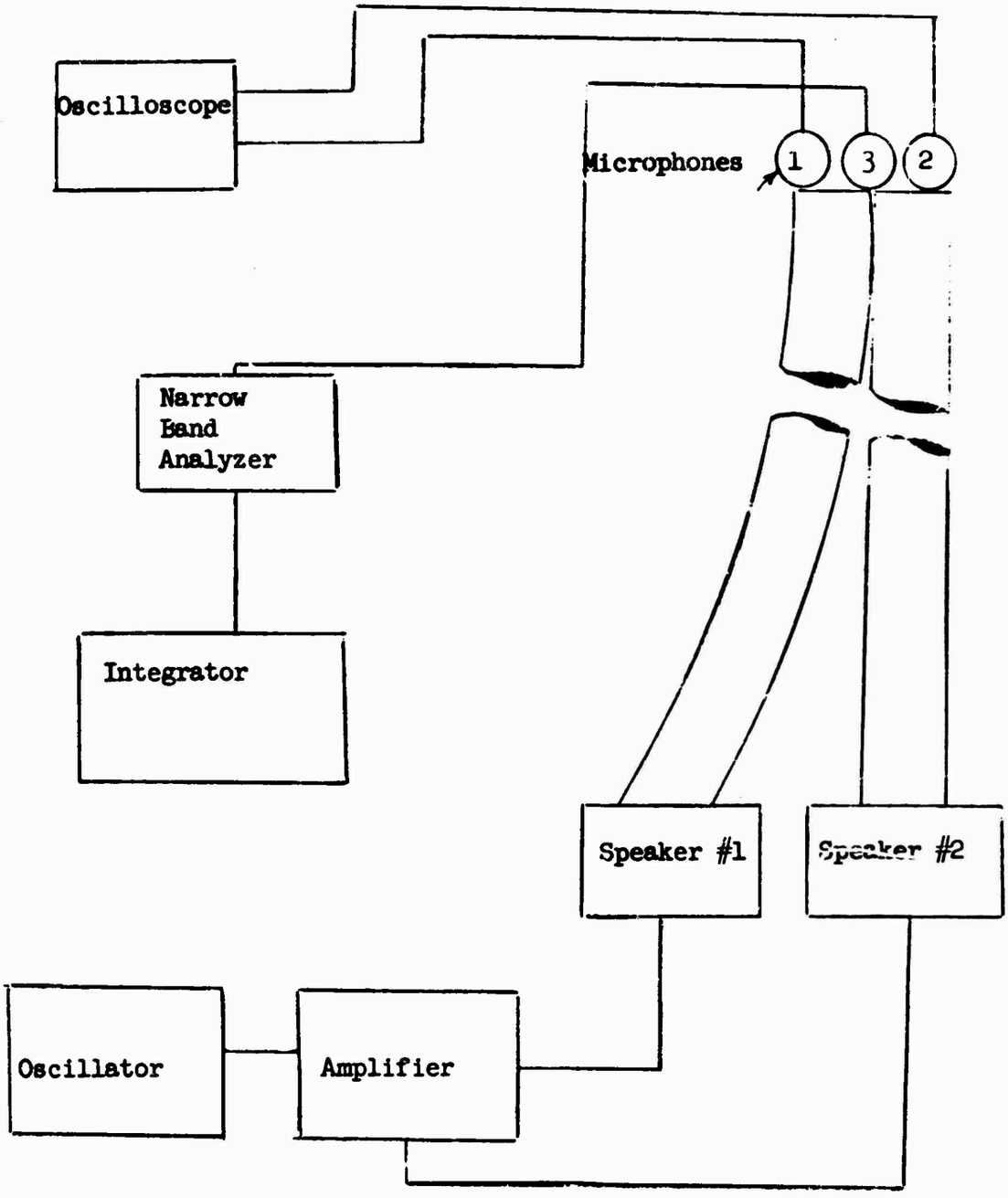

Figure 23. Schematic of Wave Cancellation Test Instrumentation.

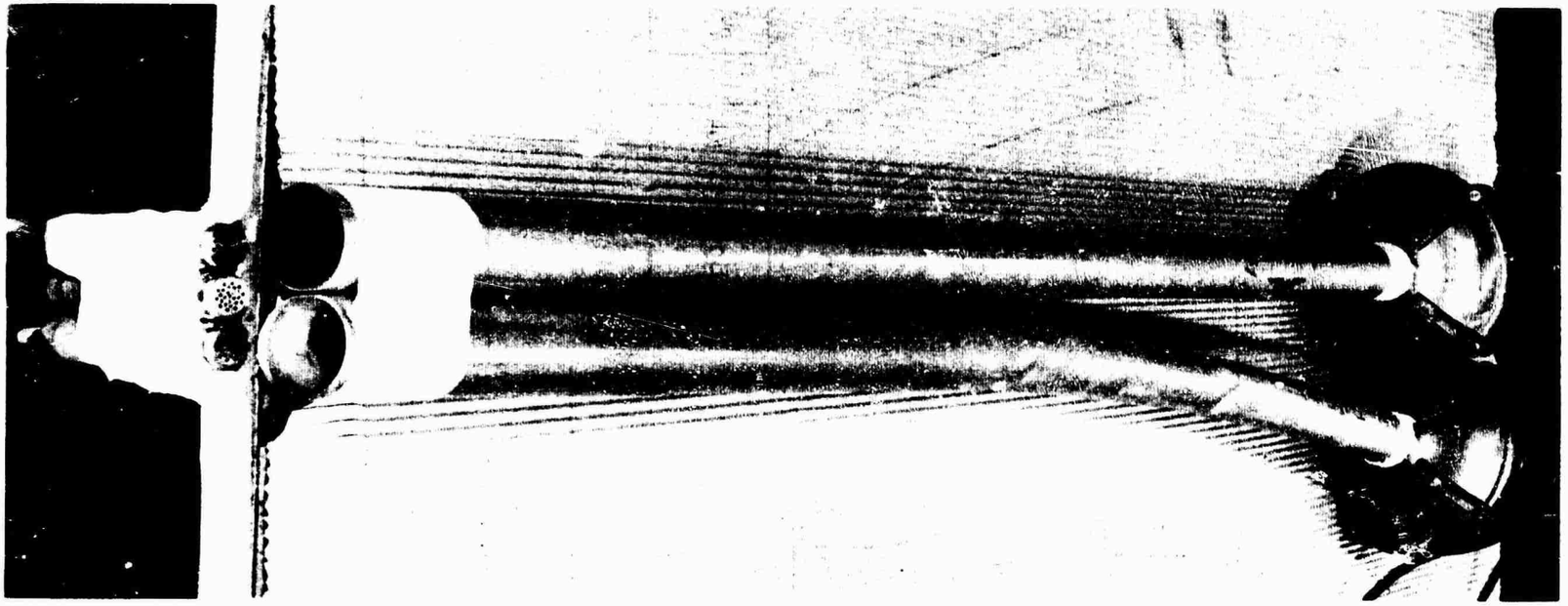

Figure 24. Arrangement of Sound Wave Passages and Microphones for Wave Cancellation Investigation.

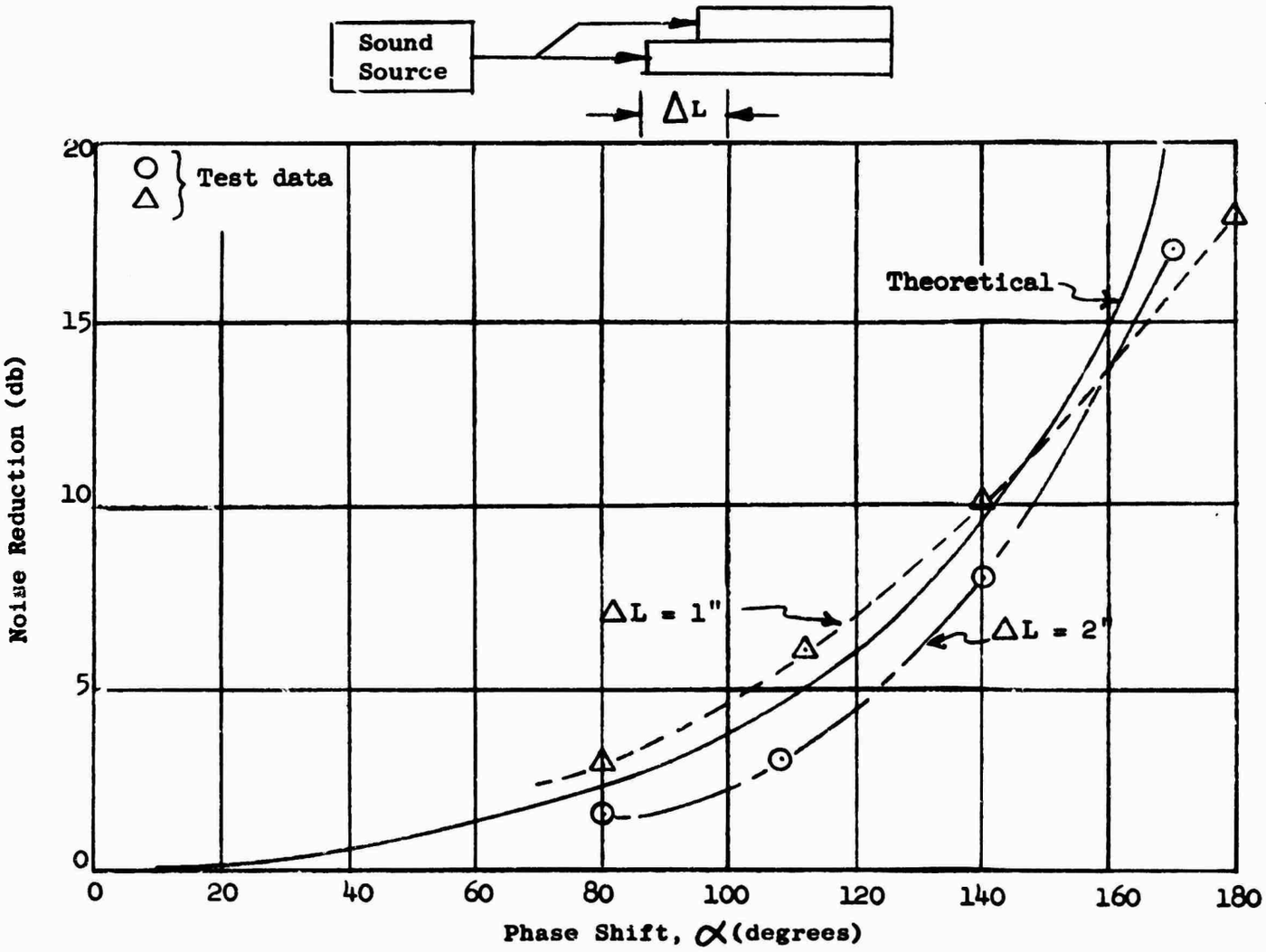

Figure 25. Noise Cancellation Obtained by Varying the Length of Wave Travel.

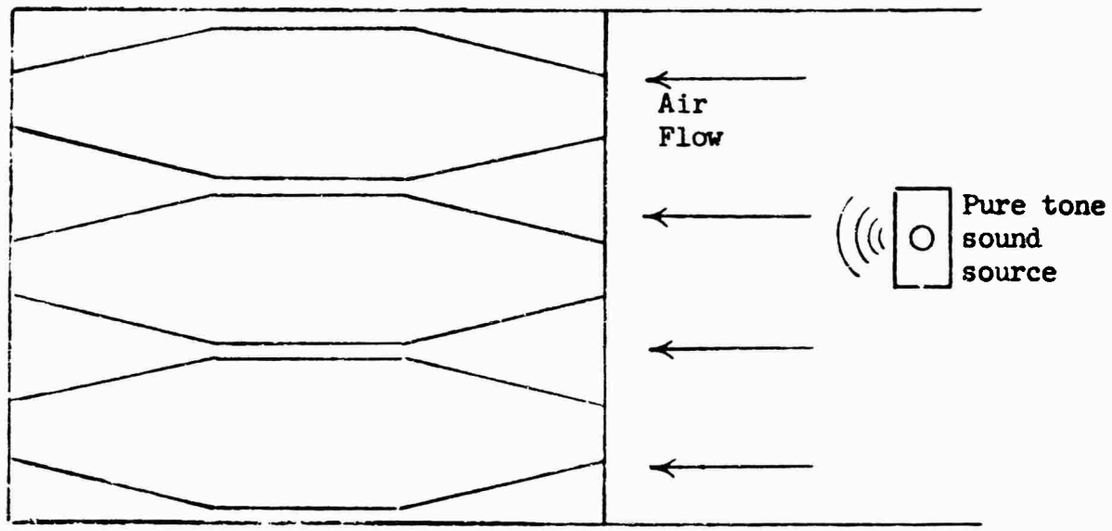

Figure 26. Schematic of Wave Cancellation Test Rig with Air Flow.

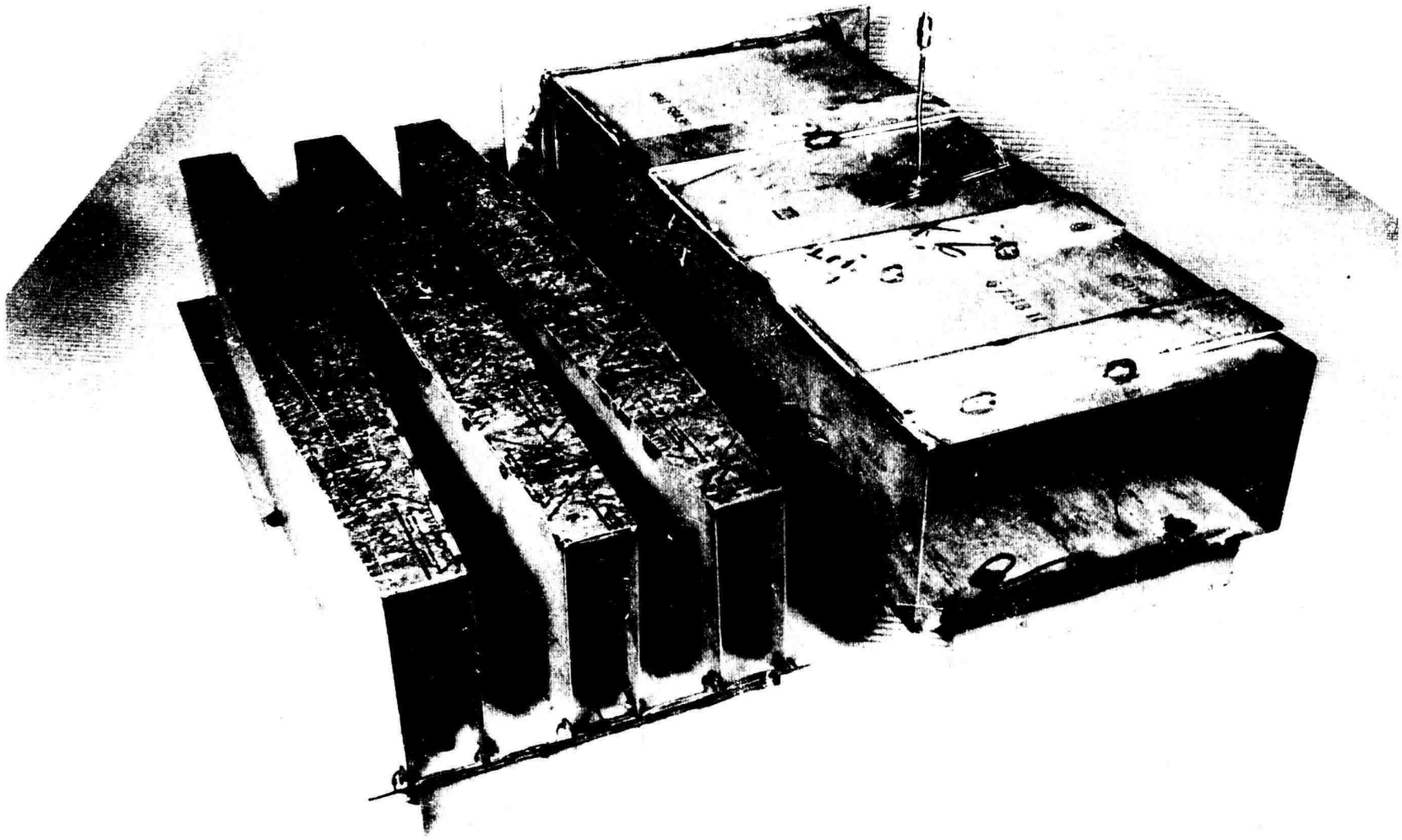

Figure 27.1 Flow Ducts for Wave Cancellation Evaluation.

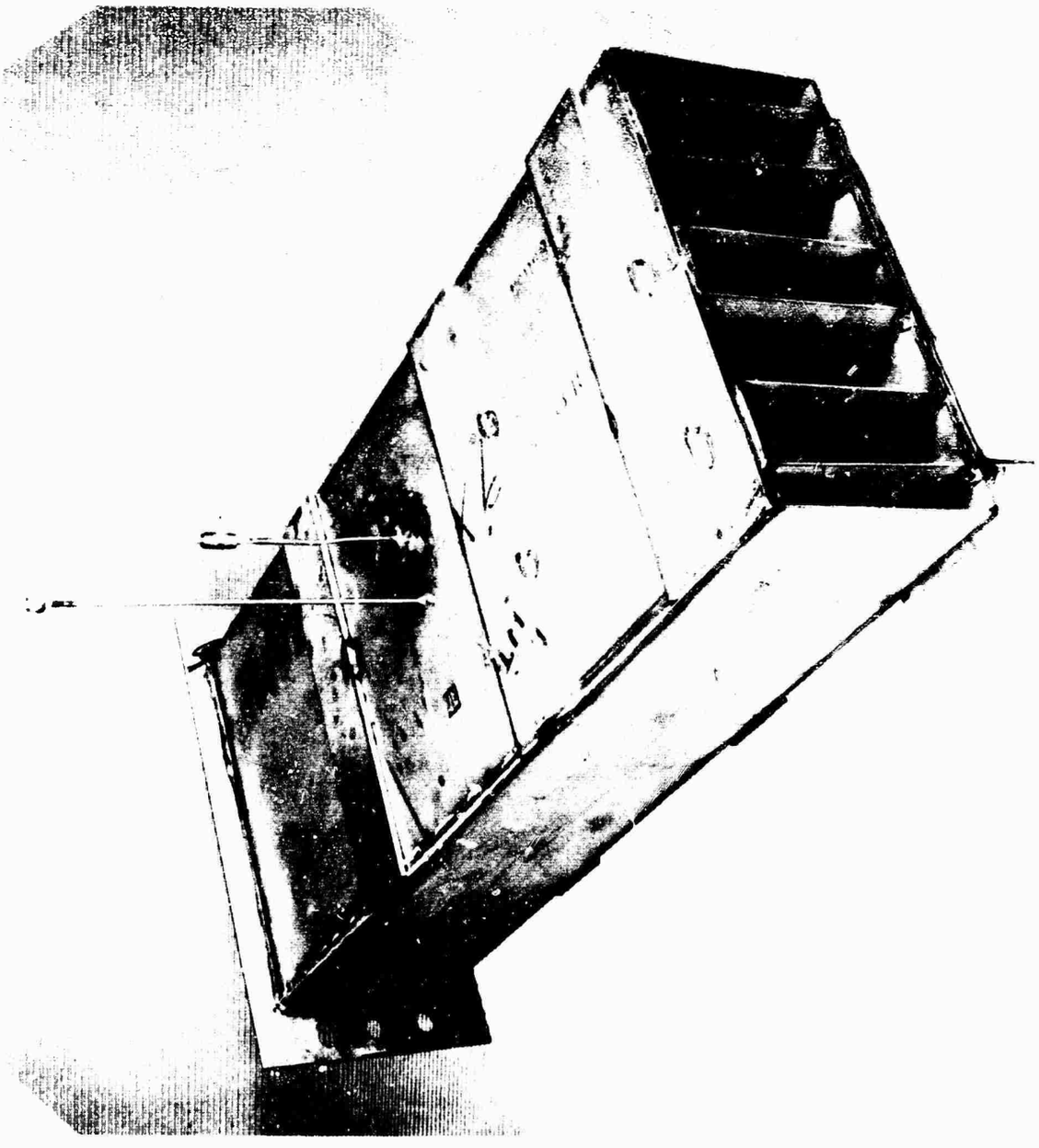

Figure 27.2 Flow Duct for Wave Cancellation Evaluation.

ABSORPTIVE SUPPRESSOR DESIGN

Absorptive suppression lends itself to several areas of physical application: outlet guide vanes, OGV, inlet guide vanes, IGV, flow passages, and, as in the case of an "in-wing" lift fan device, exhaust vectoring louvers. This latter area was chosen for design of an absorptive suppressor, as it could have a direct application to development vehicles and was readily adaptable to the VTOL scale model rotor-stator fan with exhaust louvers, Figure 28.

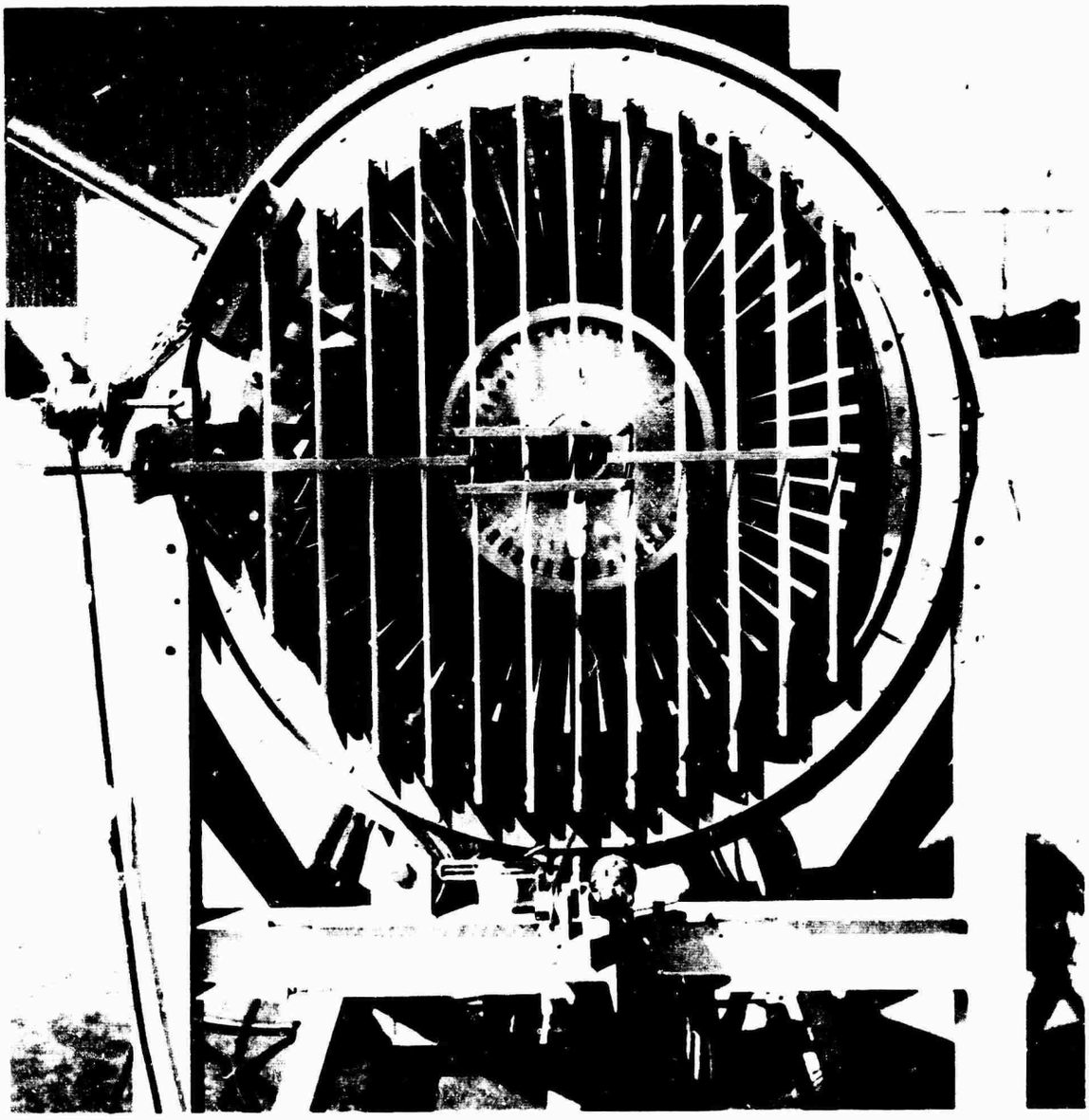

Figure 28. Exhaust Vectoring Louvers.

DESIGN METHOD

Absorptive suppressors can be designed readily by using a procedure as outlined in reference 9, page 243. The procedure utilizes a design curve shown schematically in Figure 29. The design parameters are passage width, l_x, thickness of material, t, percent open area (which are interrelated), and frequency. By varying these parameters, a specific flow resistance, R_1, can be determined for the thickness of material; and from this data the proper material can be selected by using a curve similar to Figure 30. This general outline of the procedure gives some insight into the problem of applying this type of design to a passage where there is air flow. If the aerodynamic performance is to be maintained, the proper flow conditions must be kept; but they are in general a function of the passage width, length, and percent open area. Thus, a compromise between aerodynamic and acoustical design must be made.

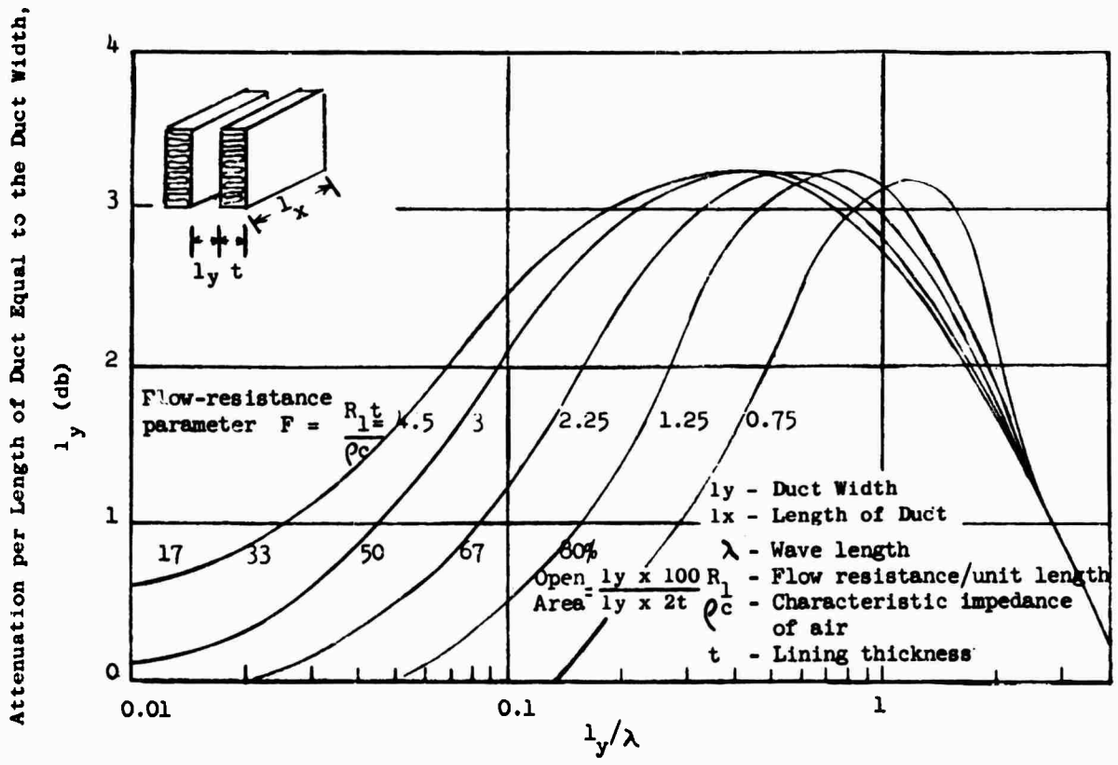

Figure 29. Design Chart for Acoustically Treated Ducts Lined on Two Sides.

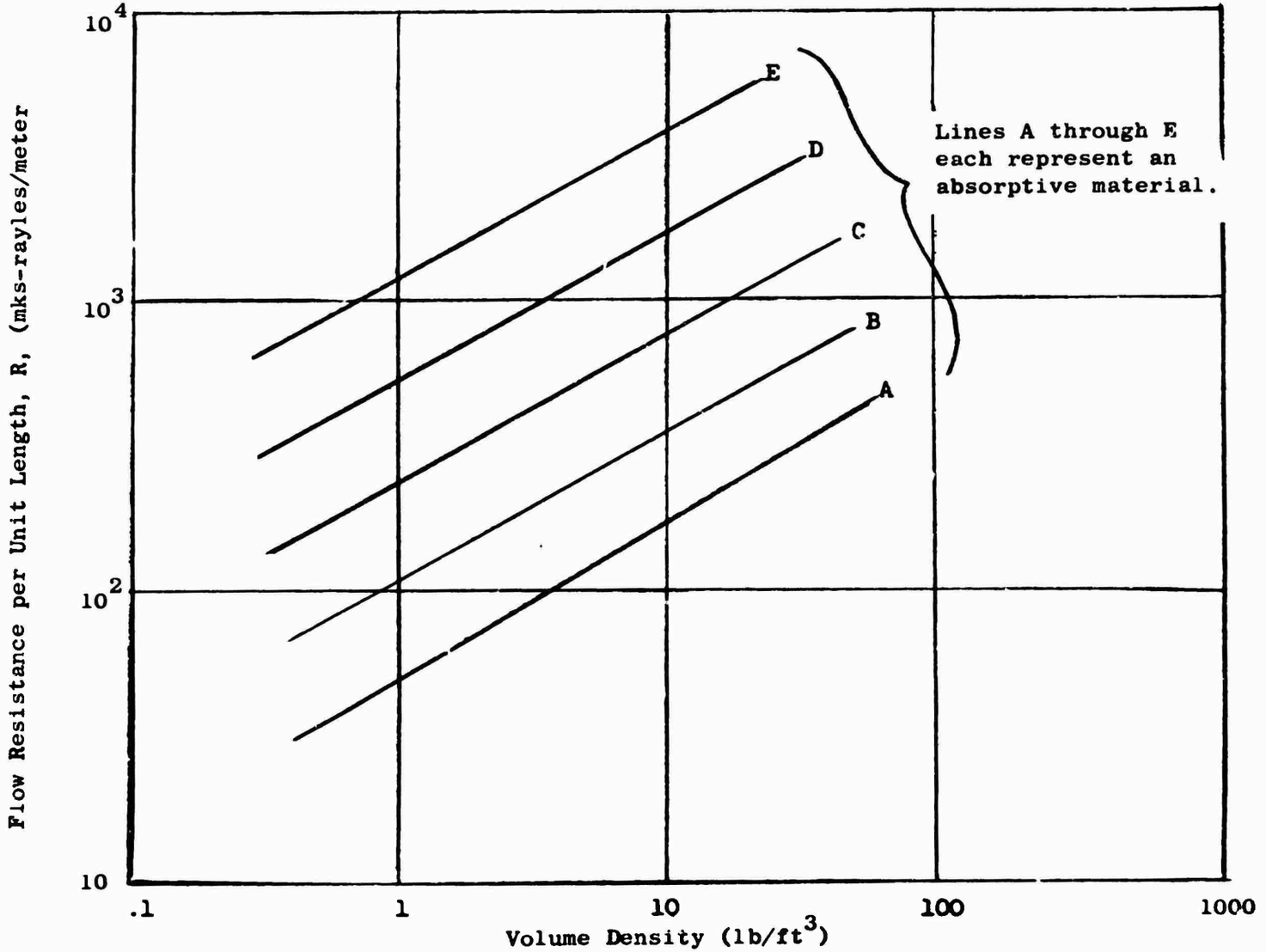

Figure 30. Schematic of Design Chart for Selection of Absorptive Material.

For fans and compressors, a basic design parameter for stator blades is (reference Figure 31):

$$\frac{c}{A_2} = \left[\frac{\sigma}{AR \cos \beta_2}\right]^{\frac{1}{2}} = \left[\frac{c/s}{h/c \cos \beta_2}\right]^{\frac{1}{2}}$$

where

β_2 = flow angle out of blades

c = chord length

A_2 = flow passage area between blades at stage exit

σ = solidity = $\frac{\text{chord length}}{\text{blade spacing}} = \frac{c}{s}$

AR = aspect ratio = $\frac{\text{blade height}}{\text{chord length}} = \frac{h}{c}$.

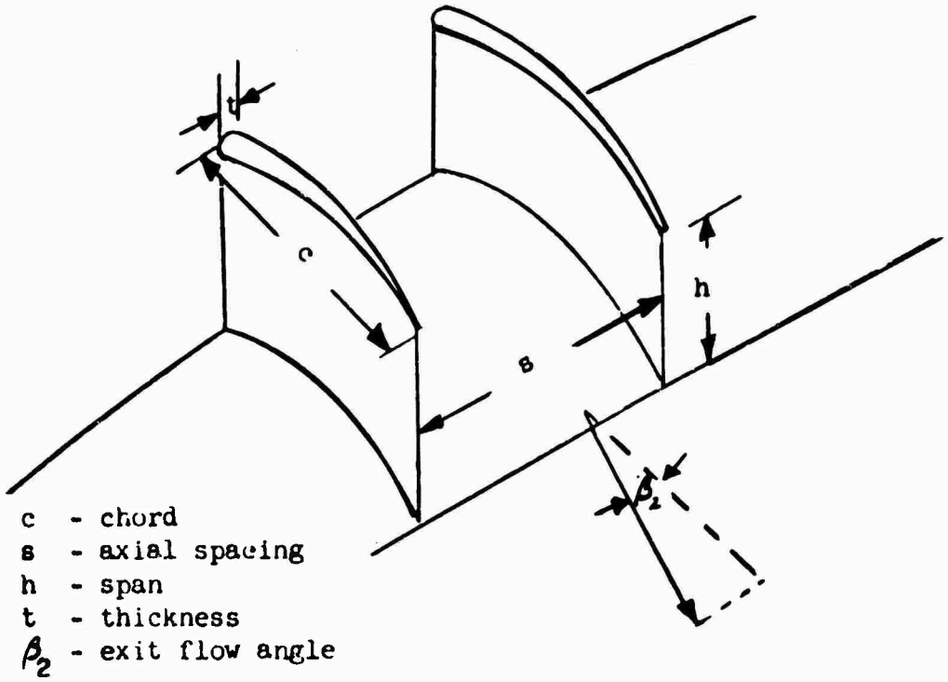

c - chord
s - axial spacing
h - span
t - thickness
β_2 - exit flow angle

Figure 31. Schematic of Compressor Blade Design Parameters.

Obviously, as the blade thickness, t, is varied for addition of absorptive material, the chord, c, must also be varied to maintain the thickness ratio, t/c, and to provide sufficient length for ample suppression. With a varying chord length, the above parameter must also be adjusted. Generally, c is increased; thus, since blade height, h, is predetermined, the spacing, s, must be increased to maintain c/hs a constant. When s is increased, the proper percent open area,

$$\frac{t}{s} \times 100,$$

must be maintained to satisfy the acoustical design parameters. This type of design procedure becomes difficult when a low-frequency signal is being attenuated in a small passage, since the material thickness is in general large for low-frequency suppression and the small open area is affected to a large degree by the increased blade thickness.

For the application of absorptive material to the exhaust louvers of the scale model fan configuration, the fundamental frequency was too low to provide a realistic louver configuration due to the large material thickness required. To demonstrate a suppressor properly, the desig was made to suppress the higher harmonics of the fan which would correspond to the fundamental frequency of a full scale vehicle. The design as made on this basis would also be of the same general physical configuration as would be required by a full scale vehicle. The absorptive louver design is shown in Figure 32, and as mounted on the scale model fan in Figure 35. The design calculations are given in Appendix VI.

TEST RESULTS

The absorptive louvers were tested initially in a reverberation room environment without air flow. The louvers were attached to a large plenum, Figure 33; by using a loudspeaker and random noise generator as a sound source, the signal was measured for the standard louver case. The tests were then repeated for the treated louver case. The results are shown in Figure 34 as a function of the SPL reduction obtained. Also shown on Figure 34 is the design suppression. The results were within two db of the predicted suppression at the maximum suppression point.

The louvers, treated and standard, were next tested in a free field environment, Figure 35, using the scale model rotor - stator fan to determine the effect of air flow. The effect of air flow on the suppression characteristics of absorptive suppressors is generally to reduce the peak suppression by 25 percent and to shift the point of maximum suppression to a higher frequency (reference 17, page 4). The test data, Figure 34, in terms of pressure level reduction indicated approximately a 35 percent reduction in suppression and a shift in the

maximum suppression point to a lower frequency. The shift to a lower frequency was not expected and is not explainable in terms of the characteristics of absorptive material. The results show a very effective reduction in noise level for the design, and the maximum suppression occurs in a region that would correspond to the fundamental frequency of a full scale vehicle. The variation in the radiated sound pressure due to the absorptive suppressor is shown in Figures 36.1 through 36.3 for the first 5 harmonics. As would be expected, the largest suppression occurs on the exhaust side of the fan.

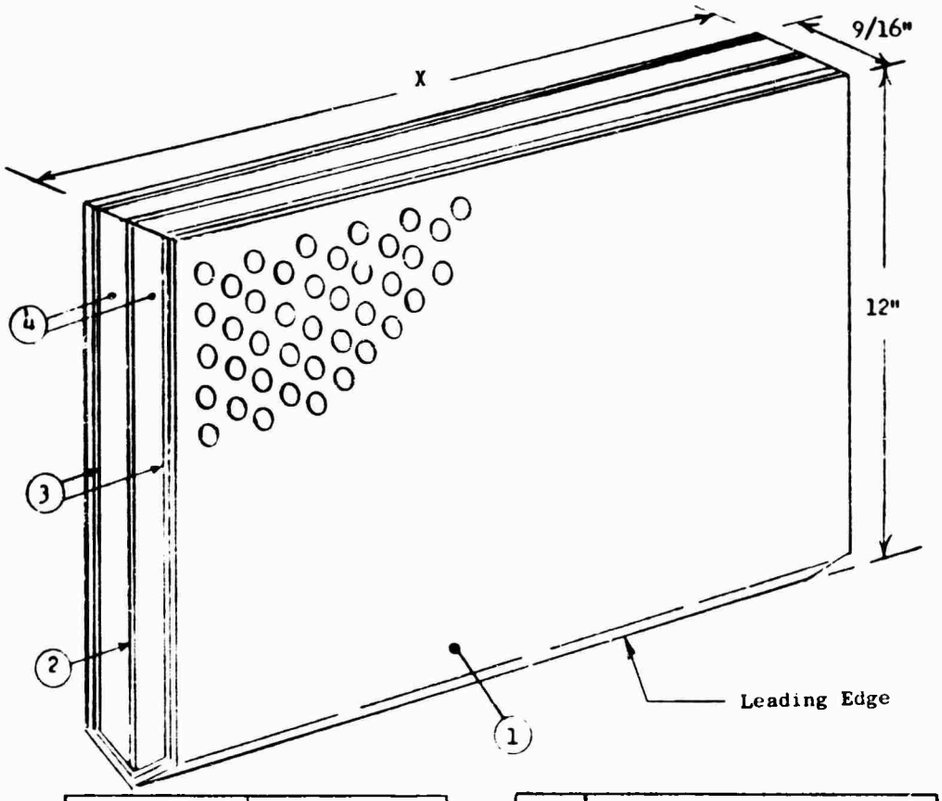

No. Louvers Required for Fan	X Dimension, in. (Reference Figure 35)
3	19
2	24
2	27
3	29

No.	Description
1	Perforated Metal, 20 Ga. 1/4" holes on 3/8" centers.
2	Flat Sheet, 1/32" thick.
3	.0045 Wire Screen, 80 mesh.
4	Absorptive Material, $\rho = 4 lb/ft^3$; $R_1 = 1.5 \times 10^5 \frac{mks\ rayles}{meter}$

Figure 32. Absorptive Louver Design for Rotor-Stator Fan (reference Table 1).

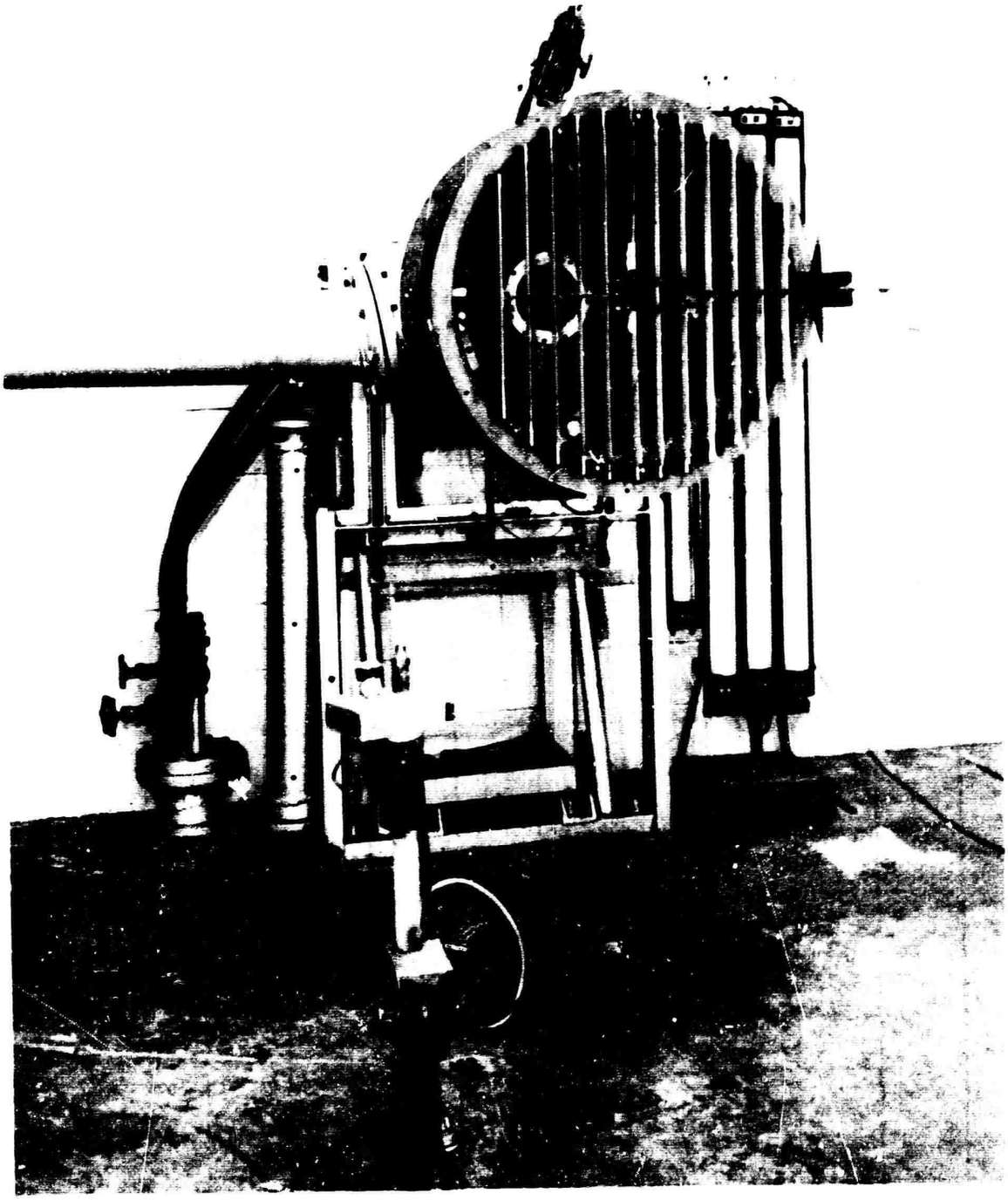

Figure 33. Exhaust Vectoring Louvers on Reverberation Room Plenum.

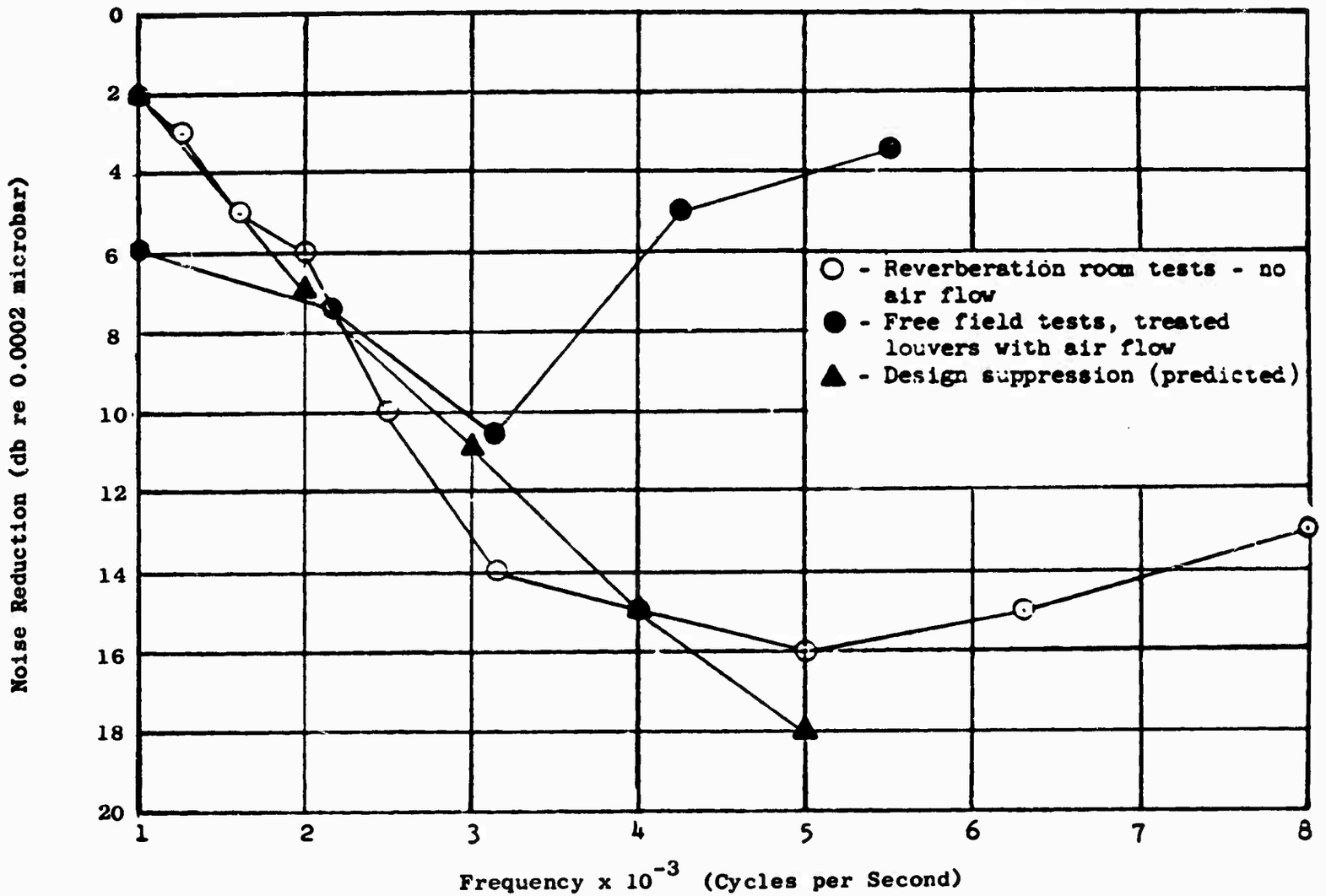

Figure 34. Noise Reduction of Acoustically Treated Louvers.

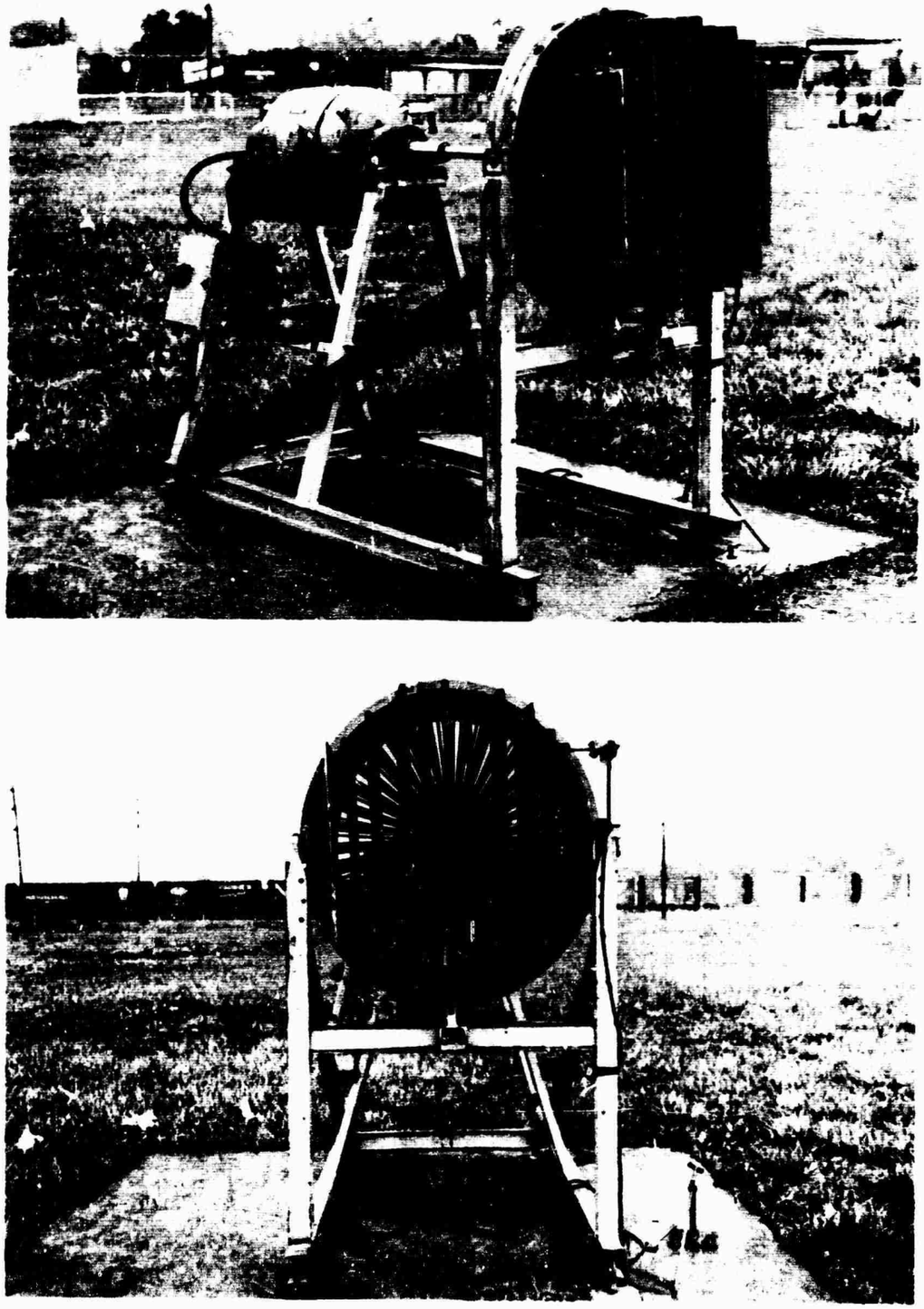

Figure 35. Rotor-Stator Fan with Treated Louvers.

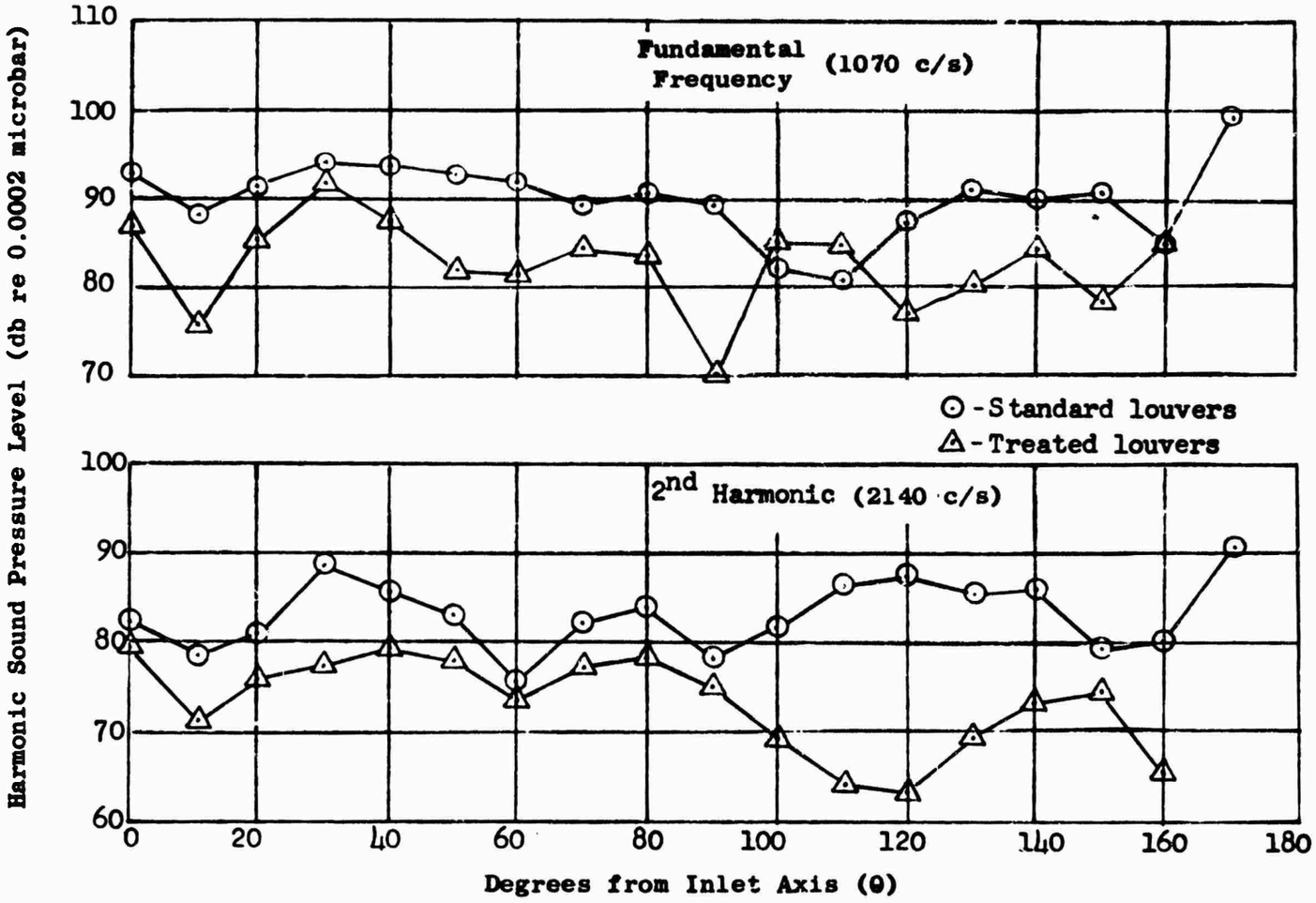

Figure 36.1 Directivity Pattern of Treated and Untreated Louvers.

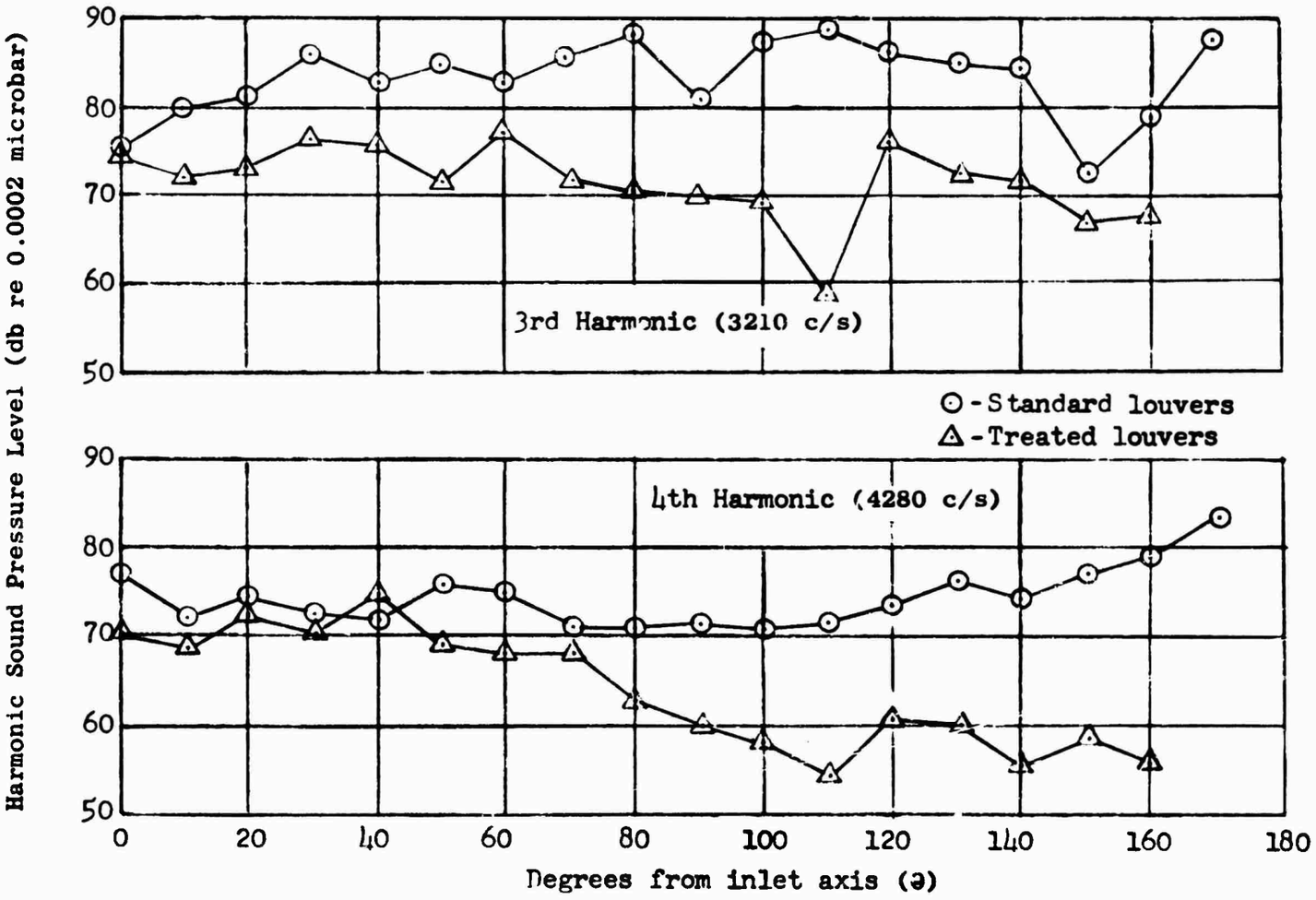

Figure 36.2. Directivity Pattern of Treated and Untreated Louvers.

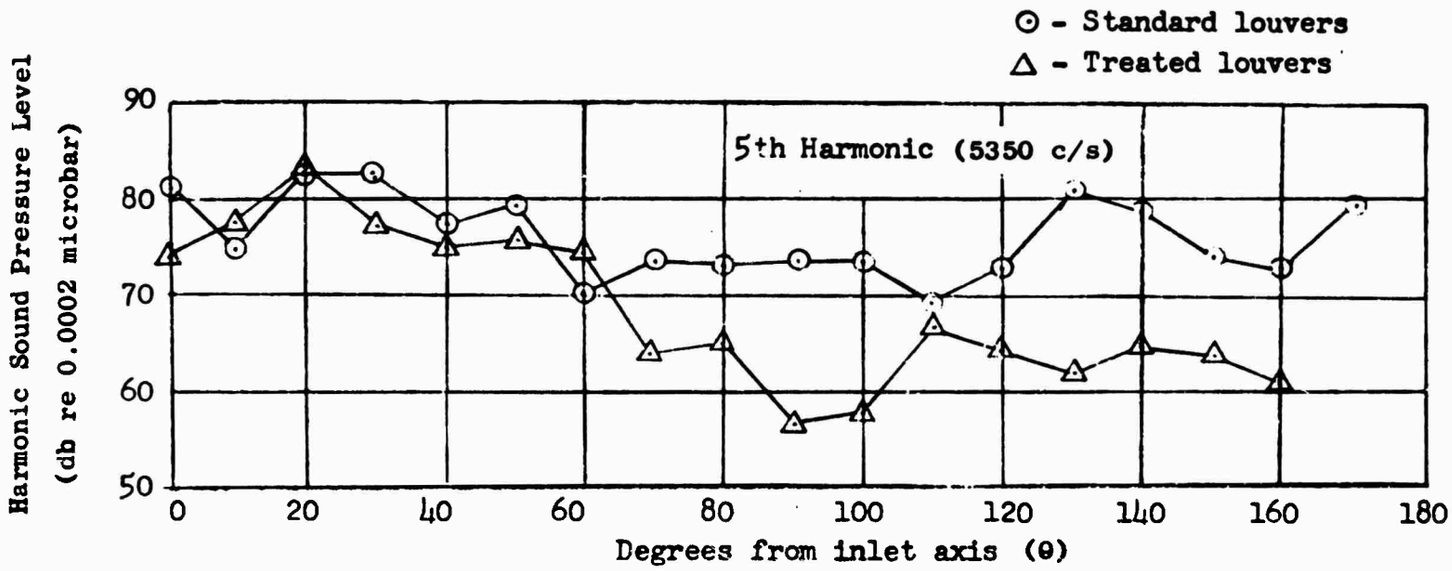

Figure 36.3 Directivity Pattern of Treated and Untreated Louvers.

SECTION FOUR - TEST DATA

TEST VEHICLES

The following data describes the various test vehicles used during the program to provide information as described in previous sections. The data given is for the basic test vehicle and does not account for various design changes as they are presented in the appropriate sections. The data is summarized in Table 1.

VTOL SCALE MODEL FANS

Two scale model fans of the same design family as the full scale VTOL lift and pitch fans used in the XV5A aircraft, Figure 1, were tested. They are designated the IGV-rotor fan and the rotor - stator fan, the first configuration being one that induces swirl ahead of the rotor and the latter being one that induces swirl in the rotor.

Inlet guide vane - rotor fan (Figure 37)

D_T = 26 inches

$\frac{D_H}{D_T}$ = .45

W = 27.8 lb/sec

RPM = 1780 (constant speed drive)

N_r = 47

N_s = 48

P_r = 1.011 (fan pressure ratio)

TABLE 1. SUMMARY OF TEST VEHICLE CONFIGURATIONS

Vehicles Tested During the Research Investigation

Name	D_T inches	D_H/D_T	W lb/sec	RPM	N_r	N_s	P_r
IGV-Rotor Fan	26	.45	27.8	1780 (Constant)	47	48	1.011
Rotor-Stator Fan	26	.40	26.1	1780 (Constant)	36	90	1.005
Lift Fan	62.5	.40	529	2640 (Maximum)	36	90	1.115
Pitch Fan	36	.45	144	4074 (Maximum)	36	90	1.08
Cruise Fan	62.5	.40	529	2640 (Maximum)	36	90	1.115
Single Stage Scale Model Compressor	26	.846	11	1780 (Constant)	56	48	1.008
Development Vehicle	Proprietary Information						

Vehicles Tested Prior to the Research Investigation

Name	Report from which Data was Obtained
Laboratory Compressor	Hunter, W.J. and Smith, L.H., Jr., Inlet Guide Vane-Rotor Interference Noise Measurements, TIS DF63FPD55, General Electric Company, Cincinnati, Ohio, January, 1963.
CJ805-3 Compressor	Semrau, W.R., Effect of Variation of Stator Vane Angle on CJ805 Compressor Noise, DIM 425, General Electric Company, Cincinnati, Ohio, May, 1961.
J93 Compressor	Data not issued as report.
Research Compressor No. 1	Smith, E.B., Noise Measurements of MJ254 Compressor FSCT at Lynn, DIM 448, General Electric Company, Cincinnati, Ohio, November, 1961.
Research Compressor No. 2	Lee, R. and Semrau, W.R., Low Speed and Transonic Speed Research Compressor Acoustics Measurements, DIM 457, General Electric Company, Cincinnati, Ohio, December, 1961.
R. Co. 12 Compressor and RA26 Compressor	Coles, G.M., Title Unknown, Rolls Royce Company, January, 1960.
CJ805-23 Fan	Dalke, C.A. and Smith, E.B., Third Noise Measurement of the GE CJ805-23 Engine and Effects of OGV's and Secondary Nozzle Sound Treatment on Aft Fan Whine, General Electric Company, Cincinnati, Ohio, November, 1959; Hallbach, J.R. and Keener, J.R., Basic Design Certification Verification Report for 7H-SSF-30 Sound Suppressor, TIS R61FPD108, General Electric Company, Cincinnati, Ohio, March, 1961.
CF700 Fan	McCann, E.O. and Smith, E.B., Noise Measurement of the CF700-2B Engine, DIM 534, General Electric Company, Cincinnati, Ohio, June, 1963.
Window Fan	Wells, R.J., Industrial Acoustics Course II Lecture Notes, Fan Noise Problem, R53GL241-6, General Electric Company, Schenectady, N.Y., May, 1954.

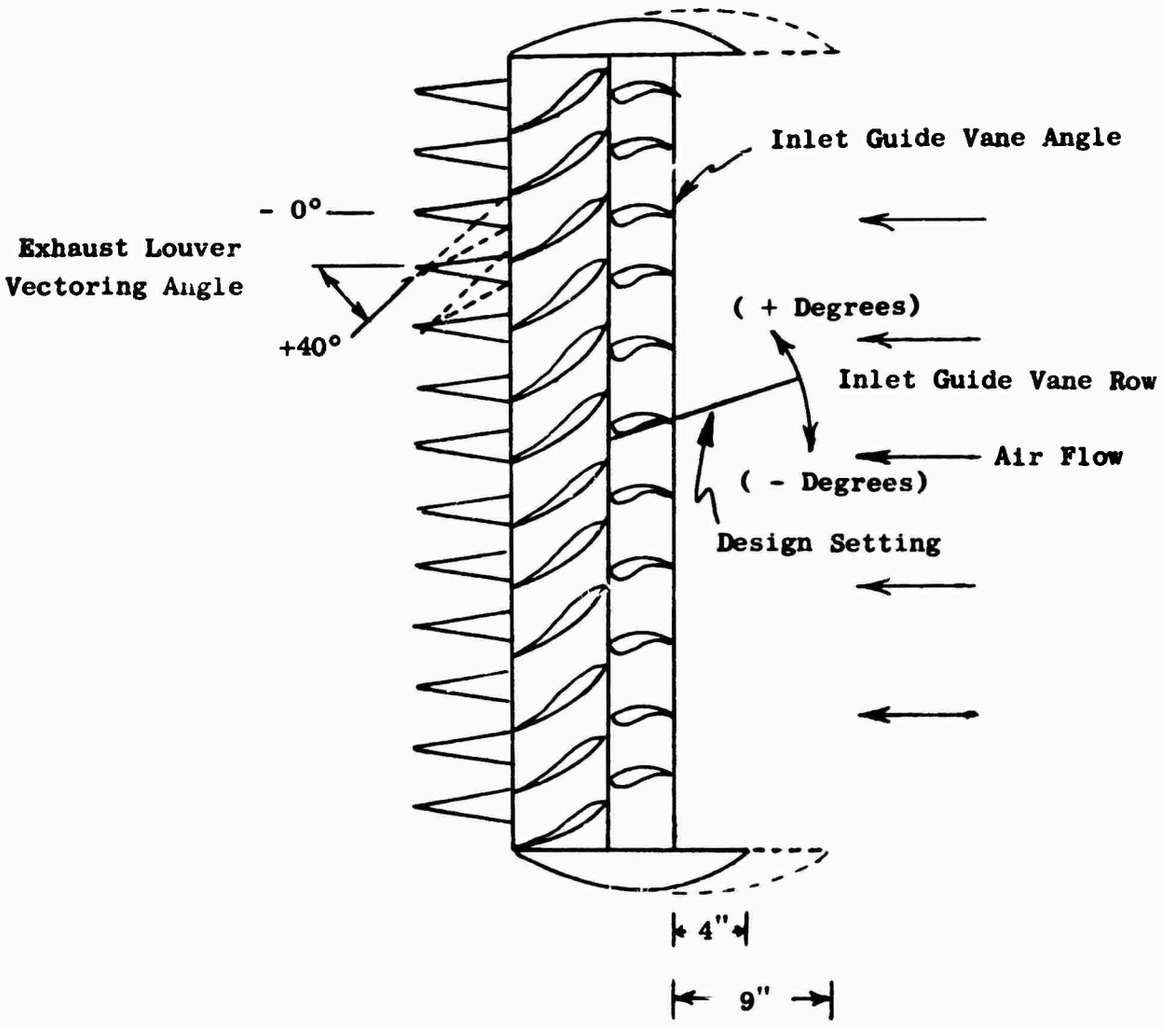

Figure 37. Test Configurations of Inlet Guide Vane - Rotor Fan (reference Table 1).

Rotor - stator Fan (Figures 38, 39 and 40)

D_T = 26 inches

$\frac{D_H}{D_T}$ = .40

W = 26.1 lb/sec

RPM = 1780 (constant speed drive)

N_r = 36

N_s = 90

P_r = 1.005

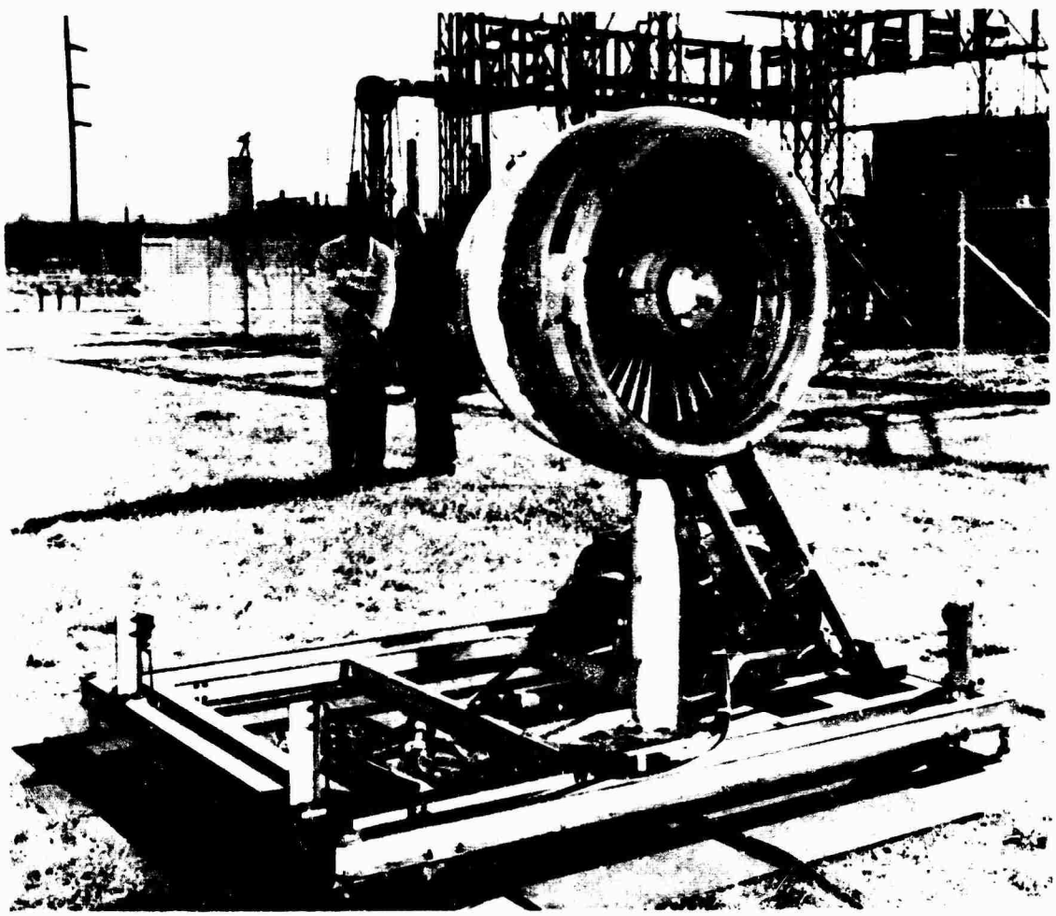

Figure 38. Rotor-Stator Fan

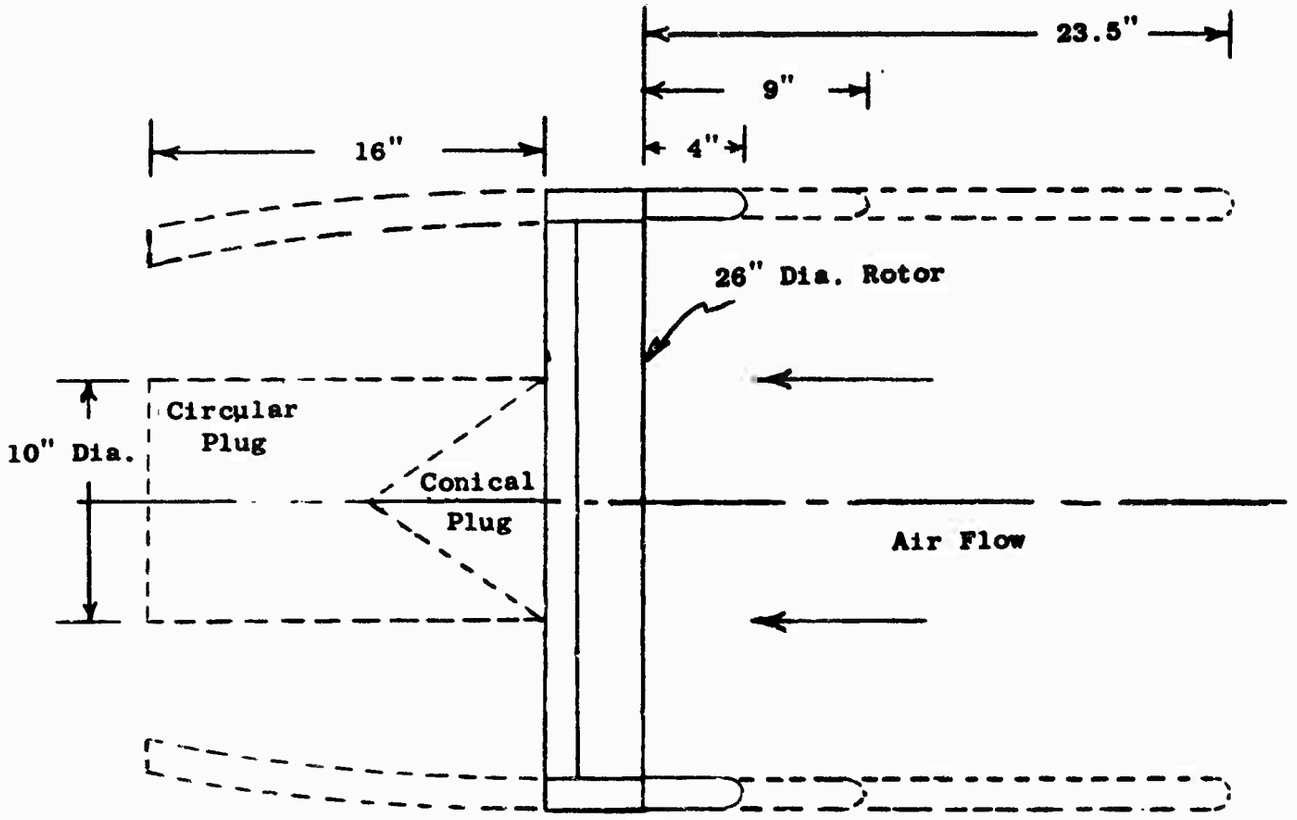

Figure 39. Test Configurations of the Rotor-Stator Fan (Reference Table 1).

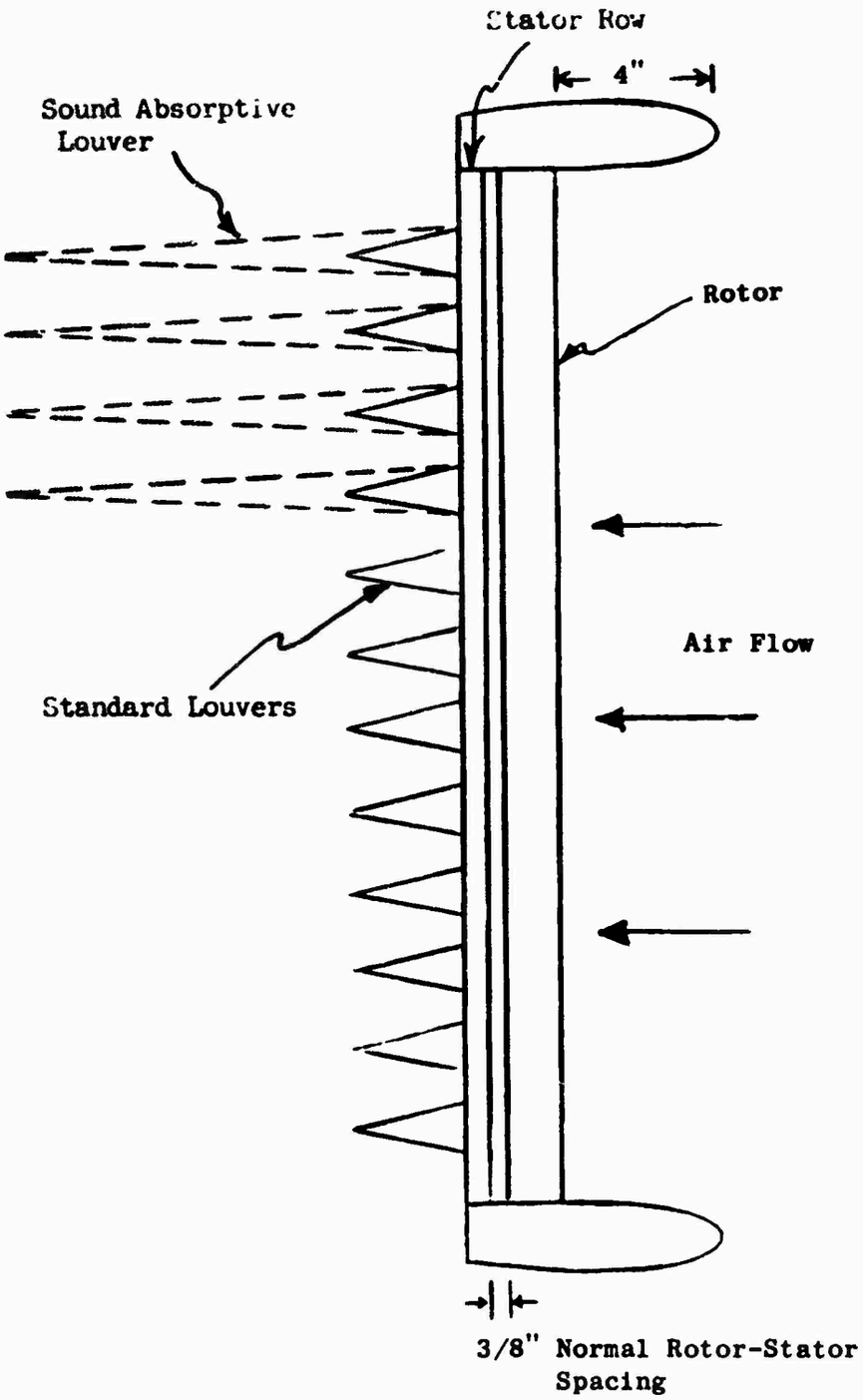

Figure 40. Test Configurations of the Rotor-Stator Fan (reference Table 1).

VTOL LIFT FAN

The VTOL lift fan is utilized in the XV5A aircraft and was tested as mounted in the aircraft and in a static test facility (Figures 1 and 41).

D_T = 62.5 inches

$\frac{D_H}{D_T}$ = .40

W = 529 lb/sec @ 2640 RPM

RPM = 2640 maximum

N_r = 36

N_s = 90

P_r = 1.115

VTOL PITCH FAN

The VTOL pitch fan is utilized in the XV5A aircraft and was tested as mounted in the aircraft and in a static test facility (Figures 1 and 41).

D_T = 36 inches

$\frac{D_H}{D_T}$ = .45

W = 144 lb/sec @ 4074 RPM

RPM = 4074 maximum

N_r = 36

N_s = 90

P_r = 1.08

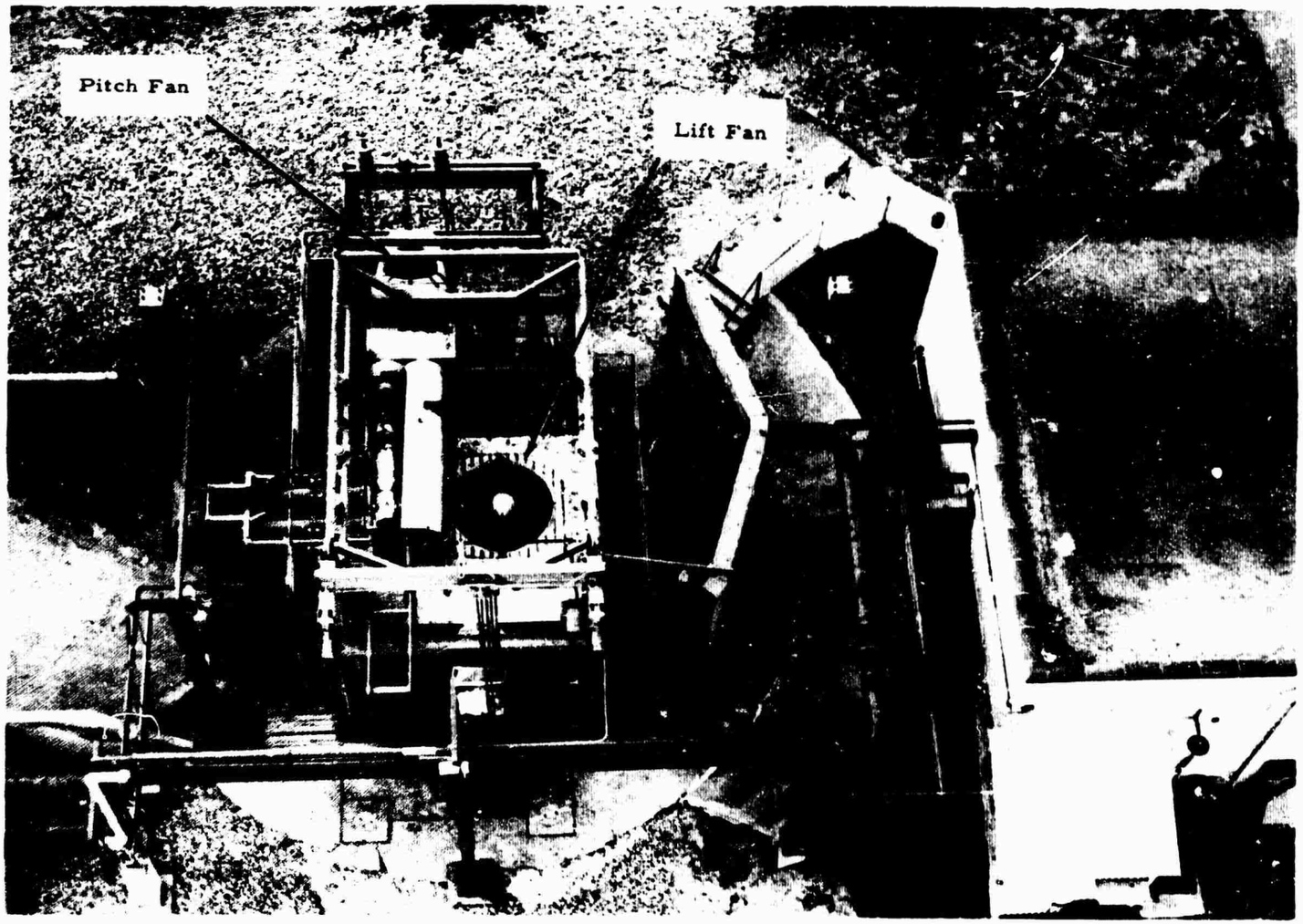

Figure 41. VTOL Static Test Facility.

CRUISE FAN

The cruise fan configuration is of the same basic design as the VTOL lift fan, but is used in a pod type installation as compared to a wing installation.

SINGLE-STAGE SCALE MODEL COMPRESSOR (Figures 42, 43, 44, and 45)

The single-stage scale model compressor was capable of having a variable rotor - stator spacing with approximately .5 inch of travel in the stator row. A significant characteristic is the high hub-tip ratio or small annulus height, which is in keeping with the basic assumption discussed in Section One.

D_T = 26 inches

$\frac{D_H}{D_T}$ = .846

W = 11 lb/sec

RPM = 1780

N_r = 56

N_s = 48

P_r = 1.008

DEVELOPMENT VEHICLE

The data presented in Figure 13 and in the following tables under development vehicle are the results of a scale model fan test utilizing a fan configuration of proprietary nature. The noise data is not classified or proprietary.

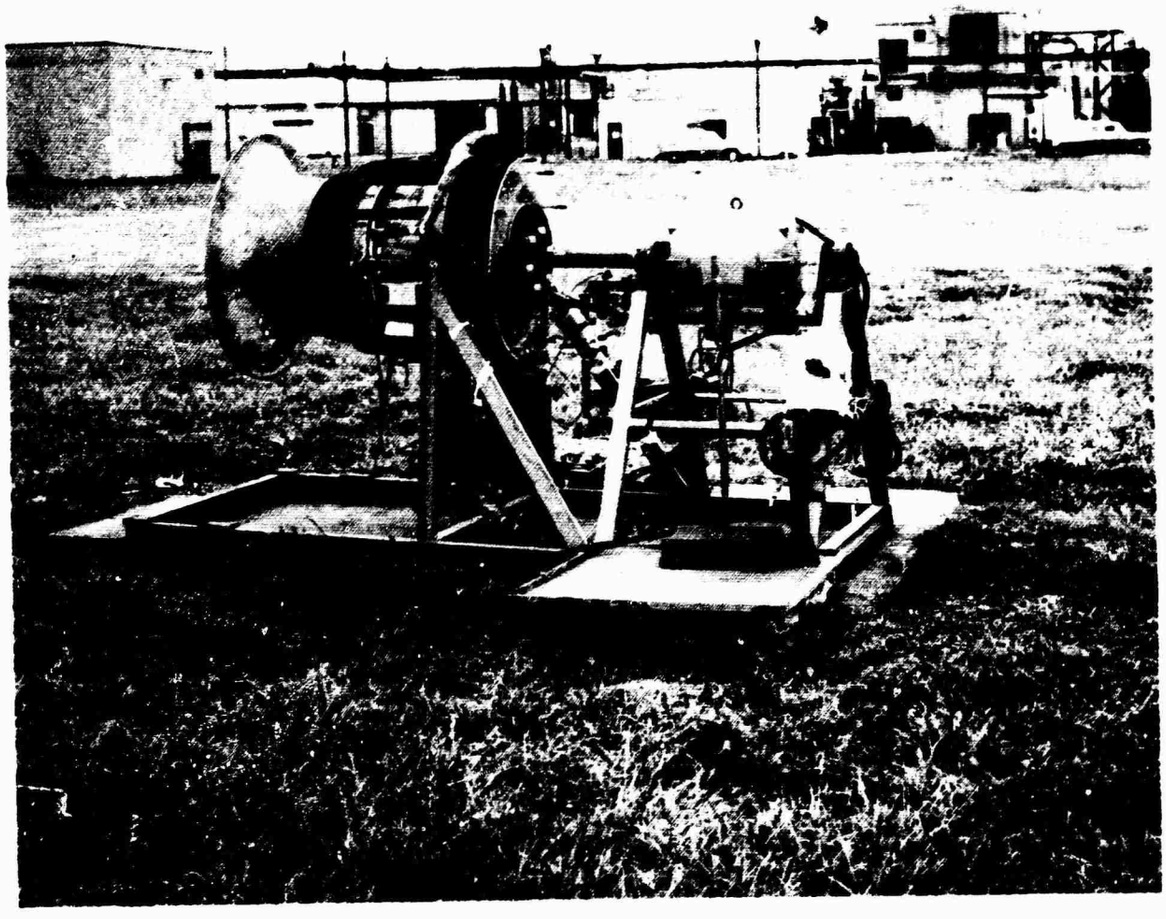

Figure 42. Single-Stage Scale Model Compressor.

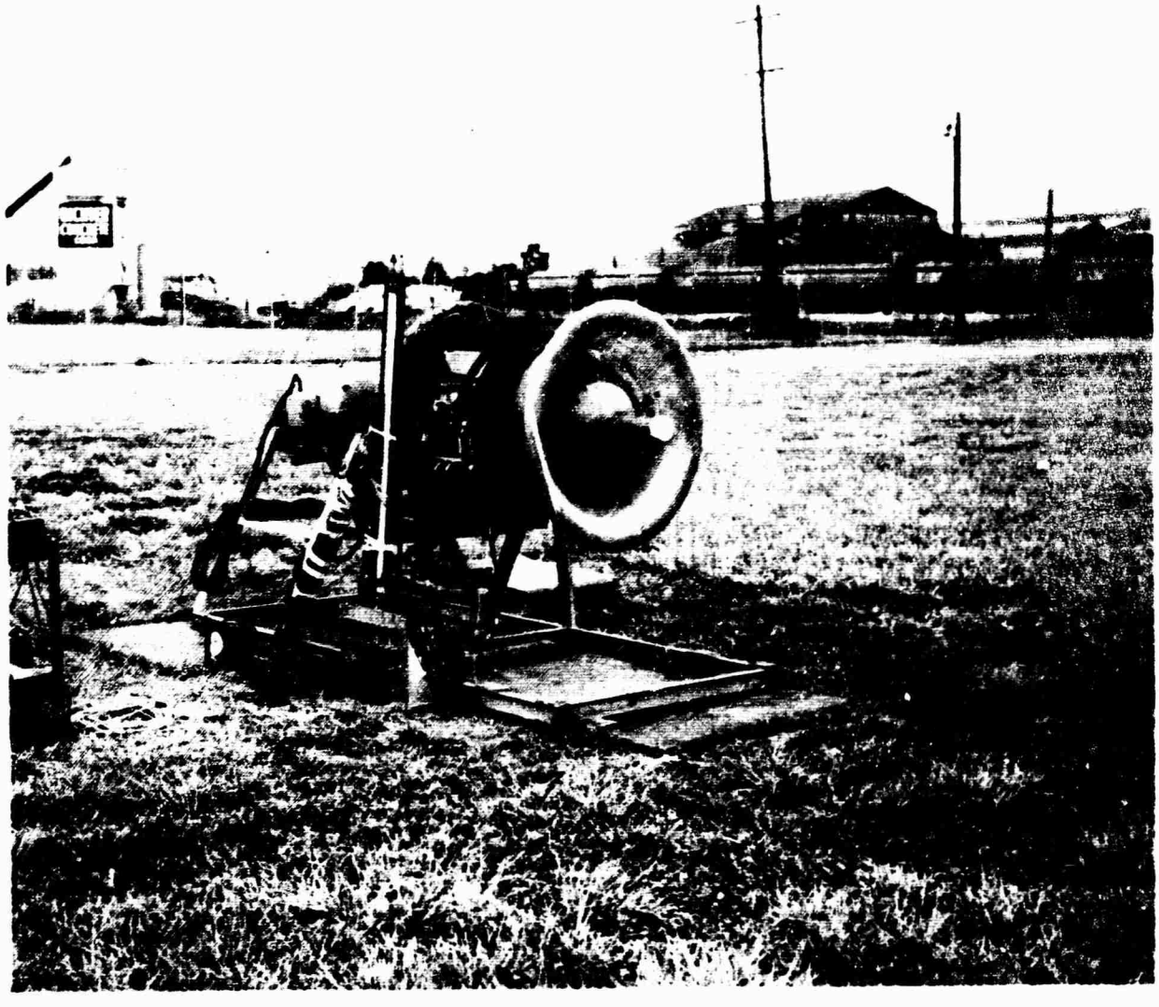

Figure 43. Single-Stage Scale Model Compressor.

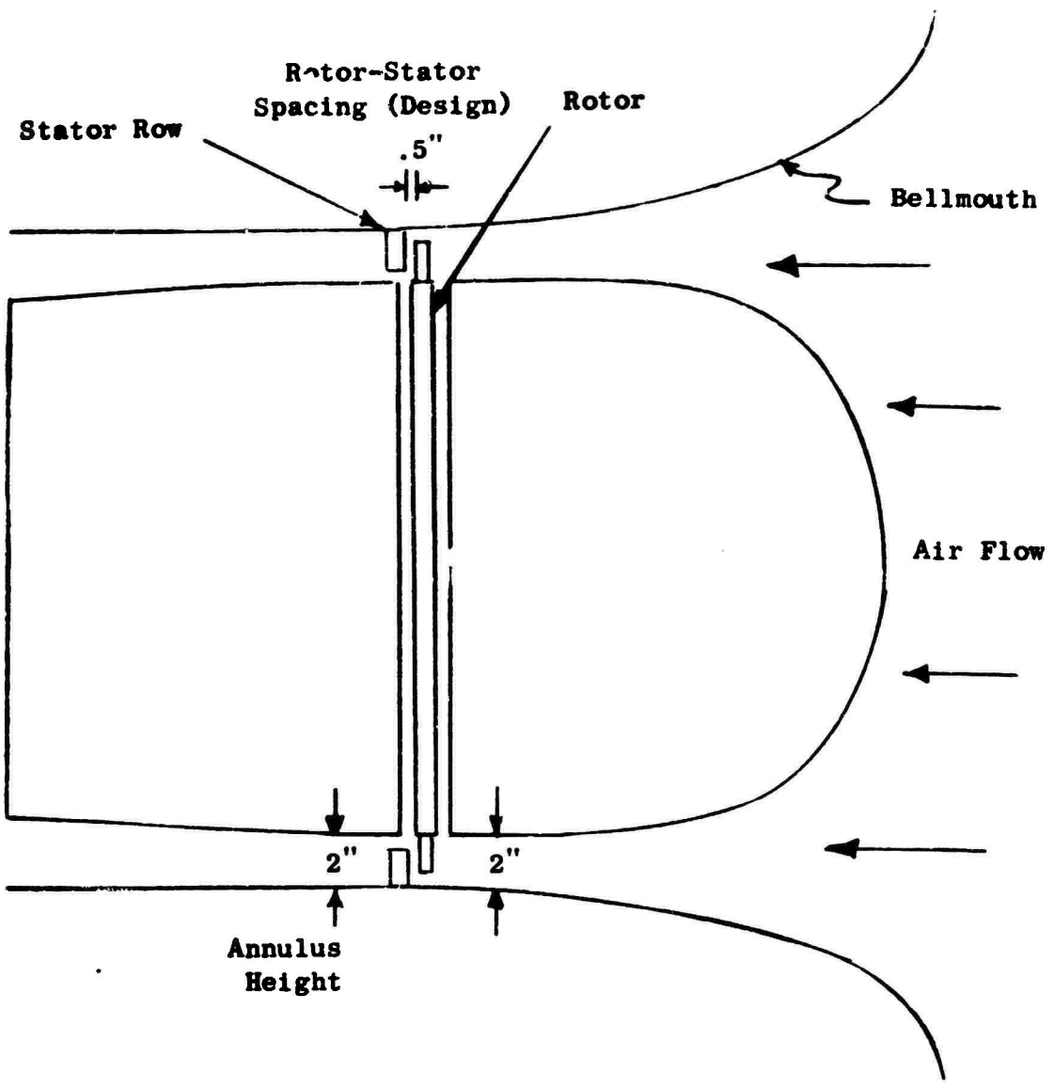

Figure 44. Test Configuration of Single-Stage Scale Model Compressor (reference Table 1).

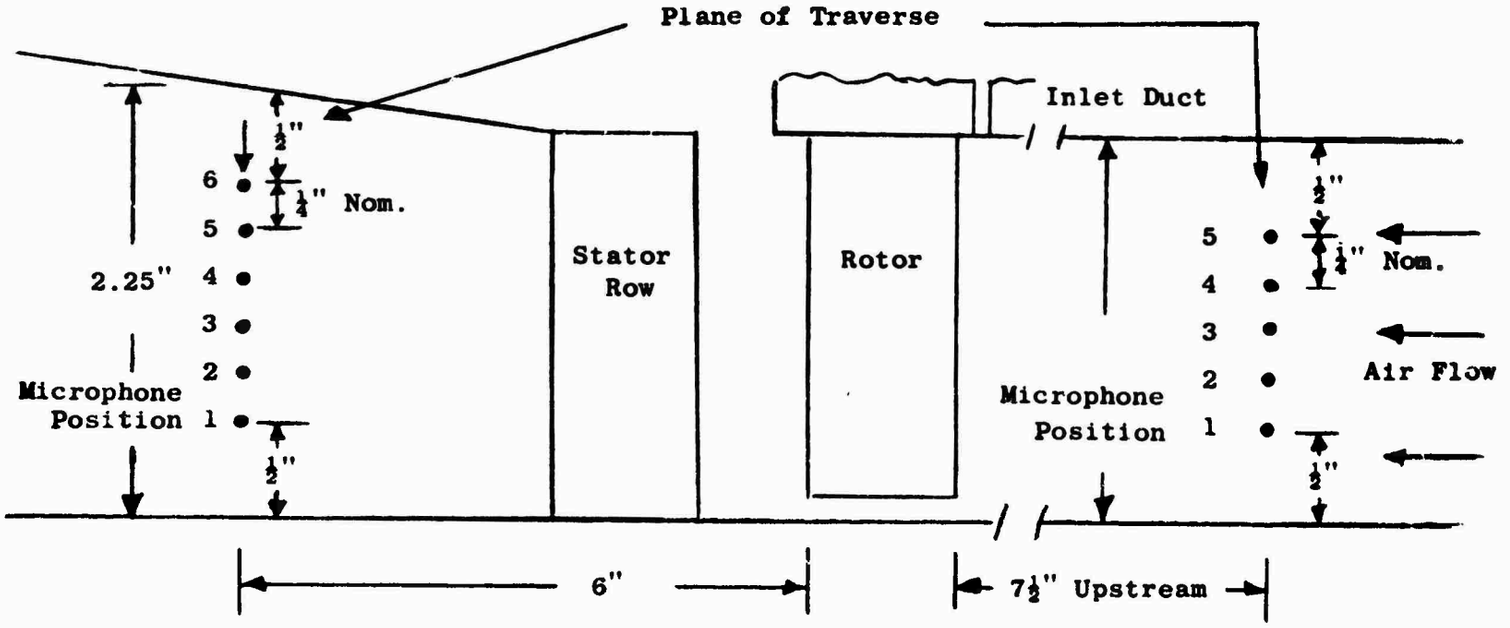

Figure 45. Location of Radial Noise Survey in the Annulus of the Single-Stage Scale Model Compressor.

TEST PROCEDURE AND EQUIPMENT

FREE FIELD MEASUREMENT

Free field noise measurement of the various scale model fan and compressor vehicles were made in generally the same manner. The test vehicles were all driven by a 25-horsepower constant-speed electric motor that was fed through a bank of reheostats used to bring the motor up to speed. When steady speed was attained, a microphone was placed at the desired location, and the sound was taped for a minimum of 15 seconds; then the microphone was moved to the next location. This procedure was the same for circumferential surveys, Figure 46, and for radial traverses of the vehicle annulus over the rotor face. A 1/2-inch microphone was used with a nose cone as required. The various systems utilized are shown in Figures 47 and 48.

The cruise fan and XV5A aircraft free field measurements were made with the recording system shown in Figure 48. The fan or aircraft was brought to the desired speed; then the data was recorded at the various circumferential locations, Figures 49 and 50, with a sufficient recording time for data analysis.

VTOL STATIC TEST FACILITY MEASUREMENTS

Measurements made of the VTOL lift and pitch fans on the VTOL static test facility, Figures 51 and 52, were done using a multiple channel recorder with 17 microphones positioned around the fans. The applicable operating conditions were provided by the test facility operator when the fans were at the desired RPM. At the desired operating condition, the microphone outputs were recorded on the multiple channel recorder in sets of three. The instrumentation is shown schematically in Figure 48.

REVERBERATION ROOM MEASUREMENTS

Reverberation room tests of the treated and untreated exhaust louvers were made using a noise source shown in Figure 53; the speaker was mounted in the plenum chamber to which the louvers were attached. The vacuum tube voltmeter was used to monitor the input to the speaker, and the oscilloscope was used to insure that the signal was not distorted. The signal was measured using a one-third octave analyzer and level recorder for comparison with and without the treated louvers.

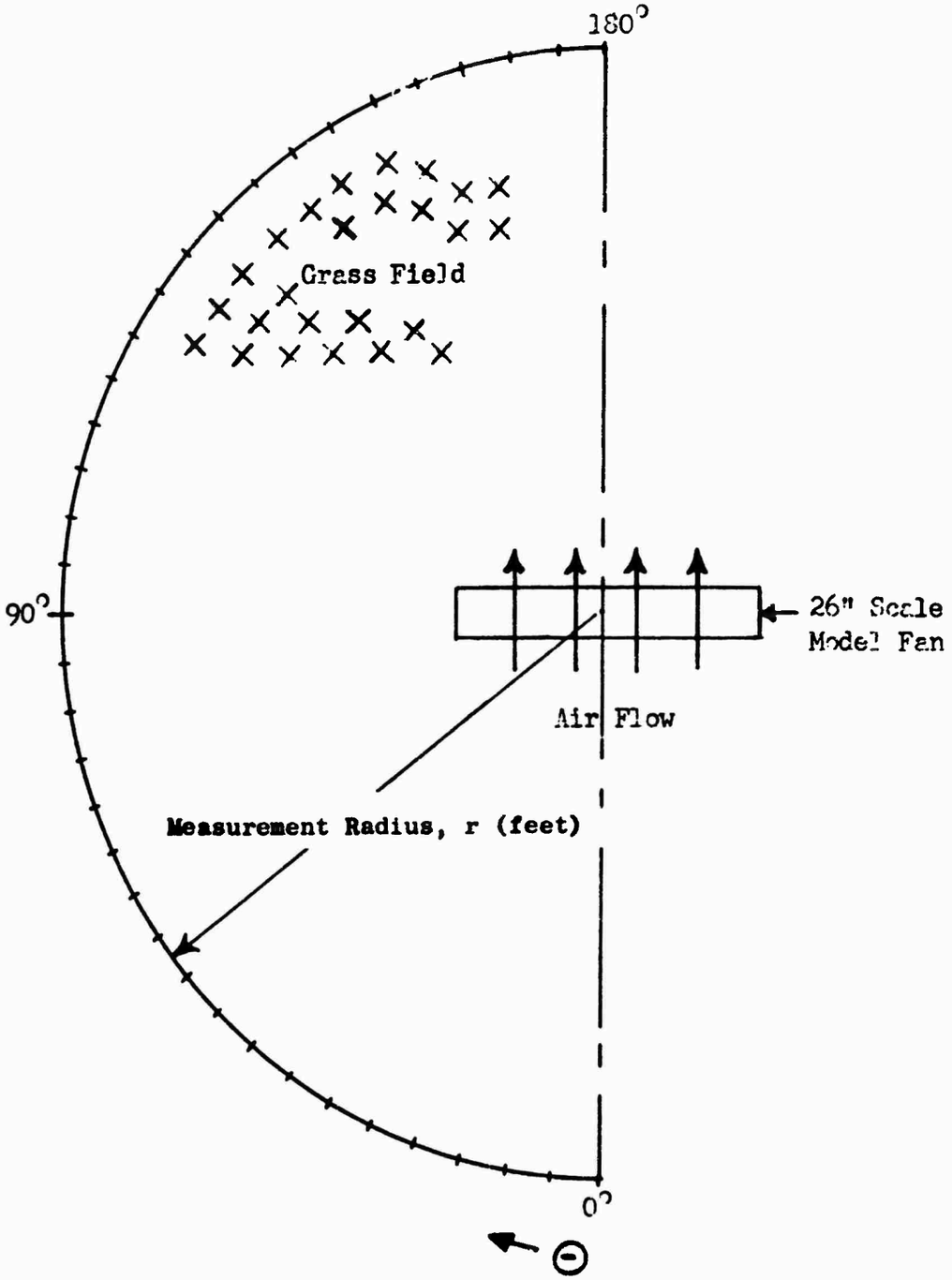

Figure 46. Test Layout and Microphone Station for Noise Evaluation of 26-inch Scale Model Fan Vehicles.

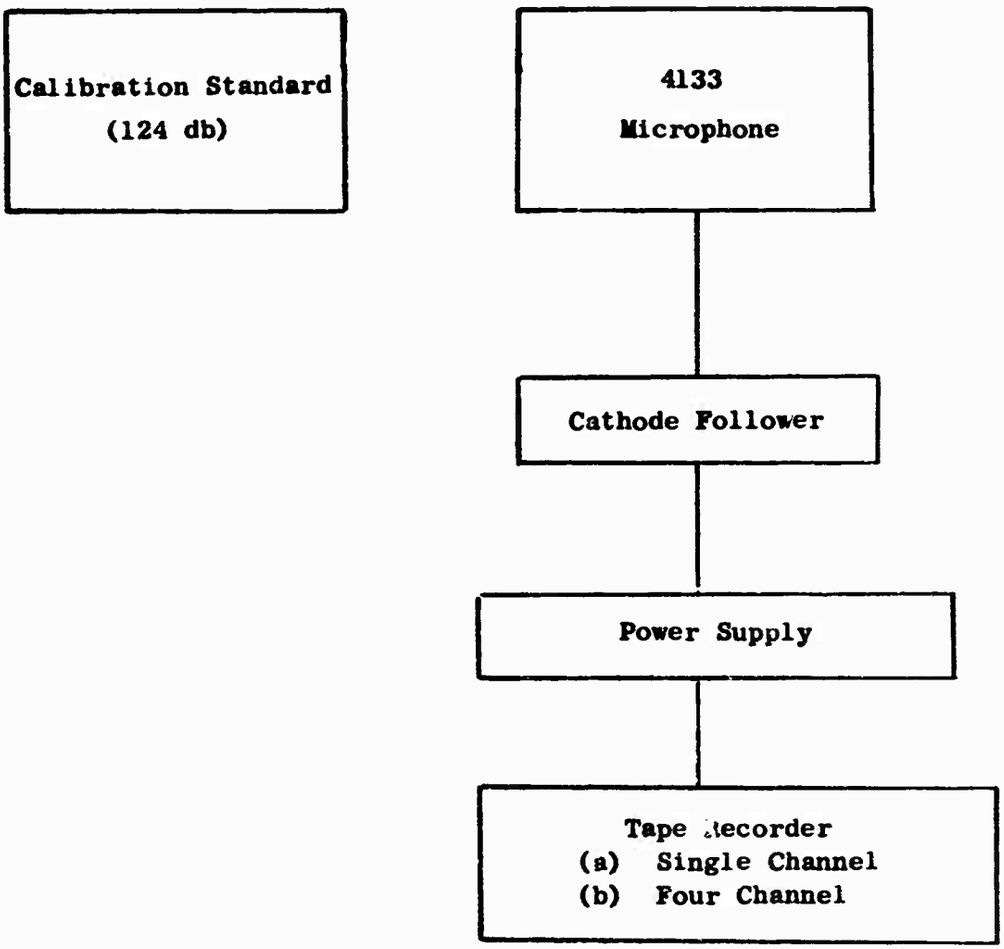

Figure 47 . Data Acquisition System - Field Test.

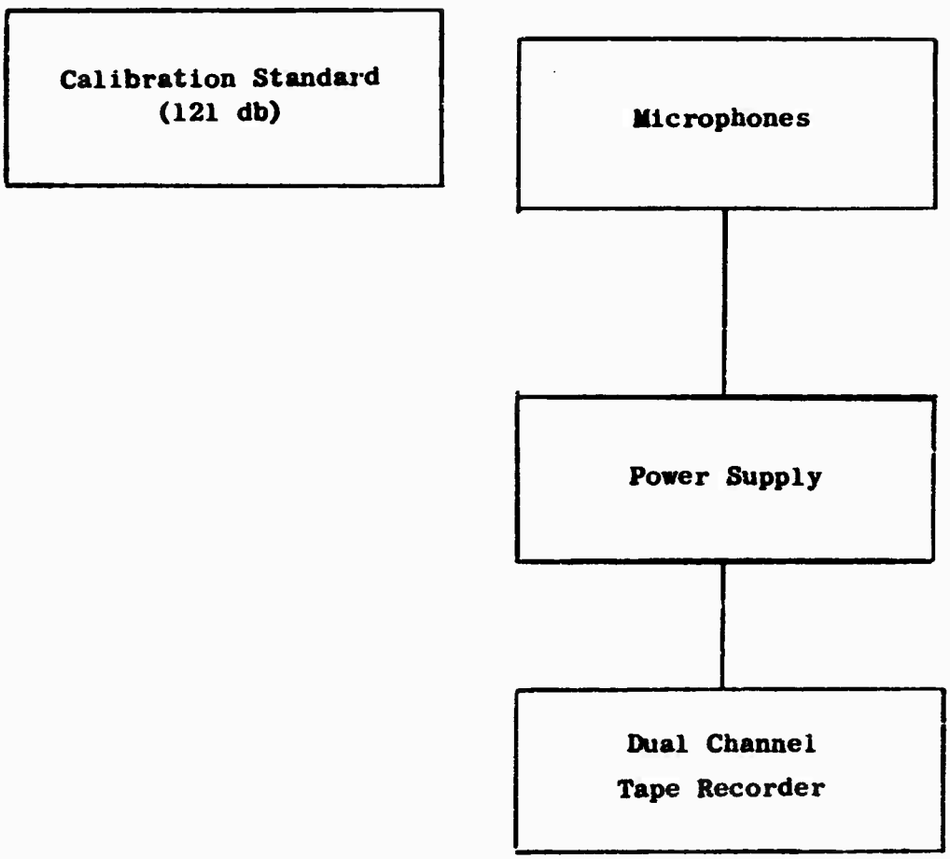

Figure 48 . Data Acquisition System - Field Test.

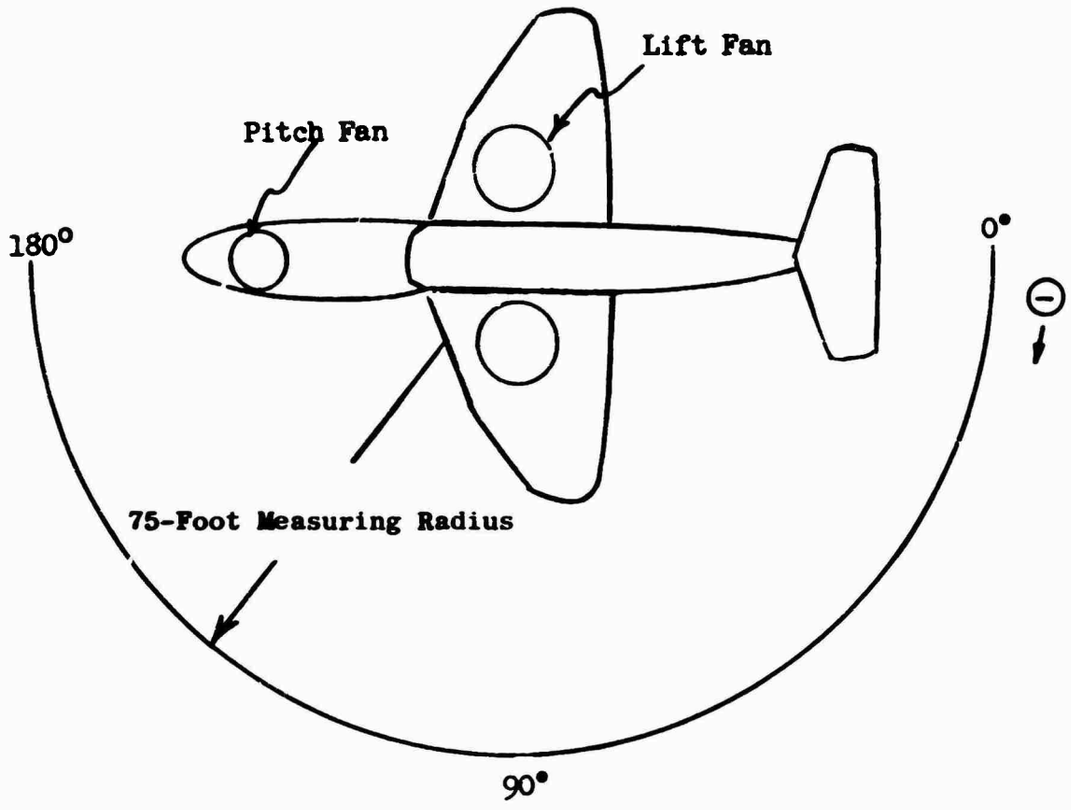

Figure 49. Test Layout of XV-5A Research Aircraft.

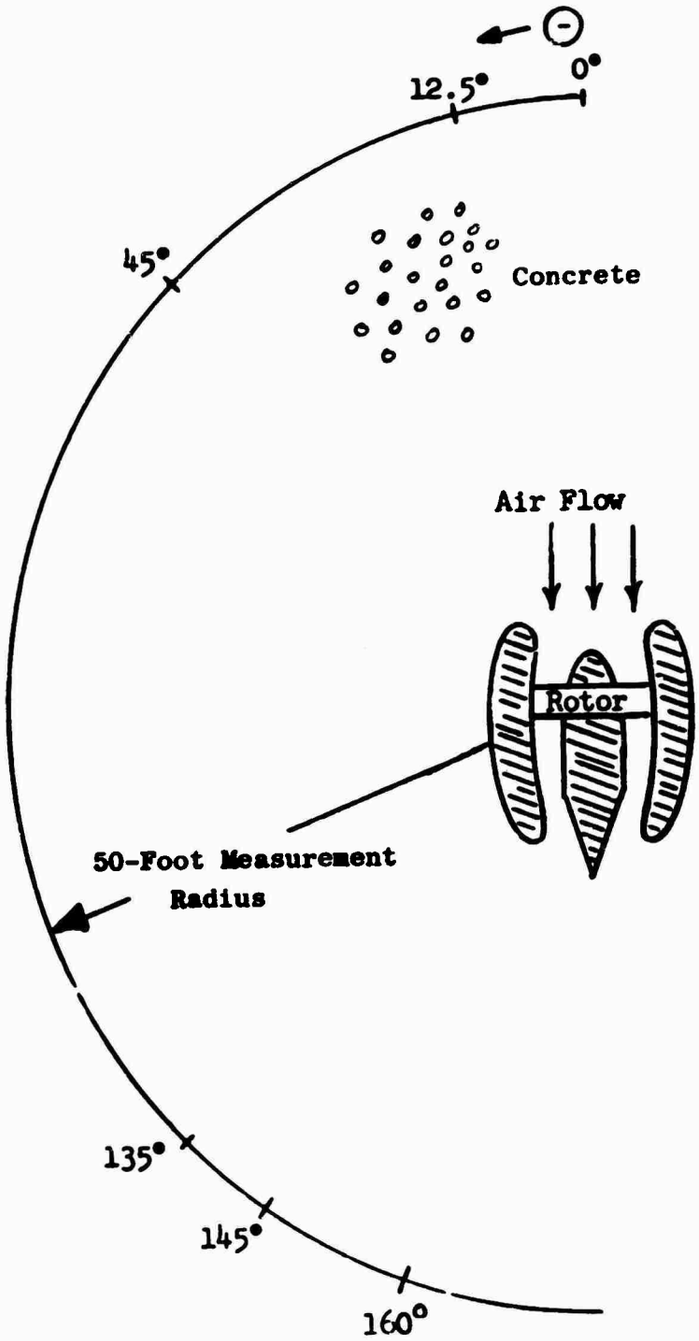

Figure 50. Test Layout for Cruise Fan Noise Evaluation.

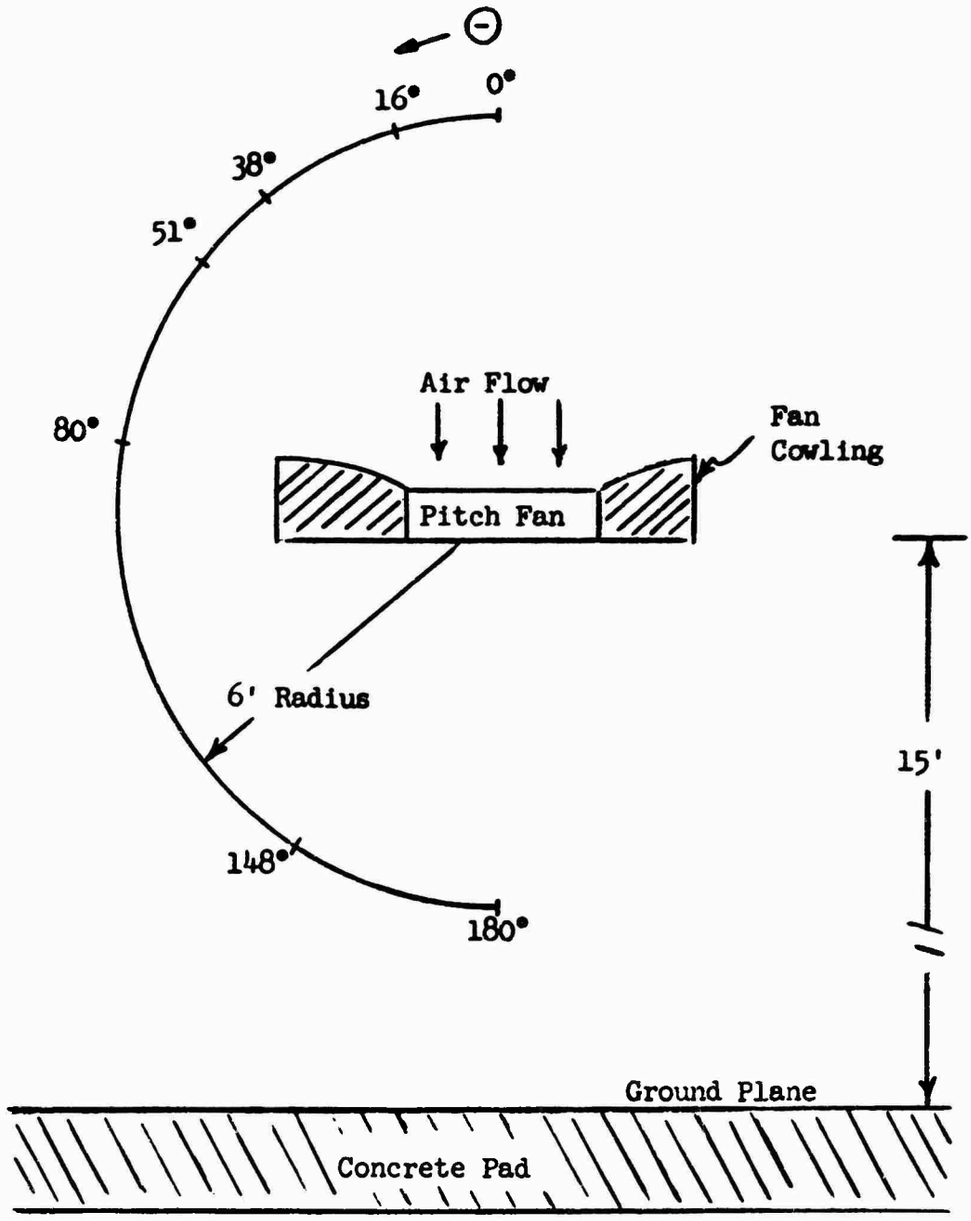

Figure 51. Test Layout for Pitch Fan Noise Evaluation.

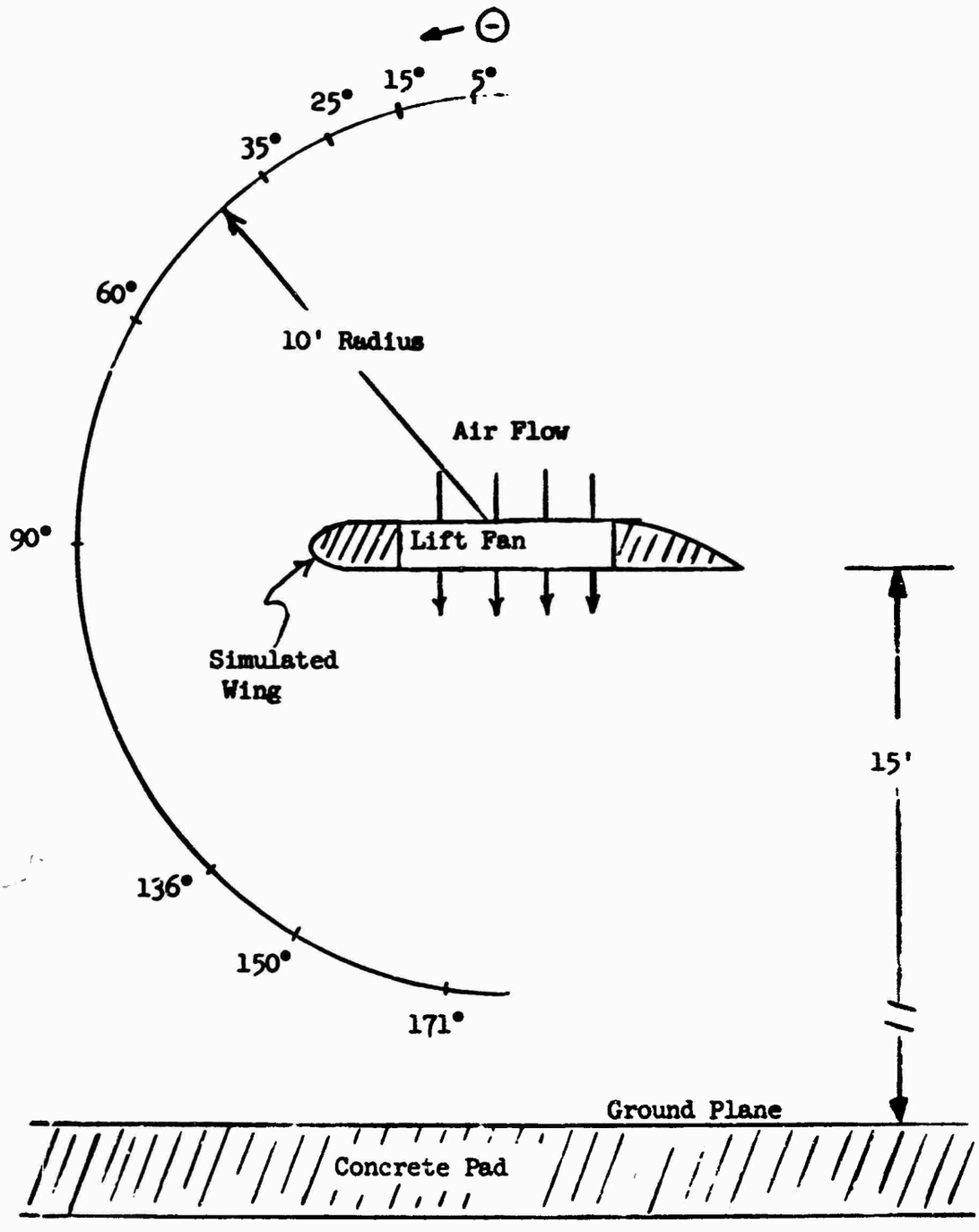

Figure 52. Test Layout for Lift Fan Noise Evaluation.

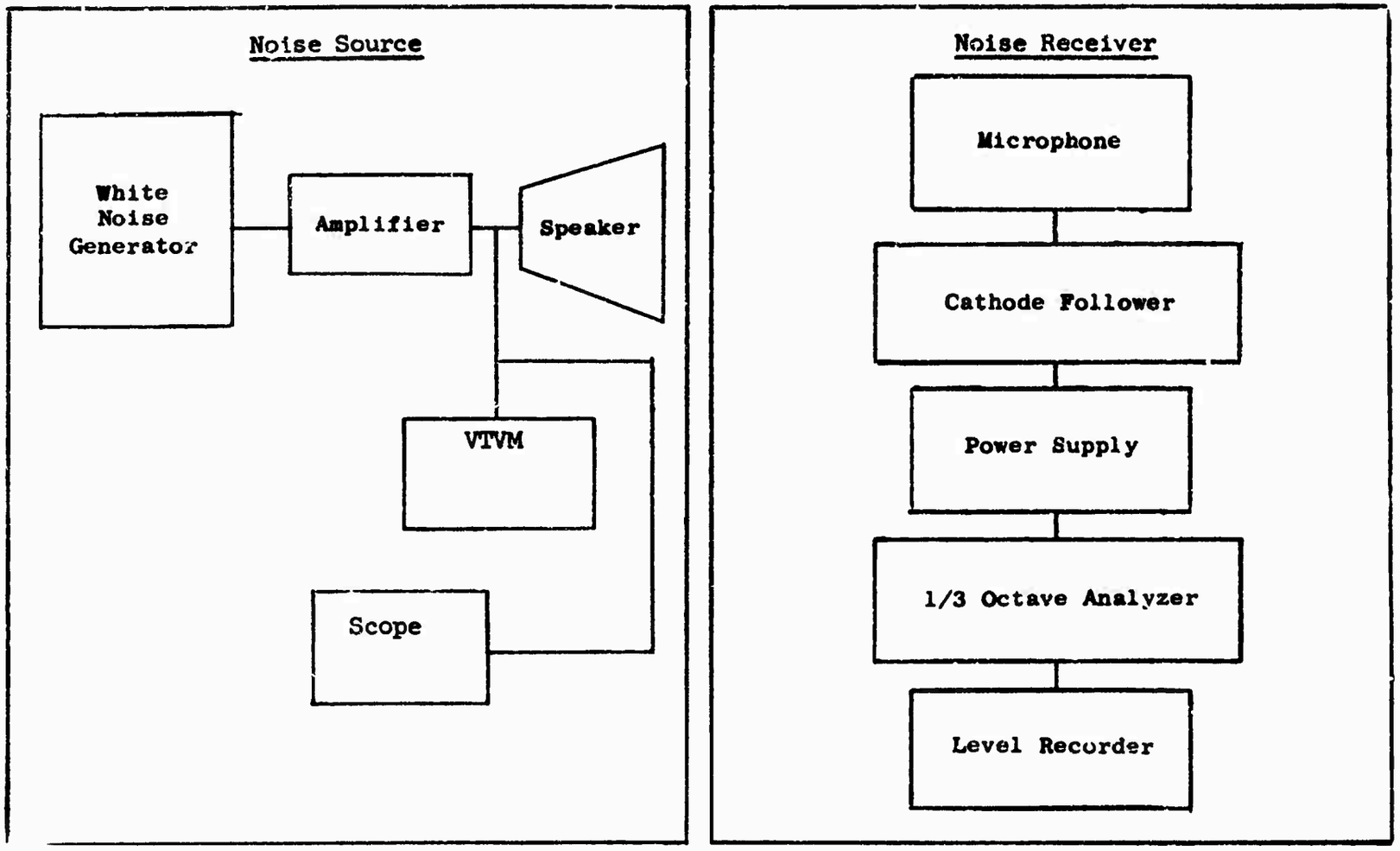

Figure 53 . Test Instrumentation - Reverberation Room.

DATA ANALYSIS

DATA REDUCTION

Data reduction of the noise tapes made on the various vehicles was done using the two systems shown schematically in Figure 54. The spectrum analyzer provided an analysis at a 10-cycle bandwidth, while the narrow band analyzer was a constant 6 percent bandwidth. The 6 percent bandwidth was sufficient for reduction of the first, second, and occasionally the third harmonic noise level of all the vehicles tested. Noise levels of higher harmonics were obtained using the 10-cycle bandwidth analyzer. The 6 percent filter was not used when the harmonic peak was not at least 5 db above the background or white noise.

SOUND POWER CALCULATIONS

The sound power levels were calculated in two manners corresponding to the circumferential surveys at constant radius and the radial measurements in the vehicle annulus near the rotor face.

The circumferential survey sound pressure levels were put into a computer program designed to calculate the sound power level based on three fourths of the surface area of a sphere having a radius equal to the measuring radius. The three-fourths surface area is a compromise between total ground reflection, 50 percent surface area, and total ground absorption, 100 percent surface area.

The sound power level was calculated from the radial sound pressure levels in the vehicle annulus using a technique developed in previous compressor measurements (reference 14, page 3.) The power level is calculated from the following equation:

$$PWL = \sum(SPL + 10 \log A)$$

where A is the annular area corresponding to each radial SPL measurement.

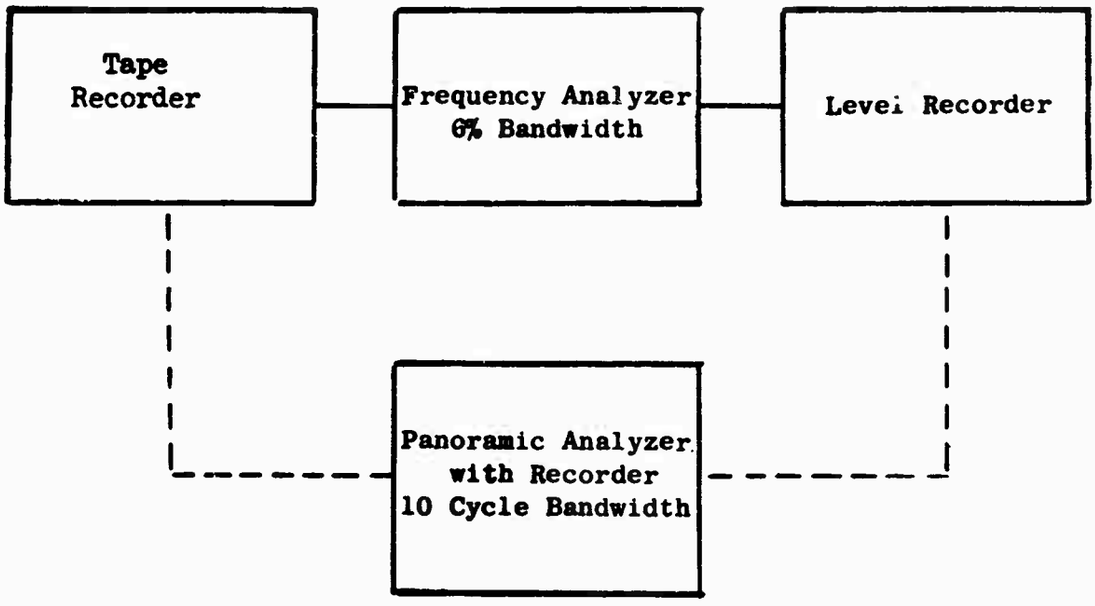

Figure 54 . Data Reduction Instrumentation.

TABLE 2. TEST DATA, INLET GUIDE VANE - ROTOR FAN

Measurement Location: see Figure 46 — Fan Speed: 1780 RPM
Measurement Radius: 20 ft — Fan Fundamental Frequency: 1395 c/s

Harmonic \ Angle, θ	Sound Pressure Level (db re .0002 microbar)										Sound Power Level (db re 10^{-13} watts)	Configuration (reference Figures 37 and 39)
	0	20	50	80	110	130	150	160				
Fundamental	79	91	86	82	83	89	87	85			121	9 in. inlet duct. 0° IGV setting and exhaust louver setting.
Second	65	80	78	71	75	72	85	78			113	
Third	73	76	78	75	72	70	77	71			110	
Fourth	68	70	71	61	66	79	72	74			108	
Fifth	62	70	68	64	68	71	73	66			104	
Harmonic \ Angle, θ	0	30	50	80	110	130	150	170	180			
Fundamental	74	84	85	80	79	85	73	81	89		119	9 in. inlet duct. 0° IGV setting and 20° exhaust louver setting.
Second	66	78	72	68	76	78	70	78	84		111	
Third	74	72	78	74	71	76	68	75	73		110	
Fourth	73	70	73	66	68	71	65	70	78		106	
Fifth	63	73	64	64	71	72	63	66	76		105	
Harmonic \ Angle, θ	0	30	50	80	110	130	160	180				
Fundamental	72	82	87	79	79	76	81	85			118	9 in. inlet duct. 0° IGV setting and 30° exhaust louver setting.
Second	67	73	75	67	82	76	79	80			112	
Third	71	68	75	75	72	71	74	80			109	
Fourth	68	67	72	66	68	73	72	80			106	
Fifth	65	73	67	66	69	72	73	78			106	
Harmonic \ Angle, θ	0	20	40	60	80	100	120	140	160	180		
Fundamental	76	91	92	86	79	83	89	89	89	89	123	9 in. inlet duct. 0° IGV setting and 40° exhaust louver setting.
Second	71	85	76	78	71	78	71	78	75	82	113	
Third	75	78	74	69	66	73	74	74	73	76	108	
Fourth	68	69	70	65	65	74	71	71	74	74	104	
Fifth	66	70	73	68	65	72	72	73	70	73	105	
Harmonic \ Angle, θ	0	20	40	60	80	100	120	140	160	180		
Fundamental	93	104	104	95	97	98	103	99	105	98	136	4 in. inlet duct. -27° IGV setting and 0° exhaust louver setting.
Second	100	99	100	96	90	93	89	94	96	90	131	
Third	84	87	91	86	86	86	87	89	87	85	123	
Fourth	81	82	79	76	75	74	81	85	81	77	115	
Fifth	78	79	78	74	70	76	80	80	82	74	113	
Harmonic \ Angle, θ	0	20	40	60	80	100	120	140	160	180		
Fundamental	87	97	98	87	82	90	96	90	94	90	129	9 in. inlet duct. -28° IGV setting and 0° exhaust louver setting.
Second	83	83	92	83	79	81	88	89	90	89	122	
Third	82	79	80	83	80	76	82	81	81	73	116	
Fourth	76	74	77	72	73	79	76	77	74	69	111	
Fifth	74	76	74	68	66	66	76	76	76	68	109	
Harmonic \ Angle, θ	0	20	40	60	80	100	120	140	160	180		
Fundamental	80	96	91	85	84	80	93	86	84	76	125	9 in. inlet duct. -16° IGV setting and 0° exhaust louver setting.
Second	80	83	85	87	81	76	82	83	80	78	119	
Third	79	82	83	78	72	74	82	82	80	68	115	
Fourth	68	73	78	70	63	66	76	79	74	67	110	
Fifth	68	74	77	68	65	67	72	76	76	67	108	

TABLE 3. TEST DATA, ROTOR-STATOR FAN

Measurement Location: see Figure 46
Measurement Radius: 10 ft
Fan Speed: 1780 RPM
Fan Fundamental Frequency: 1070 c/s

Harmonic \ Angle, θ	Sound Pressure Level (db re .0002 microbar)																		Sound Power Level (db re 10^{-13} watts)	Configuration (reference Figures 39 and 40)
	0	10	20	30	40	50	60	70	80	90	100	110	120	130	140	150	160	170	180	
Fundamental	81	79	88	92	85	90	87	80	85	85	89	87	89	91	77	84	86	90	87	117
Second	75	76	77	83	79	82	80	70	75	79	81	75	79	82	81	76	80	77	76	109
Third	68	72	77	79	81	78	80	78	77	70	77	72	77	75	80	72	77	-	77	107
Fourth	71	70	66	71	70	73	72	66	63	66	65	75	74	72	73	76	63	-	-	101
Fifth	63	67	76	70	70	65	65	66	63	59	66	64	71	67	75	72	68	-	-	98

Harmonic \ Angle, θ	0	10	20	30	40	50	60	70	80	90	100	110	120	130	140	150	160	170	Sound Power Level (db re 10^{-13} watts)	Configuration (reference Figures 39 and 40)
Fundamental	87	85	93	94	86	92	95	86	82	86	90	90	95	91	86	90	88	92	120	
Second	82	82	83	81	88	83	83	78	78	80	83	77	88	82	89	78	80	77	113	Fan equipped with 4 in.
Third	75	81	84	83	89	89	82	87	89	83	90	80	94	87	80	77	84	74	116	inlet duct and stator
Fourth	73	71	68	71	68	75	70	69	72	72	80	78	77	75	73	75	70	74	104	row. No exhaust louvers.
Fifth	85	73	90	75	68	76	73	65	62	70	66	75	75	81	81	75	73	72	105	

Harmonic \ Angle, θ	0	10	20	30	40	50	60	70	80	90	100	110	120	130	140	150	Sound Power Level (db re 10^{-13} watts)	Configuration (reference Figures 39 and 40)
Fundamental	88	86	88	91	83	88	84	82	84	86	89	88	92	86	86	90	117	
Second	83	83	84	80	83	80	78	80	79	78	79	84	84	82	89	85	112	Fan equipped with 4 in.
Third	76	77	75	80	73	74	80	75	74	71	80	80	76	81	80	77	107	inlet duct and stator
Fourth	67	72	68	74	72	74	71	72	71	73	74	71	75	75	74	79	102	row. Stator row spaced 1.0
Fifth	74	69	73	67	71	71	68	64	65	67	66	66	74	77	74	72	100	in. from rotor as compared to normal spacing of .375 in.

Harmonic \ Angle, θ	0	10	20	30	40	50	60	70	80	90	100	110	120	130	140	150	160	Sound Power Level (db re 10^{-13} watts)	Configuration (reference Figures 39 and 40)
Fundamental	87	76	86	92	88	82	82	85	84	70	85	85	77	80	84	79	85	114	
Second	80	72	77	78	80	78	75	78	78	75	69	64	64	70	73	75	66	105	Fan equipped with 4 in.
Third	75	72	73	77	77	72	78	72	71	70	69	59	77	73	73	68	68	103	inlet duct, stator row, and
Fourth	70	68	73	70	75	69	68	68	63	60	58	54	61	60	56	59	56	96	12 in. acoustically treated
Fifth	74	78	83	77	75	76	75	64	65	57	58	68	65	62	65	64	62	102	exhaust louvers (0° louver angle).

Harmonic \ Angle, θ	0	10	20	30	40	50	60	70	80	90	100	110	120	130	140	150	160	170	Sound Power Level (db re 10^{-13} watts)	Configuration (reference Figures 39 and 40)
Fundamental	93	88	92	95	94	93	93	90	91	90	83	81	88	92	90	91	85	99	120	
Second	83	79	82	88	87	84	77	83	84	78	82	87	88	86	87	80	80	91	114	Fan equipped with 4 in.
Third	75	80	82	86	84	86	84	87	88	81	88	89	86	85	84	73	79	88	115	inlet duct, stator row, and
Fourth	77	72	74	72	72	76	75	71	71	72	71	72	73	77	75	78	79	83	104	standard exhaust louvers
Fifth	82	76	83	83	78	80	70	74	73	74	74	69	73	81	79	74	73	79	106	(0° louver angle)

TABLE 4. TEST DATA, ROTOR-STATOR FAN

Measurement Location: see Figure 46
Measurement Radius: 20 ft

Fan Speed: 1780 RPM
Fan Fundamental Frequency: 1070 c/s

Harmonic \ Angle, θ	Sound Pressure Level (db re .0002 microbar) 0	20	40	60	80	100	120	140	160	Sound Power Level (db re 10^{-13} watts)	Configuration (reference Figure 39)
Fundamental	88	78	70	82	76	80	85	84		117	4 in. inlet duct. No exit duct or plug.
Second	72	74	75	76	72	70	76	70		109	
Third	74	-	-	78	80	73	82	75		112	
Fourth	74	72	72	69	68	74	72	72		106	
Fifth	84	72	72	66	69	73	73	75		106	
Harmonic \ Angle, θ	0	20	40	60	80	100	120	140	160		
Fundamental	88	81	76	81	81	83	87	90	84	120	9 in. inlet duct. No exit duct or plug.
Second	83	74	83	77	74	74	77	82	76	114	
Third	80	78	79	80	75	77	77	84	75	114	
Fourth	80	77	74	71	70	72	75	77	72	109	
Fifth	78	76	72	69	66	70	72	76	74	107	
Harmonic \ Angle, θ	0	20	40	60	80	100	120	140	160		
Fundamental	85	82	85	80	82	80	78	80	76	116	23.5 in. inlet duct. No exit duct or plug.
Second	81	83	78	71	72	71	78	82	75	113	
Third	75	76	78	76	74	80	75	82	78	113	
Fourth	70	72	72	69	66	68	71	-	72	105	
Fifth	84	78	70	67	64	67	71	75	70	106	
Harmonic \ Angle, θ	0	20	40	60	80	100	120	140	160		
Fundamental	81	79	74	75	76	72	82	82	78	114	9 in. inlet duct. 16 in. exit duct and cylindrical exit plug.
Second	75	76	76	74	69	72	75	76	68	109	
Third	80	78	76	73	74	73	70	76	74	110	
Fourth	78	76	74	68	64	64	75	74	71	107	
Fifth	77	73	72	70	64	-	69	77	72	106	
Harmonic \ Angle, θ	0	20	40	60	80	100	120	140	160		
Fundamental	86	80	82	79	79	68	82	78	82	115	9 in. inlet duct. 16 in. exit duct and conical exit plug. Fan exit duct area with plug = 446 $in.^2$
Second	76	75	72	74	75	69	68	77	74	109	
Third	82	72	77	76	70	73	71	76	74	109	
Fourth	80	74	73	71	67	66	74	74	69	107	
Fifth	79	74	72	70	63	64	70	77	74	107	

TABLE 5. TEST DATA, ROTOR-STATOR FAN

Measurement Location: see Figure 45
Measurement Radius: 50 ft
Fan Speed: 1750 RPM
Fan Fundamental Frequency: 1070 c/s

Sound Pressure Level (db re .0002 microbar)

Harmonic \ Angle, θ	0	10	20	30	40	50	60	70	80	90	100	110	120	130	140	150	160	170	180	Sound Power Level (db re 10^{-13} watts)	Configuration (reference Figures 5a and 5b)
Fundamental	77	80	79	78	80	75	71	73	75	73	67	66	73	78	78	71	77	73	75	116	Fan equipped with 4 in. inlet duct. No stator row or exhaust louvers.
Second	64	68	68	65	70	69	66	65	60	58	62	62	68	71	65	67	60	64	65	107	
Third	61	59	61	64	66	67	66	67	61	59	56	60	55	59	60	59	64	57	62	104	
Fourth	56	57	62	63	58	64	65	53	58	51	56	55	62	53	55	52	52	57	57	101	
Fifth	51	57	58	57	59	57	56	51	50	51	48	48	53	53	59	51	48	50	52	96	
Fundamental	84	82	84	80	78	73	77	77	77	75	71	72	73	80	82	72	87	82	71	120	Fan equipped with 4 in. inlet duct and stator row. Stator row spaced 1 in. from rotor as compared to normal spacing of .375 in.
Second	71	75	76	76	69	67	72	69	68	67	66	71	72	69	75	68	75	75	67	113	
Third	66	69	69	65	68	75	69	73	72	70	74	71	70	66	68	68	66	64	60	112	
Fourth	58	65	64	65	66	58	61	56	55	53	57	56	66	63	64	67	65	60	56	104	
Fifth	61	58	60	63	63	58	57	55	54	51	53	53	59	61	56	66	66	57	54	101	
Fundamental	84	77	78	79	80	76	71	72	72	74	67	66	66	73	79	72	77	70		116	Fan equipped with 4 in. inlet duct, stator row, and 12 in. acoustically treated exhaust louvers (0° louver angle).
Second	64	67	67	66	71	67	67	59	64	54	59	66	62	71	59	61	60	58		107	
Third	61	56	65	61	67	66	65	66	65	62	66	59	64	58	56	50	59	51		105	
Fourth	57	61	68	64	66	59	61	54	55	51	56	56	58	63	58	58	58	51		102	
Fifth	74	71	72	66	69	69	61	62	55	47	55	55	61	61	59	54	54	54		105	
Fundamental	81	79	77	73	76	71	84	82	82	77	68	77	78	83	82	75	80	72		121	Fan equipped with 4 in. inlet duct, stator row, and standard exhaust louvers (0° louver angle).
Second	61	69	71	73	73	67	70	72	71	70	71	70	63	70	70	74	72	67		112	
Third	61	67	70	77	74	69	73	73	66	67	70	69	75	69	69	65	69	62		113	
Fourth	60	62	64	65	64	60	61	58	56	56	58	57	63	62	62	70	58	55		103	
Fifth	73	61	61	69	72	67	61	62	62	64	57	61	64	67	69	66	60	54		107	
Fundamental	82	84	84	82	85	84	83	83	81	76	73	76	77	85	81	85	86	74	70	124	Fan equipped with 4 in. inlet duct and stator row. No exhaust louvers.
Second	66	73	73	69	76	73	64	68	62	64	62	64	68	65	72	76	75	65	60	112	
Third	65	63	68	72	79	67	75	67	78	76	72	79	73	73	61	70	63	61	62	116	
Fourth	65	61	66	69	62	67	65	62	59	60	61	61	63	68	60	65	66	58	55	106	
Fifth	79	64	74	70	63	61	62	63	59	58	70	64	73	70	60	75	62	56	56	110	

TABLE 6. TEST DATA, LIFT FAN

Measurement Location: See Figure 52 — Measurement Radius: 10 ft.

	Sound Pressure Level (db re .0002 microbar)									Sound Power Level (db re 10^{-13} watts)	Fan Speed RPM	Fundamental Frequency c/s
Angle, θ / Harmonic	5	15	25	35	60	90	136	150	171			
Fundamental	98.5	95.5	96	91	92	90.5	100	89	105	124	633	380
Second	95	98	94	91	89	89	97	88.5	102.5	122		
Third	95	97.5	92.5	93	90	87.5	96.5	87	100	121.5		
Fourth	95.5	100	94.5	94.5	91.5	90.5	97.5	87	98.5	123		
Fifth	96	101	97.5	95	92	90.5	98	88	98	124		
Angle, θ / Harmonic	5	15	25	35	60	90	136	150	171			
Fundamental	109	107.5	103.5	96.5	106	99.5	114.5	109	114	138	1124	675
Second	104	105.5	100	95	101	97	108	102	113	133		
Third	105.5	105.5	104.5	97.5	102.5	105.5	111	99.5	114	136		
Fourth	102.5	105.5	100	90.5	96	98.5	110	101.5	109	133		
Fifth	103.5	105.5	104	90	97	96	111	101.5	108	134		
Angle, θ / Harmonic	5	15	25	35	60	90	136	150	171			
Fundamental	117.5	112	108.5	113.5	113	109.5	118	115.5	132	146	1393	840
Second	106.5	108.5	112	107	104.5	106	116	110.5	126.5	142		
Third	107.5	109	110.5	106.5	105	106.5	119.5	110.5	125.5	143		
Fourth	104	106.5	107	102	100	103	115	104	122.5	139		
Fifth	104.5	107.5	106	101.5	99.5	101	118.5	104.5	122	141.5		
Angle, θ / Harmonic	5	15	25	35	60	90	136	150	171			
Fundamental	123.5	121.5	110.5	117.5	115.5	111.5	111.5	117	123	144	1736	1040
Second	112	117.5	110	113	110.5	109	113.5	114	120.5	141		
Third	113	115.5	113.5	111.5	108.5	109	111	111.5	119.5	140		
Fourth	108	111.5	110	109.5	104	104.5	114	107.5	118	139		
Fifth	108.5	113	109	108	104	101	114	109	118	139		
Angle, θ / Harmonic	5	15	25	35	60	90	136	150	171			
Fundamental	123	123.5	116	117.5	112.5	113	128	122	123.5	151	1905	1140
Second	110.5	115	114	113	104.5	110	126	111.5	121.5	149		
Third	111.5	113	117.5	108.5	105.5	108.5	120.5	111.5	120	144		
Fourth	109	111.5	112	106.5	101.5	103.5	124	110.5	118	146		
Fifth	109.5	113	111.5	106	101	100.5	122	110.5	118	144.5		
Angle, θ / Harmonic	5	15	25	35	60	90	136	150	171			
Fundamental	131	125.5	118.5	126	125.5	116	129	126.5	130.5	155	2203	1320
Second	117.5	116	117.5	117.5	116	116	123	117.5	124.5	148		
Third	118	116	117	115.5	114	112	124.5	115	126	148		
Fourth	115.5	115	114.5	112	111.5	106.5	122.5	117.5	120	146		
Fifth	113	113.5	114	109.5	110	106	122.5	117	120	146		
Angle, θ / Harmonic	5	15	25	35	60	90	136	150	171			
Fundamental	130	129.5	125	123	128	120	129.5	122.5	131	156	2327	1400
Second	118	119	118	116.5	121	116.5	125	118	126	150		
Third	119	117.5	122.5	115.5	120	114	128	117	124.5	151.5		
Fourth	114.5	116.5	116	111.5	117	108	126.5	118	121.5	150		
Fifth	107.5	114.5	117	108	115	106.5	125	118	121.5	148		

TABLE 7. TEST DATA, PITCH FAN

Measurement Location: see Figure 51 — Measurement Radius: 6 ft.

Harmonic \ Angle, θ	Sound Pressure Level (db re .0002 microbar) 0	16	38	76	80	148	180	Sound Power Level (db re 10^{-13} watts)	Fan Speed RPM	Fan Fundamental Frequency c/s
Fundamental	94.5	96.5	99	94.5	-	90.5	10[illegible]	117	1035	620
Second	98	98.5	100.5	94	-	90.5	103	118		
Third	100.5	100.5	102	97	-	92.5	102.5	120		
Fourth	101	99.5	100.5	96.5		95	101	120		
Fundamental	101.5	102.5	108	98	98	105	110.5	128	1756	1050
Second	106	101.5	105	101	97	104	111.5	126		
Third	105.5	100.5	104.5	97.5	96.5	103.5	107	125.5		
Fourth	105.5	100.5	102	96.5	96.5	103.5	105.5	125		
Fundamental	107.5	109.5	111.5	103	100.5	104.5	118	130	2255	1350
Second	108.5	103.5	103	100	99	105.5	112.5	127		
Third	106	104.5	101	98.5	96.5	103	107.5	125		
Fourth	101	101.5	100.5	99.5	96	100	109	123		
Fundamental	110.5	109	113.5	107.5	107.5	116.5	120	137	2876	1725
Second	111	108	109	109	102.5	114	116.5	134		
Third	107	107.5	106.5	104.5	101	122	113	141		
Fourth	105	105.5	106	103.5	100	120	110	139		
Fundamental	113	104	118	109.5	113	116	118	139	3066	1840
Second	108	102	116	110	115	115	116	139		
Third	108	99	103.5	104.5	112	117	112	138		
Fourth	109	99	107.5	107	111	113	110	135		
Fundamental	119	109	117.5	111	120	118.5	124.5	143	3546	2130
Second	111	107.5	117.5	107.5	112	120	122.5	141		
Third	110	105.5	111	107	110.5	117.5	119	138		
Fourth	111.5	90	110	105.5	112.5	114.5	90	137		
Fundamental	115	114.5	117	113	118.5	125	126.5	145	3956	2340
Second	114	111	117.5	117.5	116	125.5	122.5	145		
Third	114	108	111	110.5	115	119.5	117	141		
Fourth	112	105	111.5	106	114	113	113.5	137		

TABLE 8. TEST DATA, CRUISE FAN

Measurement Location: see Figure 50 — Measurement Radius: 50 ft.

Harmonic \ Angle, θ	Sound Pressure Level (db re .0002 microbar)							Sound Power Level (db re 10^{-13} watts)	Fan Speed RPM	Fan Fundamental Frequency c/s
	0	12.5	45	135	145					
Fundamental	96	92	87	90	89			131	750	450
Second	93.5	92.5	88	84	83			129		
Third	90.5	91	85	77	75			126		
Fourth	94	92.5	88.5	80	76			129		
Fifth	96	92.5	89	82	81.5			130		
Harmonic \ Angle, θ	0	12.5	45	135	145					
Fundamental	98	100	98	100	91			141	1110	666
Second	90.5	91	93.5	87	78			134		
Third	88	93	98	96	85			139		
Fourth	90	94	93	91	83			134		
Fifth	90	92	93.5	90	79			134		
Harmonic \ Angle, θ	0	12.5	45	135	145					
Fundamental	102	112	105	108	92.5			149	1400	840
Second	89	95	94	90	88			135		
Third	91	100	104.5	98	93.5			145		
Fourth	89	91	90	91	85.5			133		
Fifth	88	92	94	89	82			134		
Harmonic \ Angle, θ	0	12.5	45	135	145					
Fundamental	106.5	113.5	109	106	106.5			151	1730	1038
Second	98	104	103	99	98			144		
Third	99	106	101	99	99			143		
Fourth	91	95	94	96	91			137		
Fifth	95	96.5	95.5	94	93.5			137		
Harmonic \ Angle, θ	0	12.5	45	135	145					
Fundamental	110	111	109	106	102			150	1900	1140
Second	107	106.5	110	106	97			151		
Third	102.5	104	104	103	98			146		
Fourth	96	98	97	97	92			139		
Fifth	96.5	100	96	93	91.5			138		
Harmonic \ Angle, θ	0	12.5	45	120	135	145	160			
Fundamental	116	110.5	110	104	109.5	105	98	151	2200	1320
Second	106	108	111	117	115	103	97	157		
Third	102	104.5	104	103	106.5	95	89.5	146		
Fourth	100	101	99	101.5	101.5	94.5	90	143		
Fifth	99.5	100	98	97.5	98	93	86	140		
Harmonic \ Angle, θ	0	12.5	120	135	145	160				
Fundamental	116	110	102	112	107.5	105		149	2410	1446
Second	108	110	114	109	105	103		155		
Third	106	107	108	105	100	96.5		149		
Fourth	102	100	102	99	93.5	92		143		
Fifth	104	102.5	101	98	96	92		143		

TABLE 9. TEST DATA, XV-5A RESEARCH AIRCRAFT

Measurement Location: see Figure 49 — Measurement Radius: 75 ft

Angle, / Octave Band	Octave Band Sound Pressure Level (db re .0002 microbar)											Octave Band Sound Power Level (db re 10^{-13} watts)	Configuration
	20	30	40	50	60	80	100	120	140	160	180		
1	116	115	113	109	107	105	103	99	97	96	97	153	
2	120	120.5	118	113	110	108	104	101.5	101	100	99	157.5	Aircraft in conventional takeoff and land (CTOL) mode. Two J85 engines operating at 90% RPM (14850 RPM).
3	123	126	123.5	119	116	114.5	109	106.5	104.5	105	103	162.5	
4	125	130	128	121	118	112	110	108.5	106.5	106.5	106	166	
5	125	127	125.5	121	116.5	113	110	108.5	104.5	104	104.5	164	
6	123	123	122.5	120	117	113	110	108	104	102.5	102.5	162	
7	119	121	119.5	118	116	113	109.5	106.5	102.5	101	102	160	
8	113.5	116.5	115.5	114	112	109	105	101.5	99	101	102	156	
Angle, / Octave Band	**20**	**30**	**40**	**50**	**60**	**70**	**80**	**100**	**120**	**140**	**160**	**180**	
1	116.5	116	115	112.5	107.5	107	105.5	104.5	102.5	101	99.5	98.5	154.5	
2	119	120.5	120	117	113	111	109	108	104	103	102	100	159	Aircraft in CTOL mode. Two J85 engines operating at 100% RPM (16950 PPM).
3	123.5	126	125	124	118	115	112	109	107	106	105	104	164	
4	127	131	130	128	120	118	115	111	109	108.5	108	108	168.5	
5	127	130	130	125	120.5	119.5	117	113	110	108	107	106	168	
6	123	126	128	125	121	119.5	117	113	110	107	106	104	166	
7	116.5	121.5	124.5	122.5	119.5	117.5	115.5	111.5	107.5	104.5	103.5	101.5	163	
8	113.5	118.5	121.5	119.5	116.5	114.5	112.5	108.5	104.5	102.5	101.5	99.5	160	
Angle, / Octave Band	**20**	**40**	**50**	**60**	**80**	**100**	**120**	**140**	**150**	**160**	**170**	**180**		
1	85.5	89.5	89	86	86	86.5	86	85	84.5	83.5	86.5	87.5		
2	89	93	91	89.5	88.5	88.5	88.5	88.5	87	87	86	89		Aircraft in VTOL mode. Lift fans operating at 96.5% speed (965 PPM). Pitch fan operating at 43% speed (1755 RPM).
3	90	91	93	93.5	92	90.5	90.5	92	91	89	88.5	90		
4	94	93	96	97	96	96	97	95	95	90	91	92		
5	96	95	97	98	98	98	97.5	95.5	95	90.5	92.5	92		
6	95	96	97.5	100	98	97	98	96	95	91	93.5	93		
7	92	93	95	95.5	95.5	96	98	97	96.5	94	96	100		
8	89	91	91	91.5	94	101	100	100	100	96	100	105		
Angle, / Octave Band	**80**	**90**	**100**	**110**	**120**	**130**	**140**	**150**	**160**	**170**	**180**			
1	97	104.5	96	94	93	93	94	104.5	92	91	91.5			
2	96	102	95	94	94	93.5	93	101	92	93.5	95			Aircraft in VTOL mode. Lift fans operating at 67.5% speed. Pitch fan operating at 75% speed.
3	98	98	97	95	96.5	96.5	95	96	94	95.5	97			
4	99	100	100	101.5	101.5	102	102	98	95	97	99			
5	102	107	106	110	106	107	104	102	99	100	102			
6	104	107	106	110	105	107	106	103	100	102	103.5			
7	103.5	104.5	104.5	104.5	104.5	104.5	104.5	101	98.5	102.5	102.5			
8	98	100.5	100	100	100	100	100	96	97	101	102			
Angle, / Octave Band	**155**	**160**	**170**	**180**										
1	109	99	96	96										
2	103	95	95.5	96.5										Aircraft in VTOL mode. Lift fan operating at 82% speed. Pitch fan operating at 94% speed.
3	100	95	96.5	98										
4	100	97.5	98.5	98										
5	103	99	101.5	100										
6	104	101	105	103										
7	103	101	105	104.5										
8	97	97	101	101.5										

TABLE 10. TEST DATA, COMPRESSOR ANNULUS MEASUREMENTS IN SINGLE-STAGE SCALE MODEL COMPRESSOR

Measurement Location: see Figure 45

Fan Speed: 1780 RPM
Fan Fundamental Frequency: 1660 c/s

Harmonic \ Microphone Position	Sound Pressure Level (db re .0002 microbar) (Inlet Side) 1	2	3	4	5	(Discharge Side) 1	2	3	4	5	6	Sound Power Level (db re 10^{-13} watts) Inlet	Discharge	Configuration (reference Figure 44)
Fundamental	123	123	123	123	123	133	133	133	133	133	133	123	134	Fan in standard configuration.
Second	121	121	122	122	122	117	119	119	119	119	120	122	120	
Third	104	105	104	105	106	109	109	109	110	108	108	105	110	
Harmonic \ Microphone Position	1	2	3	4	5	1	2	3	4	5	6			
Fundamental	111	106	108	112	110	-	114	115	114	112	107	111	113	Fan stator row removed.
Harmonic \ Microphone Position	1	2	3	4	5	1	2	3	4	5	6			
Fundamental	127	129	126	125	127	124	125	125	125	126	127	127	126	Fan in design configuration, except rotor - stator spacing was increased to 1 in. as compared to normal 1/2 in.
Second	109	107	110	105	105	115	116	115	116	117	119	108	117	
Third	-	-	-	-	-	107	107	106	106	106	106		107	

TABLE 11. TEST DATA, SINGLE-STAGE SCALE MODEL COMPRESSOR

Measurement Location: see Figure 46
Measurement Radius: 40 ft

Fan Speed: 1780 RPM
Fan Fundamental Frequency: 1660 c/s

	Sound Pressure Level (db re .0002 microbar)																			Sound Power Level$_{3}$ (dl re 10^{-13} watts)	Configuration (reference Figure 44)
Angle, θ / Harmonic	0	5	10	15	20	25	30	35	40	45	50	55	60	65	70	75	80	85	90		
Fundamental	70	75	78	75	72	76	80	79	86	87	89	85	87	93	85	85	77	88	85		
Second	71	69	67	76	71	75	81	85	84	87	86	85	81	80	76	75	71	75	74		
Angle, θ / Harmonic	95	100	105	110	115	120	125	130	135	140	145	150	155	160	165	170	175	180			Standard configuration.
Fundamental	79	85	86	85	87	85	91	89	89	82	83	87	86	80	86	82	83	78		127	
Second	78	76	73	77	74	74	70	67	76	77	66	76	75	69	70	62	68	69		121	
Angle, θ / Harmonic	0	5	10	15	20	25	30	35	40	45	50	55	60	65	70	75	80	85	90		
Fundamental	65	67	70	67	65	67	66	71	70	65	68	69	64	64	61	55	57	59	56		
Second	61	63	64	65	63	63	62	61	64	64	63	61	57	55	-	53	-	53	53		
Angle, θ / Harmonic	95	100	105	110	115	120	125	130	135	140	145	150	155	160	165	170	175	180			
Fundamental	60	59	58	65	66	66	69	68	70	67	70	67	64	69	68	60	58	61		107	Stator row
Second	56	57	60	59	62	61	61	65	65	65	65	63	64	57	61	58	60	56		103	removed.
Angle, θ / Harmonic	0	5	10	15	20	25	30	35	40	45	50	55	60	65	70	75	80	85	90		
Fundamental	-	74	75	74	73	74	74	81	87	89	89	86	87	89	86	84	79	81	80		
Second	-	73	75	75	67	69	80	80	81	80	80	81	79	77	73	71	66	71	71		
Angle, θ / Harmonic	95	100	105	110	115	120	125	130	135	140	145	150	155	160	165	170	175	180			
Fundamental	76	78	81	81	80	81	87	80	85	80	77	73	81	71	73	76	64	68		125	Rotor-Stator spacing increased to 1 in.
Second	72	73	73	76	75	74	65	69	67	67	67	69	67	70	68	65	63	59		117	

TABLE 12. TEST DATA, DEVELOPMENT FAN VEHICLE

Measurement Location: see Figure 46
Measurement Radius: 40 ft
Fan Fundamental Frequency: 1185 c/s

	Sound Pressure Level (db re .0002 microbar)																			Sound Power Level (db re 10^{-13} watts)
Angle, θ / Harmonic	0	10	20	30	40	50	60	70	80	90	100	110	120	130	140	150	160	170	180	
Fundamental	74	81	77	76	75	77	70	76	70	71	74	73	75	77	74	72	75	68	65	110
Second	66	74	70	75	68	66	70	70	70	64	66	69	75	77	76	77	68	68	66	116
Third	77	75	77	72	74	75	70	68	73	64	68	62	75	78	70	81	78	73	63	114
Fourth	-	-	-	-	-	-	68	-	-	-	62	-	-	68	70	68	-	-	-	115

TABLE 13. TEST DATA, DEVELOPMENT FAN VEHICLE

Measurement Location: see Figure 46
Measurement Radius: 20 ft
Fan Fundamental Frequency: 1185 c/s

Angle, θ / Harmonic	Sound Pressure Level (db re .0002 microbar)																		Sound Power Level (db re 10^{-13} watts)
	0	10	20	30	40	50	60	70	80	90	100	110	120	130	140	150	160	170	
Fundamental	76	68	76	80	76	80	78	78	67	76	80	80	80	82	82	68	72	70	108
Second	74	76	73	71	73	75	80	78	72	74	70	72	73	71	82	82	80	80	114
Third	77	74	81	78	76	80	77	75	75	70	71	68	69	77	84	83	74	73	112
Fourth	-	-	77	-	-	-	-	71	-	66	-	-	-	72	75	-	78	-	113

BIBLIOGRAPHY

1. Beranek, L. L., Noise Reduction, McGraw-Hill, 1960.

2. Blokhintsev, D. I., Acoustics of a Non-Homogeneous Moving Medium, Leningrad, 1946.

3. Bragg, S. L., and Bridge, R., Noise from Turbojet Compressor, J. Royal Aeronautical Society, January 1964.

4. Courant, R., and Friedrichs, K. O., Supersonic Flow and Shock Waves, Interscience Publishers, Inc., New York, 1948.

5. Courant, R., and Hilbert, D., Partial Differential Equations, Interscience Publishers, New York, 1962.

6. Kinsler, L. E., and Frey, A. R., Fundamentals of Acoustics, John Wiley & Sons, New York, 1950.

7. Landau, L. D., and Lifshitz, E. M., Fluid Mechanics, Perganon Press, London, 1959.

8. Lindsay, R. B., Mechanical Radiation, McGraw-Hill, New York, 1956.

9. Lukasik, S. J., and Nolle, A. W., Handbook of Acoustic Noise Control, Volume I, Supplement 1, WADC Technical Report 52-204, Wright-Patterson Air Force Base, Ohio, 1955.

10. Morse, P. M., Vibration and Sound, McGraw-Hill, New York, 1948.

11. Morse, P. M., and Feshbach, H., Methods of Mathematical Physics, Volumes I and II, McGraw-Hill, New York, 1953.

12. Prince, D. C., Jr., The Flow of Air Through a Cascade, Sc. D. Thesis, Massachusetts Institute of Technology, 1951.

13. Prince, D. C., Jr., A General Survey of Cascade Design Methods, General Electric Report DF50FT560, General Electric Company, Cincinnati, Ohio, 1950.

14. Shapiro, A. H., The Dynamics and Thermodynamics of Compressible Fluid Flow, Ronald Press, New York, 1957.

15. Slutsky, S., Marion, S., Baronti, P., Esses, H., Analysis of Turbofan Sound Generation and Propagation, GASL Report No. 234, General Applied Science Laboratories, Westbury, L. I., New York, May 1961.

16. Smith, E. B., Cell Measurement of CJ805-23 Fan Noise, General Electric DIM 376, Cincinnati, Ohio, August 16, 1960.

17. Smith, E. B., Effect of Air Flow on Noise Reduction in a Duct Using Short Suppressor Strips, General Electric TIS R61FPD568, Cincinnati, Ohio, December 22, 1961.

18. Tyler, J. M., and Sofrin, T. G., Axial Flow Compressor Noise Studies, Paper No. 345D, 1961 SAE Aeronautic Meeting.

19. Watson, G. N., Theory of Bessel Functions, Cambridge University Press, Cambridge, England, 1948.

20. Weinig, F., Die Stromnug um Die Schauflen van Turbomaschinen, J. G. Barth publisher, Leipzig, Germany, 1935.

DISTRIBUTION

US Army Mobility Command	3
US Army Aviation Materiel Command	5
Chief of R&D, DA	1
US Army Transportation Research Command	19
US Army R&D Group (Europe)	1
US Army Engineer R&D Laboratories	2
Army Research Office-Durham	1
US Army Combat Developments Command Aviation Agency	1
US Army War College	1
US Army Command and General Staff College	1
US Army Transportation School	1
US Army Aviation School	1
US Army Transportation Center and Fort Eustis	1
US Army Aviation Test Board	1
US Army Aviation Test Activity	2
US Army General Equipment Test Activity	1
Air Force Systems Command, Wright-Patterson AFB	1
Air Force Flight Test Center, Edwards AFB	1
Air University Library, Maxwell AFB	1
Bureau of Naval Weapons	3
US Naval Postgraduate School	1
US Naval Air Station, Patuxent River	1
David Taylor Model Basin	1
Marine Corps Liaison Officer, US Army Transportation School	1
Ames Research Center, NASA	1
NASA-LRC, Langley Station	1
NASA Representative, Scientific and Technical Information Facility	2
Research Analysis Corporation	1
National Aviation Facilities Experimental Center	1
US Army Standardization Group, Canada	1
Canadian Liaison Officer, US Army Transportation School	1
British Army Staff, British Embassy, Washington	1
US Army Standardization Group, U.K.	1
Defense Documentation Center	20

APPENDIX I. JET ENGINE COMPRESSOR NOISE

PURPOSE

The purpose of this work is to review investigations on the generation of noise in the compressor assembly of jet engines and its subsequent propagation. Most of the reported material is not new but has been assembled from works that are given in the bibliography section. It has been edited in a manner, considered by this author, as systematic and logical in order. The problem of the noise of a compressor assembly of a jet engine is reduceable to a problem of generation and propagation of sound waves. If classical assumptions are acceptable physically, this type of investigation turns into an eigenvalue problem with the wave equation as its field equation. Thus the previous work of others is not essential.

Throughout Appendix I, the following symbols will be used in place of those listed on page xv.

(x, y, z)	Cartesian coordinates
(r, θ, z)	cylindrical coordinates
(ζ, θ, ξ)	nondimensional cylindrical coordinates
t, T	time, nondimensional time
c	velocity of sound
w	angular velocity of rotor
$\bar{v}$	stream velocity
$\bar{u}$	velocity of pressure disturbance
β	v_z/c
r_o, r_1	radii, outer and inner cylinder
ϕ	velocity potential
δ ( )	Dirac delta function
J_n, Y_n	Bessel functions
n, m, j, k	summation indexes
N_r, N_s	number of blades, rotor, stator
h	r_1/r_o

Interest in the study of compressor noise of jet engines centers about the problem of the generation of sound in the compressor and its subsequent propagation to an observer somewhere in space. The generation of noise is closely associated with the pressure fluctuations inflicted upon the medium under consideration by the compressor assembly. The propagation of noise is thus identical to the propagation of the pressure fluctuations. If one is interested in investigating these problems analytically, he would have to describe the nature of propagation of the pressure variations by means of equations called field equations representing faithfully this phenomenon.

The formal way of obtaining the field equations is to start with the fundamental laws of mechanics: namely (1) the conservation of matter, (2) the conservation of momentum, and (3) the conservation of energy. These are supplemented by the thermodynamic equations of state for the medium under consideration. If, however, it is assumed that the problem under consideration adheres adequately to the assumptions of classical acoustics, the above yield the well-known wave equation

$$\nabla^2 \phi - \frac{1}{c^2} \frac{\partial^2 \phi}{\partial t^2} = 0 \qquad (1)$$

as the field equation for the problem.

To complete the formulation of the problem, it remains to impose boundary and initial conditions upon it. These are usually dictated by the geometric and physical aspects of each individual case. For a jet engine, for example, the boundary is the core of the engine on the inside and the casing on the outside. On the boundary it is reasonable to assume that the velocity normal to the surface of the boundary is the same as that of the boundary itself. Thus, if the core and the casing are considered rigid, the velocity of the medium in the normal-to-the-surface direction is zero.

Another condition can be extracted from the continuity of flow. Since in classical acoustics changes of the state of medium are neglected, then the velocity of the fluid in the axial direction should have no jumps or discontinuities. Therefore, it is required that the axial velocity be continuous. The last condition is formulated from the action of the blades of the rotor and of the stator on the flowing medium. If the blades of the rotor, say, are equally spaced and if the rotor is rotating at some angular velocity, w, then the tangential component of the velocity should suffer a discontinuity every time a

blade passes by. Thus this condition can be expressed as a finite discontinuity of the magnitude of the tangential velocity. Now, the analytical problem of noise generation and propagation is completely defined by

$$\nabla^2 \phi - \frac{1}{c^2} \frac{\partial^2 \phi}{\partial t^2} = 0$$

$$u_1 (r_1) = u_1 (r_o) = 0$$

$$\left| u_2 \right|_{s = 0} = \text{continuous} \qquad (2)$$

$$\left| u_3 \right|_{s = 0} = f(r) \; \delta (\theta - wt)$$

where $\bar{u} = (u_1, u_2, u_3) = \text{grad } \phi$, ϕ is the acoustic potential, and δ is a Dirac delta function indicating a jump.

The solution of this mathematical problem will predict how the pressure fluctuations created by the compressor assembly propagate through the jet engine toward the intake and exhaust of it. Once the pressure waves find themselves at the open ends of the jet engines, they will disperse through the surrounding space. This is called radiation of the pressure waves, and the manner by which they radiate will determine the intensity, directivity and frequency by which they reach an observer. Here, again, some clarifications of the boundary conditions of the radiating surface are necessary. One simple way of looking at this part of the problem is to imagine that the whole space is separated into two parts by a surface containing the radiating faces. The radiating faces (in this case the open end of the engine) are characterized by the pressure fluctuating as predicted by the propagation part of the solution; the rest of the surface is rigid. This is all that is necessary to calculate the radiation field completely, outside of a description of the medium itself.

It should be pointed out that, while the above statements contain all the fundamental parts necessary for the study of noise generation and propagation by the compressor assembly of a jet engine, it is also a simplification of the overall problem, as it will be shown subsequently.

A schematic representation of the problem of generation, propagation and radiation of noise is given in Figure 55.

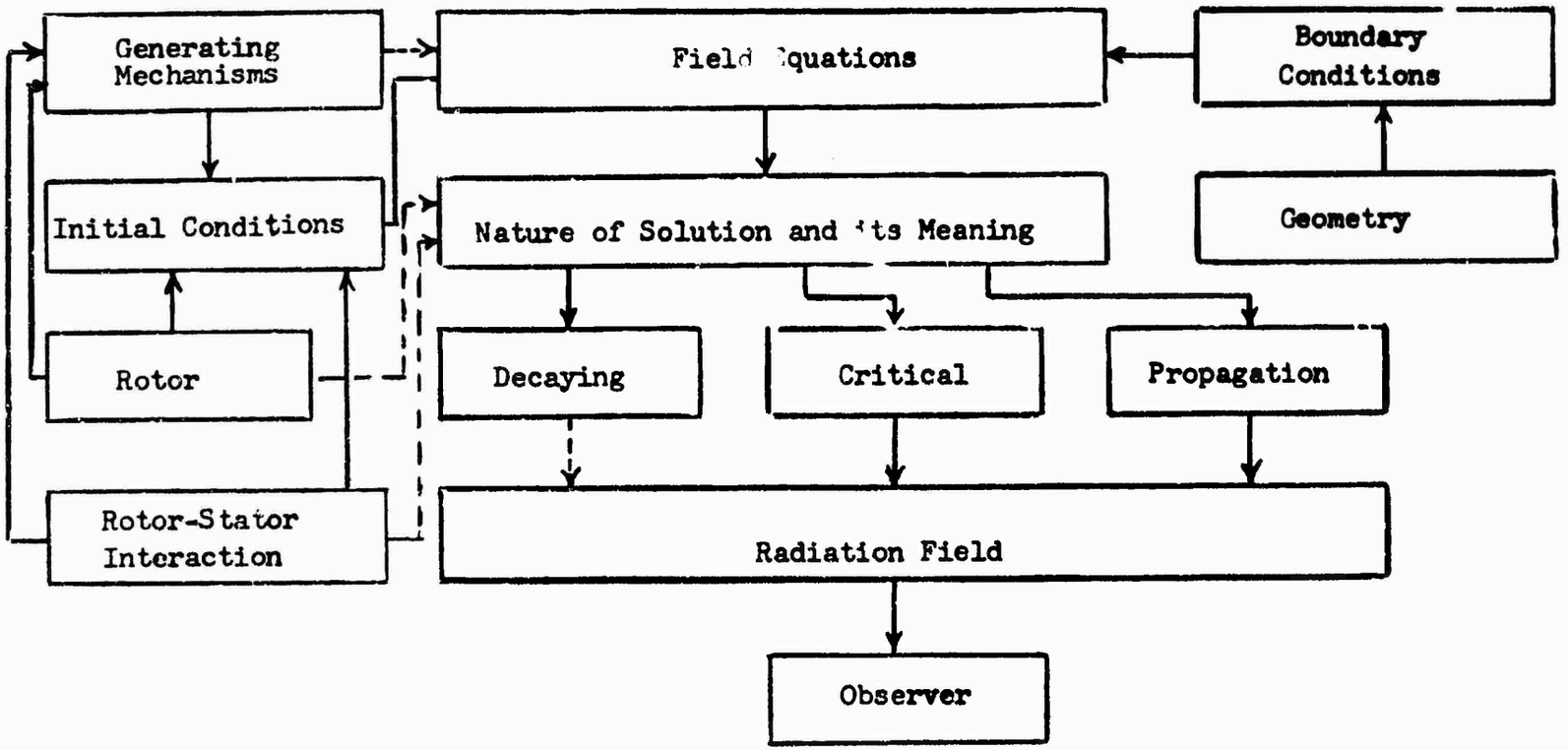

Figure 55 . Evolution of the Noise Problem.

With this brief introduction to the fundamental problem, one now can undertake the formulation and solution of the jet engine noise in a systematic manner. The basic approach is rather fixed, as indicated in Figure 55. There is, however, quite a choice in the order. Some authors prefer to start with the effect of the rotor and of the rotor - stator interaction on the solution of the field equations. Others choose to formulate the eigenvalue problem first and obtain its solution, then inject the rotor and rotor - stator effects to narrow the solution to the specific problem at hand. The final results should be the same regardless of the choice. In this review the following subjects shall be discussed.

(1) The formulation of the eigenvalue problem from the physical and geometric aspects of the jet engine.

(2) The solution and its meaning. The influence of the rotor effects and rotor - stator interaction on the critical speed.

(3) Important aspects of the obtained solution. A discussion of the design parameters which enter into the significant results of the solution and if possible their effect on noise characteristics.

The radiation of the acoustic waves into surrounding space will not be discussed in this report since it will be covered extensively in subsequent work.

THE MATHEMATICAL PROBLEM

The first commitment made here is adherence to the classical acoustics. The meaning of this assumption is that the behavior of the pressure fluctuations is described by the classical wave equation. Inherently this equation of acoustic waves implies that the pressure fluctuations are very small. This is most likely an incorrect assumption, but the price for a more accurate description is the introduction of nonlinear terms in the field equations, which mean an extremely difficult problem from the very start. Thus, it is probably wiser to accept the lack of proper description at this point for the sake of accessibility to a formal solution. Therefore, the field equation employed for this kind of work is

$$\nabla^2 \phi - \frac{1}{c^2} \frac{\partial^2 \phi}{\partial t^2} = 0$$

where ϕ is the acoustic potential, or velocity potential as sometimes called.

The second simplification is on the geometry of the jet engine. The core and the enclosure of the engine are approximated by two concentric cylinders. The region of interest to this problem is the annulus contained between the inner and outer cylinders. Furthermore, it is assumed that the annulus region extends from $-\infty$ to $+\infty$ in the axial direction. The exaggeration is imposed in order to make the subsequent mathematical problem more accessible. It means that it is not necessary to have any boundary conditions at some finite length from the compressor assembly to worry about. The introduction of this simplification has an effect on the magnitude of the reflected wave. But it has been pointed out that this influence may be neglected without great sacrifice to the practical aspects of the problem.

Next it is assumed that the surfaces (walls) of the concentric cylinders are rigid. This implies that, since the walls are non-deformable, the mechanical vibration of the core and the enclosure of the jet engine are neglected. Experts claim that the coupling between the acoustic pressure waves and the characteristics of the surrounding structures is not of importance in the problem under consideration.

Figure 56 shows what the jet engine looks like after the above simplifications have been introduced.

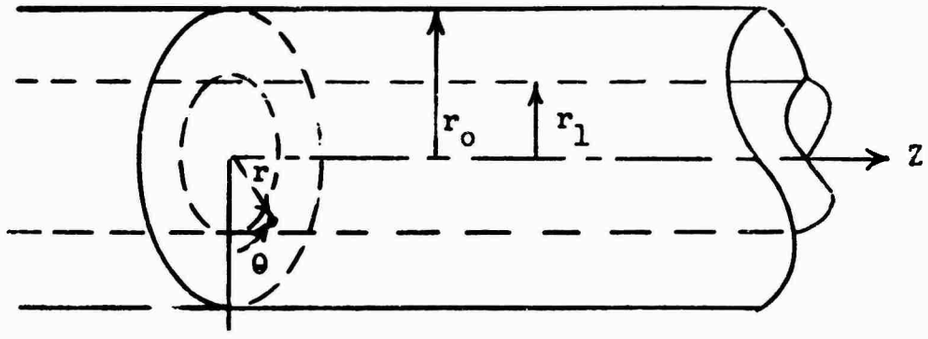

Figure 56. Mathematical Model.

Now introduce a cylindrical coordinate system (r, θ, z) as shown in Figure 56. Then the problem put in mathematical form becomes:

$$\nabla^2\phi - \frac{1}{c^2}\frac{\partial^2\phi}{\partial t^2} = 0 \qquad (3)$$

$$u_1 (r_o) = u_1 (r_1) = 0 \tag{4}$$

$$\left| u_2 (z = 0) \right| = f(r)\ \delta(\theta - wt) \tag{5}$$

$$u_3 (z = 0) = \text{continuous} \tag{6}$$

where u_1, u_2, u_3 are the velocity components in the r, θ and z directions respectively. Equations (4) through (6) are the boundary conditions of the problem. Equation (4) is a consequence of the rigidity of the walls. Equation (5) expresses the fact that the tangential component of the velocity varies with the radius and that its magnitude contains finite discontinuities due to the chopping of the blades. Equation (6) states that the flow in the axial direction is continuous. Condition (5) further states dependence of the velocity on the angular velocity of the blades and also on the position of the point. Some authors prefer to use different boundary conditions instead of (5). For example, they assume that the pressure distribution at the plane z = 0 is known.

$$p (r, \theta, 0, t) = f (r, \theta, 0, t) \tag{7}$$

This is not unreasonable since one can measure the pressure at some convenient plane and use it as a datum. This, however, commits the problem immediately to numerical methods and also divorces the analytical problem completely from the design of the compressor. The choice here is mostly dictated by the experimental approach one wishes to use. In this review the former formulation is preferred due to its possible tie with compressor-blade design.

Introducing the nondimensional coordinates (ζ , θ, ξ) such that

$$\begin{aligned} r &= r_o \zeta & Z &= r_o \xi \\ \theta &= \theta & t &= r_o \frac{\mathcal{I}}{c} \end{aligned} \tag{8}$$

Equation (3) expressed in the cylindrical coordinates (ζ, θ, ξ) and τ becomes

$$\left(\frac{\partial^2}{\partial \zeta^2} + \frac{1}{\zeta} \frac{\partial}{\partial \zeta} + \frac{1}{\zeta^2} \frac{\partial^2}{\partial \theta^2} + \frac{\partial^2}{\partial \xi^2} - \frac{\partial^2}{\partial \tau^2} \right) \phi = 0 \tag{9}$$

Now assume that $\phi = \phi(\zeta, \theta, \xi; \tau)$ is of the form

$$\phi = R(\zeta)\, Z(\xi)\, \Theta(\theta - w\tau) \tag{10}$$

where the $\Theta = \Theta(\theta - wt)$ is suggested by condition (5). Furthermore, the equal spacing of all blades and the angular velocity of the rotor suggest that Θ is periodic, and of the form

$$\Theta = e^{in(\theta - wt)};$$

therefore,

$$\phi = R(\zeta)\, Z(\xi) e^{in(\theta - wi)}. \tag{11}$$

Substituting (11) into (9), one obtains

$$\begin{aligned} Z(\xi) &= A_m e^{im\xi} + B_m e^{-im\xi} \\ R(\zeta) &= C_n J_n(\lambda_{nm}\zeta) + D_n Y_n(\lambda_{nm}\zeta) \\ \lambda^2_{nm} &= n^2 w^2 - m^2 \end{aligned} \tag{12}$$

and the velocity potential has the form

$$\begin{aligned} \phi(\zeta, \theta, \xi, \tau) = &\left\{A_m e^{im\xi} + B_m e^{-im\xi}\right\} \cdot \left\{C_n J_n(\lambda_{nm}\zeta)\right. \\ &\left. + D_n Y_n(\lambda_{nm}\zeta)\right\} \cdot \left\{e^{in(\theta - w\tau)}\right\}. \end{aligned} \tag{13}$$

Now the boundary conditions (4) through (6) are utilized to determine the arbitrary constants introduced into the analytical problem. The nondimensional variables introduced by equation (8) are used. Equation (4) yields

$$\frac{\partial}{\partial\zeta}\phi(h, \theta, \xi, \tau) = 0; \quad \frac{\partial}{\partial\zeta}\phi(1, \theta, \xi, \tau) = 0; \quad h = \frac{r_1}{r_o}$$

or

$$C_n J_n'(h\lambda_{nm}) + D_n Y_n'(h\lambda_{nm}) = 0$$
$$C_n J'(\lambda_{nm}) + D_n Y'(\lambda_{nm}) = 0$$

Solving for C_n and D_n, one obtains the characteristic equation

$$J_n'(\lambda_{nm})\, Y_n'(h\lambda_{nm}) - J_n'(h\lambda_{nm})\, Y_n'(\lambda_{nm}) = 0 , \qquad (14)$$

whose solution yields the values of λ nm which satisfy boundary conditions (4). Note again that

$$\lambda_{nm}^2 = n^2w^2 - m^2 \quad \text{or} \quad m^2 = n^2w^2 - \lambda_{mn}^2 . \qquad (15)$$

Equation (6) requires $\left|U_3\right|_s = 0$ = continuous or

$$\left.\frac{\partial \phi}{\partial \xi}\right|_{\xi = 0+} = \left.\frac{\partial \phi}{\partial \xi}\right|_{\xi = 0-} . \qquad (16)$$

Substituting (13) into (16), one finds that

$$A_m = -B_m . \qquad (17)$$

Condition (5) can be approached in the following manner: consider a vortex of intensity $\Gamma(r)$ created by a blade; then

$$\Gamma(r) = \oint u_2 ds = r_o \int \left|u_2\right| \zeta \, d\theta .$$

By equation (5) this becomes

$$\Gamma(\zeta) = r_o \zeta f(\zeta) .$$

Thus equation (5) can be written as

$$\left|u_2(\zeta, \theta, \upsilon, \tau)\right| = \frac{\Gamma(\zeta)}{\zeta r_o} \delta(\theta - w\tau) ;$$

and since there are N blades, then

$$\left| u_2 (\zeta, \theta, 0, \tau) \right| = \sum_{j=1}^{N} \frac{\Gamma_j(\zeta)}{r_o \zeta} \delta(\theta + \frac{2\pi j}{N} - w\tau) .$$

Introducing the potential function ϕ, one obtains

$$\left| \frac{\partial \phi}{\partial \theta} \right|_{s=0} = \Gamma(\zeta) \sum_{j=1}^{N} \delta(\theta + \frac{2\pi j}{N} - w\tau) \qquad (18)$$

under the assumption of identical blades, thus equal vortex intensity $\Gamma(\zeta)$. Now, using equations (13) and (17),

(19)

$$\left. \frac{\partial \phi}{\partial \theta} \right|_{s=0} = \sum_{n} \sum_{m} 2 \text{ in } A_{nm} e^{\text{in}(\theta - w\tau)} \left\{ C_n J_n(\lambda_{nm}\zeta) + D_n Y_n(\lambda_{nm}\zeta) \right\}.$$

Then by Fourier-Bessel expansion, (18) and (19) yield

$$A_{nm} = \frac{N}{4 \text{ in } \pi} \int_h' \zeta \Gamma(\zeta) \bar{R}(\zeta) \, d\zeta \qquad (20)$$

where

$$\bar{R}(\zeta) = C_n \bar{J}_n (\lambda_{mn}\zeta) + D_n \bar{Y}_n (\lambda_{nm}\zeta)$$

is the normalized form.

Thus the completely defined solution, ϕ, for this problem is

$$\phi(\zeta, \theta, \xi, \tau) = \sum_{n=KN}^{\infty} \sum_{m=1}^{\infty} A_{nm} e^{\text{in}} \left\{ (\theta - w\tau) + \sqrt{(n^2 w^2 - \lambda^2_{nm})}\xi \right\} \bar{R}(\lambda_{nm}\zeta) \qquad (21)$$

where $K = \frac{n}{N}$ = integer. This obviously is a restriction on n, which comes from mathematical considerations; but, as will be shown later, it is physically necessary also. It merely says that the index n has to be a multiple of the number of blades, N.

It is possible now to draw some conclusions without considering the rotor - stator assembly any further. Examining equation (21), it is evident that the critical component of the solution is the exponential term,

$$e^{in\left\{(\theta - wT) + \sqrt{n_2 w_2 - \lambda^2_{nm}\xi}\right\}} \quad ,$$

and in particular the coefficient of ξ. If the argument of the radical is a positive number, then the solution in z-direction will be sinusoidal in nature; thus the ϕ solution, and therefore the acoustic waves, will be propagated without attenuation in z. If the argument of the radical is negative, then the z-solution is exponentially decaying; thus the acoustic waves are attenuating. Therefore, if

$$w > \frac{\lambda_{nm}}{n} \implies \text{propagation in } z \tag{22}$$

$$w < \frac{\lambda_{nm}}{n} \implies \text{decay in } z \tag{23}$$

and

$$w = \frac{\lambda_{nm}}{n} = w^{\circ}_{nm} \quad \text{critical speed.} \tag{24}$$

This w°_{nm} is quite often referred to as the cutoff speed. It depends, so far, on the eigenvalues of the wave equation, which were imposed by the rigidity of the boundary. It will be shown, in the next paragraphs, that the critical speed depends on the interaction (or interference) of the rotor - stator system, the tip Mach number, the spin velocity, etc.

THE CRITICAL SPEED

In the previous section the motion of acoustic waves in the jet engine has been discussed and its dependence on such variables as the geometric shape of the engine (through λ_{nm}), the speed of the rotor w, and the number of blades (through n = KN) has been indicated. The influence of the rotor - stator assembly and of the flow velocity on the critical parameters $\{\lambda_{nm}, w, n, \Gamma(\zeta)\}$ and subsequently on the critical speed w°_{nm} will be undertaken in this section.

THE ROTOR EFFECTS

The formulation of the problem in the previous section is essentially the problem of generation of acoustic waves by a rotor. It remains now to justify some of the assumptions made there. At first the pressure fluctuations are created by the rotating blades. Therefore, the pressure field is spinning around with the same angular velocity as the rotor. Hence if one expressed the pressure with respect to a blade, the pressure would be expressed in terms of its position with respect to that blade. If, however, the reference frame is stationary, then the θ component of the pressure will have to be corrected by wt, the arc traveled by the blade in time t. Thus the dependence of the pressure field on θ and t has the general form

$$P(\theta, t) = P(\theta - wt).$$

This is consistent with the form of traveling waves.

If the blades are assumed to be equally spaced and identical in design, then the pressure fluctuations will be periodic in nature with a period $\frac{1}{Nw}$, N being the number of blades. Thus the pressure function has the form

$$P(\theta, t) = P\left\{N(\theta - wt)\right\},$$

which is the same as obtained previously, where the index of summation is $n = kN$, k = integer, rather than $n = 1, 2, 3 \ldots$. As for the critical speed $w^{\bullet}_{nm}$, the previous remarks remain unchanged, for the "rotor only" case.

THE ROTOR - STATOR INTERFERENCE

The interaction of the rotor - stator assembly is caused by the cutting of rotor waves by the stator blades, the cutting of the stator wakes by the rotor, and interference on rotating pressure patterns. While their relative influence depends on the geometry of the blades, their relative distance, the aerodynamic aspects of flow, and whether one deals with viscous wakes or nonviscous vorticity sheds, they all have one common property: the same periodic recurrence. Therefore, the periodic behavior of these interactions will be discussed first.

Consider a rotor and a stator, concentric to each other, the rotor having N_r blades and the stator having N_s blades, both being equally spaced

over a 2 π interval. The periodic nature of the pressure field in θ and t is expressed by the relationship

$$P(\theta, t) = P(\theta + \bar{\theta}, t + \bar{t}) \tag{25}$$

The intervals $\bar{\theta}$ and $\bar{t}$ can be obtained as follows: Let, at time t_o, a blade of the rotor, say, number 1, be located opposite a blade of the stator, say, also number 1. If $N_r \neq N_s$, then the rest of the blades are not centered with respect to their rotor or stator counterparts. Since the rotor is rotating with angular velocity w, it will take

$$t = \frac{\Delta\theta}{w} \quad ; \quad \Delta\theta = \frac{2\pi}{N_s} - \frac{2\pi}{N_r} \quad \text{for } N_r > N_s \tag{26}$$

time to have the next pair of rotor and stator blades centered with respect to each other. This relatively equivalent position of the stator and rotor position is repeated at intervals of time of intergal multiples of $\frac{\Delta\theta}{w}$. Thus

$$\bar{t} = \frac{\Delta\theta}{w} \quad . \tag{27}$$

In the period of time $\bar{t}$, the pressure pattern has traveled along from stator blade 1 to a neighboring stator blade, say, 2. The arc interval is obviously $\frac{2\pi}{N_s}$. As the rotor rotates by another $\Delta\theta$, the pressure pattern shifts by another $\frac{2\pi}{N_s}$. Therefore,

$$\bar{\theta} = \frac{2\pi}{N_s} \quad . \tag{28}$$

The angular velocity with which the pressure field swirls around is now

$$\bar{w} = \frac{\bar{\theta}}{\bar{t}} = \frac{N_r}{N_r - N_s} \, w = \frac{N_r}{\Delta N} \, w \quad . \tag{29}$$

Next it is realized that the period on θ is $\frac{2\pi}{\Delta N}$; thus, in view of the comment under "The Rotor Effects", one can express the pressure field as

$$p(\theta, t) = \psi(\theta - \bar{w}\, t) \quad f(t) \tag{30}$$

where f (t) is a time function due to the fact that θ and t do not rotate. However, since the frequency on time is $\frac{\bar{w}}{\bar{\theta}}$, f (t)

may be expanded in series

$$f(t) = \sum_{j} e^{-2i\pi j \frac{\bar{w}}{\bar{\theta}} t} \tag{31}$$

and consequently (30), after similar expansion, yields

$$P(\theta,t) = \sum_{j,k} e^{ik\Delta N(\theta-\bar{w}t)} e^{-2\pi ij\frac{\bar{w}}{\bar{\theta}} t} \tag{32}$$

or

$$P(0,t) = \sum_{j,k} e^{ik\Delta N\theta} e^{-i\bar{w}\left(k\Delta N + \frac{2\pi}{\bar{\theta}} j\right) t} . \tag{33}$$

Examination of equations (32) and (33) yields the following information:

(1) The pressure field rotates with angular velocity

$$\frac{N_r}{N_r - N_s} w \tag{34}$$

in distinction to w for the pure rotor case.

(2) The general expression of the harmonics generated is given by

$$\bar{w}\left(k\Delta N + \frac{2\pi}{\theta} j\right) = w\left(kN_r + j\frac{N_r N_s}{\Delta N}\right). \tag{35}$$

Equations (32) and (33) define the nature of the acoustic potential in θ and t for the case of rotor - stator interaction. The wave propagation for this case is identical to the problem solved previously except for the $\ominus$ component, which assumes the form given by equations (32) and (33). Thus the potential is given by

$$\phi = r_o c \sum_{k} \sum_{j} \sum_{m} A_{kjm}\left(e^{ik\Delta N(\theta-\bar{w}t)} e^{-2i\pi j\frac{\bar{w}}{\bar{\theta}}t} e^{-ik_{kjm}\xi}\right)\left(\bar{R}(\lambda_{nm}\zeta)\right) \tag{36}$$

where row the coefficient of ξ, k_{kjm} is given by

$$k_{kjm} = \left[\left(kN_r + j\,\frac{N_r\,N_s}{\Delta N}\right)^2 w^2 - \lambda_{n\,m}^2\right]^{1/2} \qquad (37)$$

with the restriction on n = k . N, n = integer.

The critical speed, in general, will be

$$w_{nm}^{\circ} = \frac{\lambda_{nm}\,\Delta N}{kN_r\Delta N + j\,N_r\,N_s} \quad . \qquad (38)$$

Assuming j = 0, since it appears that the contribution of the j's will be in high harmonics, one obtains

$$w_{nm}^{\circ} = \frac{\lambda_{nm}}{k\,N_r} = \frac{\Delta N}{N_r}\left(\frac{\lambda_{nm}}{n}\right) \quad . \qquad (39)$$

Equation (39) compared with equation (24) indicates that the critical speed changes by a factor of $\Delta N/N_r$, with frequencies of the interaction between rotor and stator being harmonics of N_r w (of the pure rotor case), for the case of j = 0.

THE EFFECT OF CONSTANT SUBSONIC FLOW

So far, the problem under consideration has been for sound propagation in a medium standing still. The case of the stream moving with a velocity $\bar{V}$,/ $\bar{V}$ / <C, subsonic and constant in magnitude will be developed. The same result may be obtained if one considers the medium at rest and the sound source moving with - $\bar{V}$ velocity. The field equation to start with is the same,

$$\nabla^2 \phi - \frac{1}{c^2}\,\frac{\partial^2 \phi}{\partial t^2} = 0,$$

and the position of the source is (x* (t), y* (t), z* (t)). Introducing the new variables,

$$\begin{aligned} \bar{x} &= x - x^*(t) \\ \bar{y} &= y - y^*(t) \\ \bar{z} &= z - z^*(t) \\ t &= t\,. \end{aligned} \qquad (40)$$

The transformation introduces the change in ϕ:

$$\phi(x, y, z, t) = \phi\left\{\bar{x} + x^*(t), \bar{y} + y^*(t), \bar{z} + z^*(t); \quad t\right\} . \quad (41)$$

Substituting into the wave equation, one obtains the proper form of the field equation for a moving medium:

$$\nabla^2 \phi - \frac{1}{c^2} \frac{\partial^2 \phi}{\partial t^2} + \frac{1}{c^2} \left\{2(\bar{v}\cdot\nabla) \frac{\partial \phi}{\partial t} - (\bar{v}\cdot\nabla)(\bar{v}\cdot\nabla)\phi + \left(\frac{\partial \bar{v}}{\partial t}\cdot\nabla\right)\phi\right\} = 0. \quad (42)$$

Uniform Axial Flow

This case is characterized by

$$\bar{v} = \left[0, 0, v_z\right] \quad (43)$$

$$v_z = \text{constant} .$$

Substituting equation (43) into (42) yields

$$\nabla^2\phi - \frac{1}{c^2} \frac{\partial^2 \phi}{\partial t^2} + \frac{2v_z}{c^2} \frac{\partial^2 \phi}{\partial t \partial \bar{z}} - \frac{v_z^2}{c^2} \frac{\partial^2 \phi}{\partial \bar{z}^2} = 0 . \quad (44)$$

Introduce now the variables in cylindrical coordinates

$$r = r_o \zeta \quad ; \qquad \bar{z} = r_o \frac{\xi - \beta\tau}{\sqrt{1-\beta^2}}$$

$$\theta = \theta \quad ; \qquad t = r_o \frac{\tau}{c} \quad ; \quad \beta = \frac{v_z}{c} \quad (45)$$

and the field equation assumes the form

$$\nabla^2\phi - \frac{\partial^2 \phi}{\partial \tau^2} + \frac{2\beta}{\sqrt{1-\beta^2}} \frac{\partial^2 \phi}{\partial \xi \partial \tau} = 0 . \quad (46)$$

The solution to equation (46) is obtained, as shown previously, by the method of separation of variables, and is of the same form as equation (21). The difference is in $\bar{z}$, where the factor $\frac{1}{\sqrt{1-\beta^2}}$ is included in ξ and τ.

Thus

$$\phi(\zeta, \theta, \xi, \tau) = \sum_n \sum_m A_{nm} e^{in\left\{(\theta - \bar{w}\tau) + \alpha_{nm}\xi\right\}} \bar{R}(\lambda_{nm}\zeta) \quad (47)$$

and

$$\bar{w} = \frac{w}{\sqrt{1-\beta^2}}$$

$$\alpha_{nm} = n\left\{\pm\left[\left(\frac{\bar{w}}{1-\beta^2}\right)^2 - \frac{\lambda_{nm}^2}{n^2(1-\beta^2)}\right]^{\frac{1}{2}} - \frac{\bar{w}\beta}{1-\beta^2}\right\}. \quad (48)$$

The critical speed is obtained by setting $\alpha_{nm} = 0$; thus, from equation (26), one gets

$$\bar{w}_{nm}^{\circ} = \frac{\lambda_{nm}}{n} \quad (49)$$

or

$$\bar{w}_{nm}^{\circ} = \sqrt{1-\beta^2}\ \frac{\lambda_{nm}}{n}. \quad (50)$$

This indicates that the critical speed or cutoff speed decreases as v_z or β increases. Similarly, one can obtain the effect of moving medium on the rotor - stator system. The critical or cutoff speed in the case of a one-stage compressor becomes

$$w_{nm}^{\circ} = \frac{\sqrt{1-\beta^2}}{kN_r + j\frac{N_s N_r}{\Delta N}}\ \lambda_{nm} \quad (51)$$

in contradistinction to equation (38). For more complicated cases, such as the inclusion of swirl velocity, one proceeds in a similar way by introducing a set of variables, as in equation (44), where

$$\textcircled{H} = r_o \frac{\theta \gamma T}{\sqrt{1 - \gamma^2}} \qquad \gamma = \frac{w^* r_o}{c} \qquad (52)$$

where w^* is the swirl velocity.

APPENDIX II. THE INCOMPRESSIBLE PRESSURE FIELD OF A FLAT PLATE CASCADE

Weinig (reference 20) concluded that the incompressible, inviscid flow performance of any cascade could be described in terms of an "equivalent flat plate cascade". Weinig and many others, including the present author (references 12 and 13), have developed techniques for quantitative demonstration of the equivalence between real cascades and flat plate cascades. With the help of modern computing machinery, some of these methods could be used to evaluate pressure fields for real cascades. For qualitative evaluation, however, consideration of the flat plate cascade can be useful.

The development of reference 20 shows that the field of velocity components of a flat plate cascade (Figure 57) may be described parametrically in terms of a "picture plane", Figure 58.

$$w = u_x - iu_y = c\,\frac{\zeta - \zeta_s}{\zeta - \zeta_L} \tag{53}$$

$$\frac{x}{s} + i\,\frac{y}{s} = \frac{1}{2\pi}\left\{\ln\,\frac{\zeta + 1 - ih}{\zeta - 1 - ih} + e^{2i\beta}\,\ln\,\frac{\zeta + 1 + ih}{\zeta - 1 + ih}\right\} \tag{54}$$

Suitable algebraic expressions are available relating picture plane parameters h, ζ_L, ζ_s to the physical plane geometric parameters u_s and β, and the aerodynamic variables β_1 and β_2. The identification of values of the parameter corresponding to physical plane points on a desired contour, such as a vertical line at a specified distance from the cascade, is a formidable job for a desk calculation, but can be done expeditiously with the help of the IBM 7094 computer. Some representative results are shown on Figure 2. It is clear that the magnitude of the velocity fluctuations seen by an observer moving parallel to the cascade axis diminishes very rapidly with distance, either upstream or downstream.

An analytical expression for the decay rate may be deduced from equations (53) and (54) . In the region far upstream from the cascade, equation (54) is effectively

$$\frac{x}{s} + i\,\frac{y}{s} = \frac{1}{2\pi}\,\ln\,(\zeta + 1 - ih) + c_1 \,. \tag{55}$$

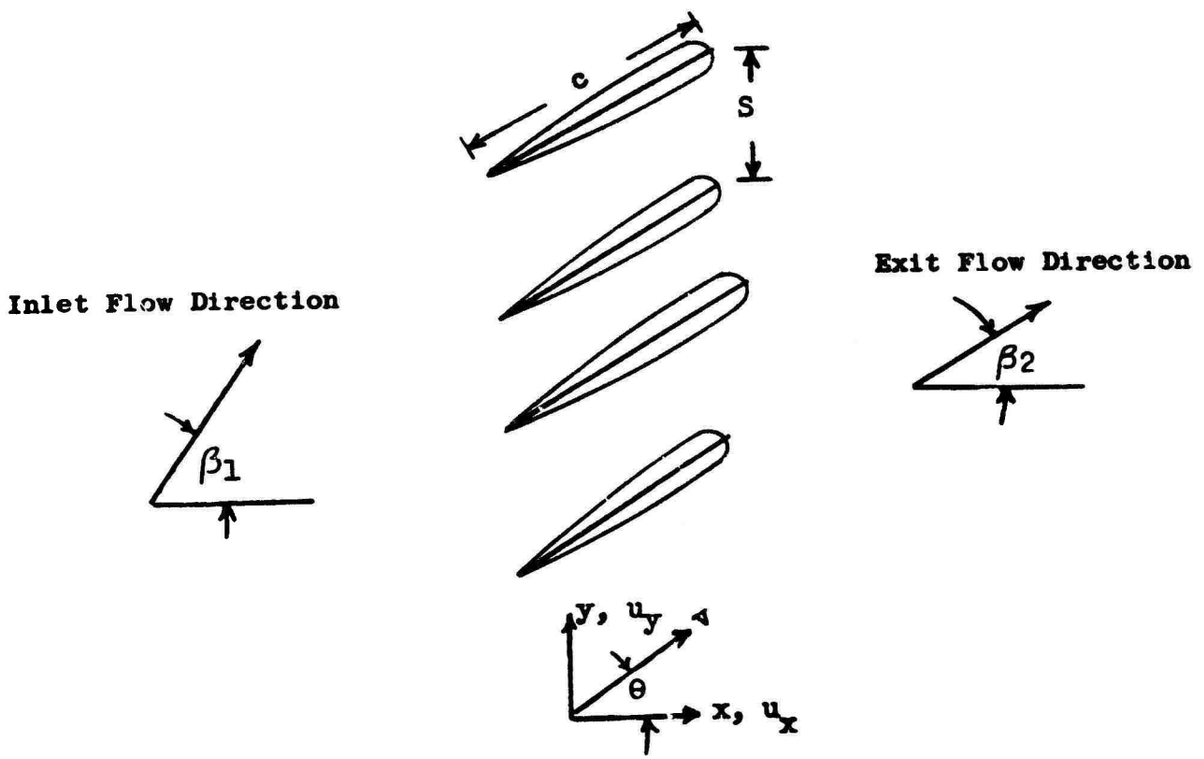

Figure 57. Velocity components of a flat plate cascade

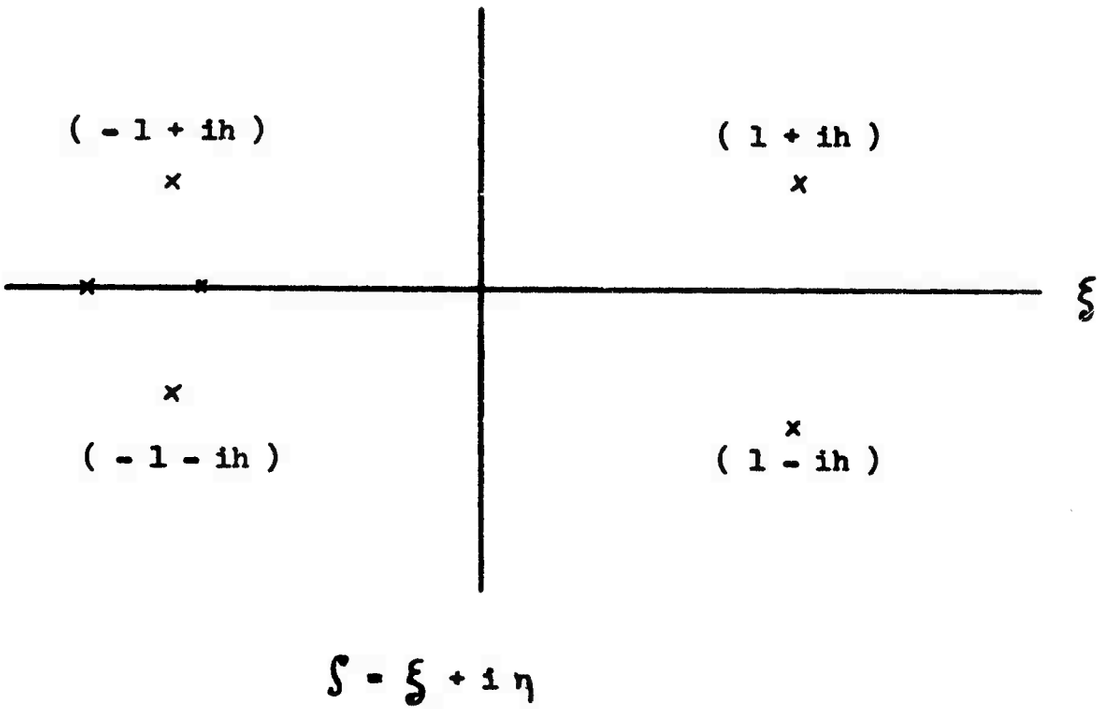

Figure 58. Picture Plane for Flat Plate Cascade.

If the vector distance of the parameter ζ from the image of upstream infinity, $(-1 + ih)$, is expressed in polar form, $r\,(e)^{i\theta}$, then

$$\ln (\zeta + 1 - ih) = \ln r + i\,\theta \tag{56}$$

so that the distance between two points (x_1, y_1) and (x_2, y_2) is

$$\frac{x_2 - x_1}{s} + i\,\frac{y_2 - y_1}{s} = \frac{1}{2\pi} \ln \frac{r_2}{r_1} + i \left(\frac{\theta_2 - \theta_1}{2\pi} \right) . \tag{57}$$

Then, if the two points have the same ordinate, $(y_2 = y_1)$,

$$\frac{r_2}{r_1} = \exp \left[2\pi \frac{(x_2 - x_1)}{s} \right] . \tag{58}$$

Equation (53), conveniently expressed in logarithmic form, can be developed as a Taylor series based on the image of upstream infinity:

$$W = \ln(u_x - i\,u_y) = \ln c + \ln (\zeta - \zeta_s) - \ln (\zeta - \zeta_L)$$

$$= W_\infty + \left[\frac{1}{(-1 + ih) - \zeta_s} - \frac{1}{(-1 + ih) - \zeta_L} \right] (\zeta + 1 - ih) + 0\,(\zeta + 1 - ih)^2 . \tag{59}$$

Neglecting the quadratic and higher order terms, and using the polar form for the vector distance, as in (56),

$$W - W_\infty = c'\, r\, e^{i\theta} . \tag{60}$$

It is also convenient to use a polar form for the velocity vectors

$$\left.\begin{aligned} u_x - i\,u_y &= v\, e^{-i\phi} \\ W &= \ln v - i\,\phi \end{aligned}\right\} .$$

Now, applying (60) and (61) to a point far upstream from the cascade, where the local velocity magnitude is not much different from that at infinity,

$$\ln \frac{v}{v_\infty} - i\,(\phi - \beta_\infty) = \ln\left(1 + \frac{v - v_\infty}{v_\infty}\right) - i\,(\phi - \beta_\infty)$$

$$\approx \frac{v - v_\infty}{v_\infty} - i\,(\phi - \beta_\infty)$$

$$= r\left[\mathrm{Re}\,(c')\cos\theta - \mathrm{Im}\,(c')\sin\theta\right] + in\left[(\mathrm{Re}\,(c')\sin\theta + \mathrm{Im}\,(c')\cos\theta\right] . \quad (62)$$

Then the real part of (62) may be applied to the two points (x_1, y_1) and (x_2, y_2) with the same ordinates $(y_2 = y_1)$:

$$\frac{\dfrac{v_2 - v_\infty}{v_\infty}}{\dfrac{v_1 - v_\infty}{v_\infty}} = \frac{r_2}{r_1} \quad . \quad (63)$$

Now, substituting (58) into (63),

$$\frac{v_2 - v_\infty}{v_1 - v_\infty} = \exp\left[2\pi\,\frac{(x_2 - x_1)}{s}\right] . \quad (64)$$

If (x_2, y_2) is farther from the cascade than (x_1, y_1), the exponential is negative, demonstrating a rapid decay rate. This rate is approximately a factor of 530 for each blade spacing away from the cascade, which is consistent with Figure 2. The rate is also approximately 55 db for each blade spacing, and appears to be quite close to Figure 14 of reference 18.

The analysis downstream of the cascade is similar, except that the logarithm in (55) is negative, which leads to a sign change in the exponent of (64).

APPENDIX III. SUBSONIC COMPRESSIBLE FLOW INFLUENCE ON THE PRESSURE FIELD OF A CASCADE

In the study of noise generation and propagation from the compressors and fans of aircraft jet engines, one of the mechanisms investigated has been the inviscid pressure field associated with an isolated cascade. Reference 18 gives a treatment of this feature which makes it appear to be fundamentally dependent on cylindrical geometry. Actually, the subsonic results appear to be primarily two-dimensional, as can be seen in the following analysis based on the Karman-Tsien approach.

A logarithmic hodograph plane, Figure 59, is the basis for the quasi-conformal transformation relating the complex velocity potential, the complex velocity, and the physical plane coordinates, Figure 60, far away from a cascade. In this plane

$$\zeta = \omega_\infty - i\beta_\infty \tag{65}$$

represents the flow conditions without the disturbances due to individual blades.

$$\begin{aligned}\zeta &= \omega - \omega_\infty - i(\lambda - \beta_\infty) \\ &= \omega' - i\lambda'\end{aligned} \tag{66}$$

represents the disturbance velocity, which, if related to physical plane coordinates, produces the sound sensation. The compressible velocity function, ω, is related to the ratio of the actual velocity to the undisturbed velocity, $\frac{V}{V_\infty}$, with the Mach number M of the undisturbed flow as parameter, by

$$\omega = \ln \frac{2\left(\frac{V}{V_\infty}\right) M_\infty / \sqrt{1 - M_\infty^2}}{1 + \sqrt{1 + \left[\left(\frac{V}{V_\infty}\right)^2 M_\infty^2 / \sqrt{1 - M_\infty^2}\right]}} . \tag{67}$$

A suitable complex velocity potential is

$$\begin{aligned}\omega &= \phi + i\,x \\ &= \Gamma \exp(\zeta_\infty) / 2\pi \ln(\zeta') + 0(\zeta').\end{aligned} \tag{68}$$

In the regime of interest, the terms $0(\zeta')$ may be neglected in comparison with the logarithm.

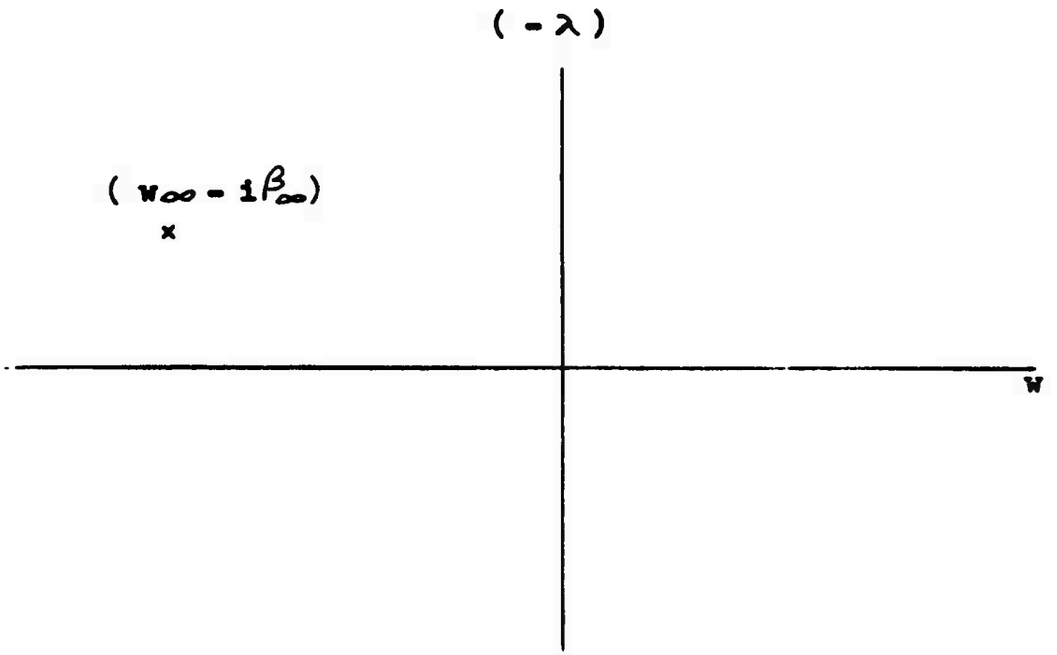

Figure 59. Logarithmic Modograph Plane.

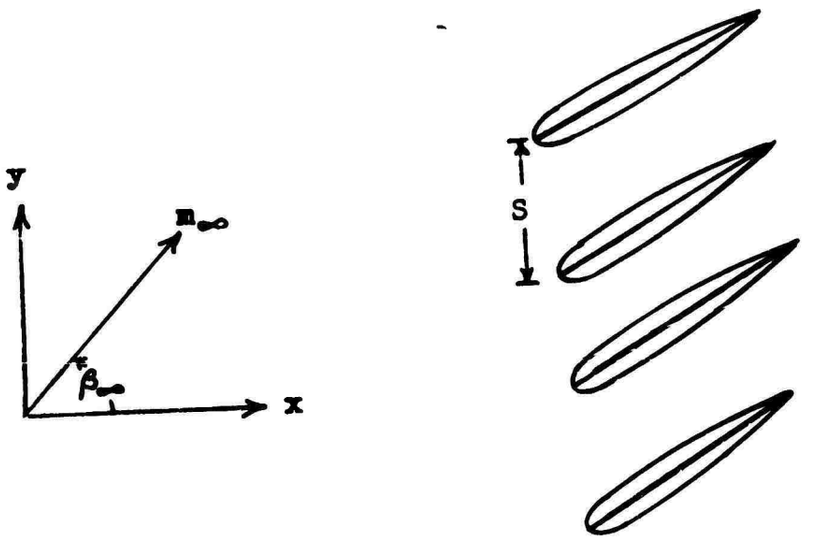

Figure 60. Physical Plane Coordinates.

The transformation from hodograph plane to physical plane is defined by

$$d\left(\frac{x + iy}{s}\right) = \left[B \exp\left(-\zeta'\right) d\zeta'\right] \Big/ \left(2\pi\zeta'\right) - 1/4 \left[B \exp\left(\zeta'\right) \exp\left(2\zeta_\infty\right) d\zeta'\right] \Big/ \left(2\pi\zeta'\right). \tag{69}$$

The constant B is the same in equations (68) and (69) and is to be determined so that one circumnavigation of ζ_∞ in the hodograph plane corresponds exactly to one movement across a blade space s parallel to the cascade. This condition is satisfied if the real and imaginary points of B are respectively

$$B_R = \frac{1 - \exp\left(2\omega_\infty\right) \cos 2\beta_\infty \Big/ 4}{1 - \exp\left(4\omega_\infty\right) \Big/ 16} \tag{70}$$

$$B_I = -\frac{\exp\left(2\omega_\infty\right) \sin 2\beta_\infty \Big/ 4}{1 - \exp\left(4\omega_\infty\right) \Big/ 16} . \tag{71}$$

A useful measure of the decay of the pressure field of the cascade going away is the ratio of the disturbance velocities

$$\begin{aligned} v'_1 &= v_1 - v_\infty , \\ v'_2 &= v_2 - v_\infty , \end{aligned} \tag{72}$$

found at distances x and x_2 from the cascade. Using (66) and (67), this ratio becomes

$$\frac{v_2 - v_\infty}{v_1 - v_\infty} = \frac{v_2/v_\infty - 1}{v_1/v_\infty - 1} = \frac{\left[4 \exp\left(\omega'_2\right) \exp\left(\omega_\infty\right) \sqrt{1 - M_\infty^2}\right] - 1}{\left[4 - \exp\left(2\omega'_2\right) \exp\left(2\omega_\infty\right)\right] M_\infty} \Bigg/ \frac{\left[4 \exp\left(\omega'_1\right) \exp\left(\omega_\infty\right) \sqrt{1 - M_\infty^2}\right] - 1}{\left[4 - \exp\left(2\omega'_1\right) \exp\left(2\omega_\infty\right)\right] M_\infty} . \tag{73}$$

(73) may be simplified considerably by using a relation between ω_∞ and M_∞ implied by (67). The end result is

$$\frac{v_2 - v_\infty}{v_1 - v_\infty} = \left(\frac{\exp(\omega'_2) - 1}{\exp(\omega'_1) - 1}\right)\left(\frac{4 + \exp(\omega'_2)\exp(2\omega_\infty)}{4 + \exp(\omega'_1)\exp(2\omega_\infty)}\right). \tag{74}$$

For

$$\omega'_2 \ll 1,$$

$$\omega'_1 \ll 1, \tag{75}$$

a further simplification is possible:

$$\frac{v_2 - v_\infty}{v_1 - v_\infty} \approx \frac{\omega'_2}{\omega'_1} . \tag{76}$$

A path of integration for (69) which is restricted to real $d\zeta'$ and ζ serves to identify a locus of maximum velocity difference from the free stream; then, retaining the restriction (68),

$$\frac{d(x + iy)}{s} = \frac{1}{2\pi}\left[B - 1/4\ \bar{B}(\cos 2\beta_\infty - i \sin 2\beta_\infty)\right]\frac{d\omega'}{\omega'} \tag{77}$$

or

$$2\pi(x_2 - x_1)/s = \frac{\left[1 - 2(1/2 \exp \omega_\infty)^2 \cos 2\beta_\infty\right]\ln(\omega'_2/\omega'_1)}{1 - (1/2 \exp \omega_\infty)^4} + \frac{(1/2 \exp \omega_\infty)^4 \ln(\omega'_2/\omega'_1)}{1 - (1/2 \exp \omega_\infty)^4} . \tag{78}$$

Inverting (78) and substituting in (76),

$$\frac{v_2 - v_\infty}{v_1 - v_\infty} = \exp\frac{2\pi(A_2 - A_1)}{s}\ \frac{1 - (1/2 \exp \omega_\infty)^4}{1 - 2(1/2 \exp \omega_\infty)^2 \cos 2\beta_\infty + (1/2 \exp \omega_\infty)^4} \tag{79}$$

which is equivalent to equation (64), Appendix II, for the limiting case of zero Mach number.

APPENDIX IV. ACOUSTIC PRESSURE FIELDS DUE TO INTERFERENCE BETWEEN SUCCESSIVE BLADE ROWS

ROTOR - STATOR INTERFERENCE ANALYSIS

Several investigations (references 3, 15, 18) have studied the possibility of production of propagating sound waves due to rotor - stator interference. All three of these analyses are quite similar and lead to, among other results, the concept of a cutoff frequency given by a rather complicated expression, involving the radius ratio of an annular configuration and one or more Bessel functions, usually of high order. Some of these analyses have been supported by experimental investigations confirming the existence of a cutoff frequency. The extent of experimental confirmation has usually been rather slight. Other experiments often show that rotor - stator combinations are noisy over a wide speed range, with no particular speed at which the noise production changes quantitatively. Consequently, a tentative conclusion was reached, that the interference model may have been unrealistic or that the sophistication of the analysis might have hidden the essential meaning of the phenomena being studied.

A different model is proposed, which will permit a study of sound wave propagation due to interferences between adjacent blade rows, without dependence on a cylindrical geometry. Analysis of the model may be separated into two parts: (1) production and propagation of a cylindrical wave, starting from a cylinder the minimal size of the stator leading edge (this analysis is made for a stator following a rotor, but is expected to apply also to a rotor following an inlet guide vane row); and (2) interaction and combination of cylindrical wave fronts, with periodically spaced and time-sequenced origins, to form plane wave fronts which can propagate without attenuation.

The wave front chosen here as a fundamental component is cylindrical to represent the signal propagation from an interference condition over the entire blade span at the same time. This is inconvenient in that the cylindrical wave does not have a simple acoustic potential like those for plane and spherical waves (reference 6, pages 127 - 128, 163). However, the techniques of the unsteady flow method of characteristics (reference 14, pages 933 et seq) may be adapted to study the propagation of a cylindrical wave with the initial conditions: zero particle velocity at zero time for all radii; sinusoidally varying particle velocity at the initial radius for one period, followed by zero particle velocity thereafter. The FORTRAN source list for this computer program follows the analysis. Realistic numerical results from this program have not yet been obtained.

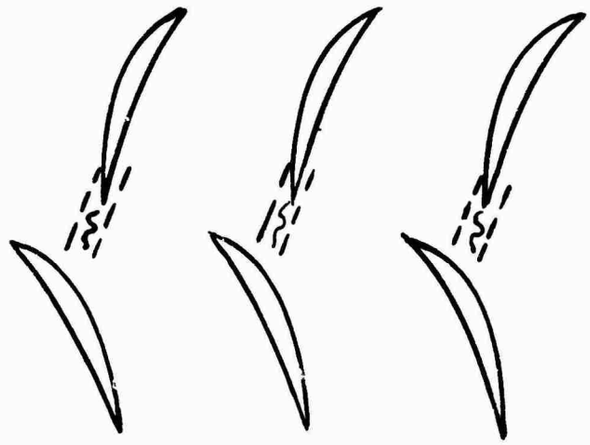

Figure 61. Equal Rotor and Stator Blade Numbers.

The summation of cylindrical wave fronts to form a plane front requires a determination of the proper time relationship between reference points on interference signals originating on successive stator vanes. The simplest situation occurs when the number of rotor blades is the same as the number of stator vanes (Figure 61). Then interferences take place at the same instant on all stator vanes. The symmetry of the situation indicates that the individual signals will combine to form a plane wave front parallel to the blade rows, which propagate in the axial direction away from the blade rows. The next more complex situation occurs when the number of rotor blades is slightly different from the number of stator vanes, and when the time required for a signal to travel from the leading edge of one stator to the leading edge of the next stator is constant.

Figure 62. Varying Rotor and Stator Blade Numbers.

In Figure 62 the number of rotor blades is greater than the number of stator vanes, in the ratio 5 to 4. Interferences occur later on each successive stator vane in the direction of rotation, by an interval one-fifth of the time required for one rotor blade to move from one stator vane to the next. If this time delay is less than the travel time of a signal from one stator leading edge to the next, the signal continuing down a stator vane passage will be a combination of the two signals. If, however, the first signal reaches the next leading edge before the signal starts there, there will be no intersection between the waves. Instead the signals will travel independently.

Although none of the cutoff frequency analyses states this explicitly, it seems likely that this lack of wave intersection may be the mechanism behind the cutoff frequency. Some qualitative study has suggested that wave interactions leading to plane wave formation may occur between signals originating farther apart in time. Quantitative confirmation of this possibility is one of the objectives of the computer program that follows. Such confirmation might imply a desirability of revising the cutoff frequency concept.

THE METHOD OF CHARACTERISTICS FOR CYLINDRICAL WAVE PROPAGATION

Propagation is based on the following equations (reference 4, pages 14, 15, 28, 29) relating dependent variables (pressure, p; density, ρ ; sound velocity, c; and particle velocity, u) in terms of independent variables (time, t; and radius, r).

Continuity:

$$\frac{\partial \rho}{\partial t} + \frac{1}{r} \frac{\partial \rho r u}{\partial r} = 0 \tag{80}$$

Momentum:

$$\frac{\partial u}{\partial t} + u \frac{\partial u}{\partial r} + \frac{1}{\rho} \frac{\partial p}{\partial r} = 0 \tag{81}$$

Isentropic flow of a perfect gas:

$$p = k\rho^{\gamma} \tag{82}$$

Definition of sound velocity:

$$c^2 = \frac{dp}{d\rho} = k\gamma\rho^{\gamma-1} \tag{83}$$

or

$$\frac{2dc}{c} = (\gamma - 1)\frac{d\rho}{\rho} = (\gamma - 1)\, d \ln\rho \tag{83A}$$

Using (83), (81) becomes

$$\frac{\partial u}{\partial t} + u\frac{\partial u}{\partial r} + c^2 \frac{\partial}{\partial r}(\ln\rho) = 0 . \tag{84}$$

(80) may also be written

$$\frac{\partial \rho}{\partial t} + \frac{\rho}{r}\frac{\partial (ru)}{\partial r} + u\frac{\partial \rho}{\partial r} = 0$$

or

$$\frac{\partial \ln\rho}{\partial t} + u\frac{\partial \ln\rho}{\partial r} + \frac{u}{r} + \frac{\partial u}{\partial r} = 0 . \tag{85}$$

The potential velocity and density are to be continuous, single-valued functions of radius and time, so that an exact differential formulation is possible:

$$d \ln\rho = \frac{\partial \ln\rho}{\partial r} dr + \frac{\partial \ln\rho}{\partial t} dt ; \tag{86}$$

$$d u = \frac{\partial u}{\partial r} dr + \frac{\partial u}{\partial t} dt . \tag{87}$$

Equations (84), (85), (86), and (87) are to be taken as simultaneous equations for the partial derivatives $\frac{\partial \ln\rho}{\partial r}$, $\frac{\partial \ln\rho}{\partial t}$, $\frac{\partial u}{\partial r}$, $\frac{\partial u}{\partial t}$. A typical derivative, $\frac{\partial u}{\partial r}$, may be expressed in determinant form as

$$\frac{\partial u}{\partial r} = \frac{\begin{vmatrix} 0 & 1 & c^2 & 0 \\ -\frac{u}{r} & 0 & u & 1 \\ du & dt & 0 & 0 \\ d(\ln\rho) & 0 & d_r & d_t \end{vmatrix}}{\begin{vmatrix} u & 1 & c^2 & 0 \\ 1 & 0 & u & 1 \\ d_r & d_t & 0 & 0 \\ 0 & 0 & d_r & d_t \end{vmatrix}} \quad . \tag{88}$$

The principle of the method of characteristics is that $\frac{\partial u}{\partial r}$ may not be uniquely defined if the denominator vanishes; i.e., if

$$\frac{dr}{dt} = u \pm c \quad . \tag{89}$$

For present purposes, attenuation will be confined to cases where u may be disregarded in comparison with c, so that

$$\frac{dr}{dt} = \pm c \quad . \tag{90}$$

Thus, lines along which

$$r = r_o \pm c\,t \tag{91}$$

are lines across which there may be a discontinuity in $\frac{\partial u}{\partial r}$, or any other of the partial derivatives, or, put in a different way, lines along which an acoustic signal is transmitted.

If u is to be continuous along a line such as 12, $\frac{\partial u}{\partial r}$ may not be infinite, so the numerator of (88) must also vanish. Using the plus sign in (90),

$$\begin{vmatrix} 0 & 1 & c^2 & 0 \\ -\underline{u} & 0 & u & 1 \\ du & dt & 0 & 0 \\ d(\ln\rho) & 0 & c^{dt} & dt \end{vmatrix} = 0 \qquad (92)$$

or making use of (83A),

$$du + \frac{2}{\gamma-1}\, dc + \frac{uc}{r}\, dt = 0 \quad . \qquad (93)$$

(93) defines the relation between changes in c and changes in u along lines such that radius increases with time. Alternatively, if the minus sign in (90) had been used in (92), a result would have been

$$-du + \frac{2}{\gamma-1}\, dc + \frac{uc}{r}\, dt = 0, \qquad (94)$$

which gives the relation between changes along lines such that radius decreases with increasing time.

The process of exploring the propagation of a wave involves specification of u on all radii at zero time, and over all time at the initial radius. Then (93) and (94) provide the necessary relations to construct the field at all times.

FORTRAN SOURCE LIST FOR CYLINDRICAL WAVE PROPAGATION

```
CCYLWVPRP CYLINDRICAL ACOUSTIC WAVE PROPAGATION
      DIMENSION U(60,100),CTR(60),DIST(100),STORE(4,1830),LIST(60),
     1    JSTOR(4,1830),ALIST(10,60),JLIST(10,60),RATIO(100),BLIST(60)
      DIMENSION X(101,7),VX(101),VY(101),VR(101),VANG(101),VNORM(101),
     1    VTANG(101)
      DIMENSION BCD(11),TITLE(8),LABEL1(7),LABEL2(7),LABEL3(7),LABEL4(7)
     1   ,LABEL5(7),LABEL6(7),LABEL7(2)
      COMMON U,JSTOR,CTR,DIST,BLDSPD,SPACE,NBLADR,NBLADS,WAVE,RAD,KPRINT
     1   ,NPRINT,NDIST,KDIST,RATIO,J,J1,J2,J3,I11,DR,GAMMA,GAM1,SDVEL,
     2    GAM11
      EQUIVALENCE (ALIST,JLIST,BLIST),(U,STORE),(X,JSTOR),(VX,JSTOR(102)
     1    ),(VY,JSTOR(203)),(VR,JSTOR(304)),(VANG,JSTOR(405)),(VNORM,JST
     2    OR(506)),(VTANG,JSTOR(607))
      TABLE LIST (15,$(SDVEL,RAD,TIME,NTIME,RADEND,GAMMA,RATIO,
     1    BLDSPD,SPACE,NBLADR,NBLADS,DIST,WAKE,LTAPE,KLIST))
      TABLE BCD(66HTIME  ACOUSTIC PARTICLE VELOCITY / INITIAL DISTURBANC
     1E VELOCITY   )
      TABLE TITLE(48HCYLINDRICAL ACOUSTIC WAVE PROPAGATION ANALYSIS
      TABLE LABEL1(42HBLADE SPEED / SOUND VELOCITY              =)
      TABLE LABEL2(42HWAKE THICKNESS / BLADE SPACE              =)
      TABLE LABEL3(42HNUMBER OF ROTOR BLADES                    =)
      TABLE LABEL4(42HNUMBER OF STATOR VANES                    =)
      TABLE LABEL5(42HDISTANCE FROM STATOR LE / BLADE SPACE     =)
      TABLE LABEL6(42HANGLE OF MAXIMUM PARTICLE VELOCITY (DEG) =)
      TABLE LABEL6(12HVNORM VTANG )
      IF(SENSE LIGHT 1)48,1
 48   GOTO(37,49,38,38),KERROR
 49   KERROR=3
      GOTO 142
    1 IOF=1
      KERROR=1
      GAMMA=1.4
      SDVEL=1120.
      NTIME=50
      LTAPE=0
      CALL DING(LIST,IOF)
      IF(SENSE LIGHT 1)1,2
    2 DR=TIME/FLOATF(NTIME)*SDVEL/2./RAD
      NPRINT=LCOUNT(1,100,RATIO,1)
      KPRINT=1
      GAM1 = (GAMMA-1.)/2.
      GAM11 = -GAM1
      DT=TIME/FLOATF(NTIME)
      IF(SENSE LIGHT 2)44,44
   44 REWIND 6
      IF(LTAPE)3,3,80
    3 JSTOR(1,1)=1
      JSTOR(2,1)=0
      JSTOR(3,1)=0
      JSTOR(4,1)=0
```

```
      STORE(1,1)=1.
      STORE(2,1)=0.
      STORE(3,1)=0.
      STORE(4,1)=0.
      JBEFOR=1
      JFIRST=2
      I11=0
      LANE=1
      JLANE=1
      ARG1=6.283185/FLOATF(NTIME)
      ARG=ARG1
      JSTOR(1,JFIRST)=JFIRST+I11
      JSTOR(2,JFIRST)=JBEFOR+I11
      JSTOR(3,JFIRST)=0
      JSTOR(4,JFIRST)=0
      STORE(1,JFIRST)=STORE(1,JBEFOR)+DR
      STORE(2,JFIRST)=STORE(2,JBEFOR)+DR
      STORE(3,JFIRST)=0.
      STORE(4,JFIRST)=0.
      J=JFIRST
      J1=JBEFOR
      J2=0
      J3=0
      JJ1=J1+JLANE
    5 IF(JSTOR(4,JJ1 ))9,9,6
    6 J2=J
      J3=J1
      J=J+1
      J1=J1+1
      CALL CYLWVE
    7 GOTO 5
    9 JSTOR(1,J+1)=J+1+I11
      JSTOR(2,J+1)=0
      JSTOR(3,J+1)=J1+I11
      JSTOR(4,J+1)=J+I11
      STORE(1,J+1)=1.
      STORE(2,J+1)=STORE(2,J)+DR
      GOTO(13,12,12,12),LANE
   12 STORE(3,J+1)=0.
      GOTO 14
   13 STORE(3,J+1)=SINF(ARG)
   14 STORE(4,J+1)=STORE(4,J)+GAM1*(STORE(3,J+1)-STORE(3,J)+(STORE(3,J+1
     1     )/STORE(1,J+1)+STORE(3,J)/STORE(1,J))*DR/2.)
      GOTO (10,16,17,17),LANE
   10 ARG=ARG+ARG1
      IF(ARG-6.283)11,15,15
   15 LANE=2
      ARG = 0.
   11 JBEFOR=JFIRST
      JFIRST=J+2
```

```
      GOTO 4
   16 LANE=3
      JLANE=2
      IF(RATIO(1)-1.)39,39,22
   22 LANE=4
      GOTO 11
   17 JSTOR(2,J+1) = J2 + 1 +111
      IF(STORE(1,J)-RATIO(KPRINT))24,18,18
   39 JJ = J+1
      GOTO 40
   18 JJ = J
   40 KLIST =JJ-JFIRST + 1
      RATIO(KPRINT)=STORE(1,JJ)*RAD
      KK=KLIST
   19 JLIST(1,KK)=JSTOR(1,JJ)
      JLIST(2,KK)=JSTOR(2,JJ)
      JLIST(3,KK)=JSTOR(3,JJ)
      JLIST(4,KK)=JSTOR(4,JJ)
      ALIST(5,KK)=STORE(1,JJ)
      ALIST(6,KK)=STORE(2,JJ)
      ALIST(7,KK)=ALIST(6,KK)-ALIST(5,KK)
      ALIST(8,KK)=STORE(3,JJ)
      ALIST(9,KK)=STORE(4,JJ)
      ALIST(10,KK)=ALIST(8,KK)*ALIST(5,KK)
      CTR(KK)=ALIST(7,KK)*RAD/SDVEL
      IF(KK-1)21,21,20
   20 JJJ=JJ
   25 JJJ=JJJ-1
      IF(JSTOR(1,JJJ)-JSTOR(3,JJ))26,27,25
   26 CALL ERROR
   27 JJ=JJJ
      KK=KK-1
      GOTO 19
   21 WRITE(3,1000)SDVEL,GAMMA,RAD,DR,DT,TIME,((ALIST(K,KK),
     1    K=1,10),KK=1,KLIST)
      KPRINT=KPRINT+1
      DO 41 KK=1,KLIST
   41 BLIST(KK)=ALIST(10,KK)
      CALL FNWTB(6,1,BLIST,KLIST,IERCOD)
      IF(IERCOD-3)42,43,43
   43 WRITE(3,1001)KPRINT,IERCOD
      SENSE LIGHT 2
   42 GOTO(11,11,22,23,38),LANE
   23 IF(KPRINT-NPRINT)24,24,45
   24 IF(JSTOR(2,J2))11,11,8
    8 JJJ=1
      JHOLD=JSTOR(1,1)
      NMOVE=1
      JMOVE=JJJ+NMOVE
   28 DO 29 I=1,4
```

```
      JSTOR(I,JJJ)=JSTOR(I,JMOVE)
   29 STORE(I,JJJ)=STORE(I,JMOVE)
      JJJ=JJJ+1
      JMOVE=JMOVE+1
      IF(JMOVE-J)32,32,33
   32 IF(JSTOR(3,JMOVE))28,28,30
   30 IF(JSTOR(3,JMOVE)-JHOLD)28,31,28
   31 JHOLD=JSTOR(1,JMOVE)
      JMOVE=JMOVE+1
      GOTO 28
   33 III=JSTOR(1,JJJ-1)-JJJ+1
      JFIRST=JJJ
   34 JJJ=JJJ-1
      IF(JSTOR(4,JJJ))35,35,34
   35 JBEFOR=JJJ
      DO 36 I=JFIRST,J
      DO 36 II=1,4
      STORE(II,I)=0.
   36 JSTOR(II,I)=0
      GOTO 4
   37 LANE=5
      GOTO 18
   38 CALL EXIT
 45   CALL FNWTB(6,2,CTR,KLIST,RATIO,NPRINT,IERCOD)
      IF(IERCOD-3)46,47,47
   47 WRITE(3,1001)KPRINT
      GOTO 1
   46 IF(LTAPE)1,80,80
   80 REWIND 6
      KERROR=2
      DO 79 I=1,7320
 79   STORE(I)=0.
      DO 81 KPRINT=1,NPRINT
      CALL FNRTB(6,1,U(1,KPRINT),KLIST,IERCOD)
      IF(IERCOD-6)81,82,82
   82 WRITE(3,1002)KPRINT,IERCOD
      GOTO 1
   81 CONTINUE
      CALL FNRTB(6,2,CTR,KLIST,RATIO,NPRINT,IERCOD)
      IF(IERCOD-6)84,83,83
   83 WRITE(3,1002)KPRINT,IERCOD
      GOTO 1
*  SPACE IS THE DISTANCE BETWEEN TWO STATOR VANES.
   84 BLADR=NBLADR
      BLADS=NBLADS
      NDIST=LCOUNT(1,100,DIST,1)
*  TMEVNT REFERS TO THE TIME BETWEEN INTERFERENCE EVENTS ON ADJACENT
*  STATOR VANES.
*  CYCLE REFERS TO THE TIME BETWEEN PASSAGE OF SUCCESSIVE ROTOR
*  BLADES PAST A POINT.
```

```
*  TIME REFERS TO PASSAGE OF A BLADE WAKE PAST A POINT.
      TMEVNT=(BLADR/BLADS-1.)*SPACE/BLDSPD
      CYCLE=SPACE*BLADS/BLADR/BLDSPD
      TIME=WAKE/BLDSPD
      DO 147 KDIST=1,NDIST
      NAXIS=DIST(KDIST)/SPACE*20.
      NAXIS=XMAXOF(NAXIS,30)
*  CYCTIM GIVES THE TIME AFTER THE START OF SOME SINE WAVE SIGNAL
*  AT THE SOURCE WHEN A SIGNAL REACHES THE POINT BEING STUDIED.
*  CYCTMM GIVES THE TIME WHEN THE END OF THE SIGNAL REACHES THE POINT.
      CYCTIM=MODF(DIST(KDIST)/SDVEL,CYCLE)
      LANE1=1
      CYCTMM=CYCTIM+TIME
      IF(CYCTMM-CYCLE)101,101,100
  100 CYCTMM=CYCTMM-CYCLE
      LANE1=2
  101 CYCTX=0.
      DO 108 JCYC=1,100
      VY(JCYC)=0.
      GOTO(105,102),LANE1
  102 IF(CYCTX-CYCTMM)103,103,104
  103 CALL BILAG(CYCTX-CYCTIM+CYCLE,DIST(KDIST)*SPACE,UCOMP)
      VX(JCYC)=UCOMP*RAD/DIST(KDIST)
      GOTO 108
  104 LANE1=1
  106 VX(JCYC)=0.
      GOTO 108
  105 IF(CYCTX-CYCTIM)106,106,107
  107 LANE1=2
      GOTO 103
  108 CYCTX=CYCTX+CYCLE/100.
  150 DUM = DUM
      DO 133 KAXIS=1,NAXIS
      AXIS=KAXIS
      DISTT=SQRTF(DIST(KDIST)**2+AXIS**2)*SPACE
      CYCTIM=MODF(DISTT/SDVEL,CYCLE)
      SINANG=SPACE*AXIS/DISTT
      COSANG=DIST(KDIST)/DISTT * SPACE
      TIMPLS=CYCTIM+TMEVNT*AXIS
      TIMMNS=CYCTIM-TMEVNT*AXIS
  148 IF(TIMPLS)109,110,110
  109 TIMPLS=TIMPLS+CYCLE
      GO TO 148
  110 IF(TIMPLS-CYCLE)112,111,111
  111 TIMPLS=TIMPLS-CYCLE
      GOTO 110
  112 IF(TIMMNS)113,114,114
  113 TIMMNS=TIMMNS+CYCLE
      GO TO 112
  114 IF(TIMMNS-CYCLE)116,115,115
```

```
115 TIMMNS=TIMMNS-CYCLE
    GOTO 114
116 CYCTX=0.
    TIMPLX=TIMPLS+TIME
    LANE1=1
    IF(TIMPLX-CYCLE)118,118,117
117 LANE1=2
    TIMPLX=TIMPLX-CYCLE
118 DO 124 JCYC=1,100
    GOTO(122,119),LANE1
119 IF(CYCTX-TIMPLX)120,120,121
120 CALL BILAG(CYCTX-TIMPLS+CYCLE,DISTT,UCOMP)
    VX(JCYC)=VX(JCYC)+UCOMP*RAD/DIST(KDIST)*COSANG
    VY(JCYC)=VY(JCYC)-UCOMP*RAD/DIST(KDIST)*SINANG
    GOTO 124
121 LANE1=1
    GOTO 124
122 IF(CYCTX-TIMPLS)124,124,123
123 LANE1=2
    GOTO 120
124 CYCTX=CYCTX+CYCLE/100.
    CYCTX=0.
    TIMMNX=TIMMNS+TIME
    LANE1=1
    IF(TIMMNX-CYCLE)126,126,125
125 LANE1=2
    TIMMNX=TIMMNX-CYCLE
126 DO 132 JCYC=1,100
    GOTO(130,127),LANE1
127 IF(CYCTX-TIMMNX)128,128,129
128 CALL BILAG(CYCTX-TIMMNS+CYCLE,DISTT,UCOMP)
    VX(JCYC)=VX(JCYC)+UCOMP*RAD/DIST(KDIST)*COSANG
    VY(JCYC)=VY(JCYC)+UCOMP*RAD/DIST(KDIST)*SINANG
    GOTO 132
129 LANE1=1
    GOTO 132
130 IF(CYCTX-TIMMNS)132,132,131
131 LANE1=2
    GOTO 128
132 CYCTX=CYCTX+CYCLE/100.
133 CONTINUE
    VRMAX=0.
    DO 140 JCYC=1,100
    VR(JCYC)=SQRTF(VX(JCYC)**2+VY(JCYC)**2)
    IF(VX(JCYC))134,135,136
134 VANG(JCYC)=3.14159
    GOTO 137
135 VANG(JCYC)=SIGNF(VY(JCYC),1.5708)
    GOTO 138
136 VANG(JCYC)=0.
```

```
137 VANG(JCYC)=VANG(JCYC)+ATANF(VY(JCYC)/VX(JCYC))
138 VRMAX=MAX1F(VRMAX,ABSF(VR(JCYC)))
    IF(VRMAX-ABSF(VR(JCYC)))139,139,140
139 LVRMAX=JCYC
140 CONTINUE
    DO 141 JCYC=1,100
    X(JCYC+1)=.01*FLOATF(JCYC)
    VNORM(JCYC)=VR(JCYC)*COSF(VANG(JCYC)-VANG(LVRMAX))
141 VTANG(JCYC)=VR(JCYC)*SINF(VANG(JCYC)-VANG(LVRMAX))
    X(1) = 0.
    VX(101)=VX
    VY(101)=VY
    VR(101)=VR
    VANG(101)=VANG
    VNORM(101)=VNORM
142 VTANG(101)=VTANG
    CALL ORG(0.,5.)
    CALL SCALEM(1.6,0.,+VRMAX,-VRMAX,16.,10.)
    CALL XAXISA(0.,0.,BCD(1),-4,16.,0.)
    CALL YAXISA(0.,-5.,BCD(2),57,10.,90.)
    CALL SYMBLA(.75,10.,.21,TITLE,0.,46)
    CALL SYMBLA(10.,9.5,.14,LABEL1,0.,42)
143 XPLOT=BLDSPD/SDVEL
    CALL NUMBRA(15.2,9.5,.14,XPLOT,0.,3)
    CALL SYMBLA(10.,9.2,.14,LABEL2,0.,42)
144 XPLOT=WAKE/SPACE
    CALL NUMBRA(15.2,9.2,.14,XPLOT,0.,3)
    CALL SYMBLA(10.,8.9,.14,LABEL3,0.,42)
    CALL NUMBRA(15.2,8.9,.14,BLADR,0.,-1)
    CALL SYMBLA(10.,8.6,.14,LABEL4,0.,42)
    CALL NUMBRA(15.2,8.6,.14,BLADS,0.,-1)
    CALL SYMBLA(10.,8.3,.14,LABEL5,0.,42)
145 XPLOT=DIST(KDIST)/SPACE
    CALL NUMBRA(15.2,8.3,.14,XPLOT,0.,2)
    CALL SYMBLA(10.,8.,.14,LABEL6,0.,42)
146 XPLOT=VANG(LVRMAX)*57.296
    CALL NUMBRA(15.2,8.0,.14,XPLOT,0.,2)
    CALL LINE(X,VNORM,101,1)
    CALL LINE(X,VTANG,101,1)
    CALL SYMBLA(X(LVRMAX)-.25,VNORM(LVRMAX)+.05,.14,LABEL7(1),
   1    0.,5)
    CALL SYMBLA(X(LVRMAX)-.25,VTANG(LVRMAX)+.05,.14,LABEL7(2),
   1    0.,5)
    GOTO (147,147,38,38),KERROR
147 CONTINUE
    GOTO 1
1000 FORMAT
    RESTORE
    CYLINDRICAL ACOUSTIC WAVE PROPAGATION ANALYSIS
    SPACE
```

```
      SOUND VELOCITY          -0PF1
      GAMMA                     -F2
      INITIAL RADIUS            -1PG3 FT.
      RADIUS INCREMENT          -1PG3   (DELTA R)/R
      TIME INCREMENT              -G3 SEC.
      TOTAL WAVE DURATION         -G3 SEC
      SPACE
    PN   PNRC  PNDG  PNLC    R/RO      TIME (CT-R)     U      (C-CO)    RO/R
X*U
      SPACE
-X   -I    -I    -I    -I    -0PF4     -F4      -F4      -F4      -F4
XF4
      REPEAT 1
      END OF FORMAT
 1001 FORMAT
      TAPE RECORD NO   -I WAS NOT WRITTEN SUCCESSFULLY, CODE  -I
      END OF FORMAT
 1002 FORMAT
      TAPE RECORD NO   -I WAS NOT READ SUCCESSFULLY, CODE  -I
      END OF FORMAT
      END
```

```
C CYLWVE  CHARACTERISTIC INTERSECTION SUBROUTINE
      SUBROUTINE CYLWVE
      DIMENSION U(60,100),CTR(60),DIST(100),STORE(4,1830),JSTOR(4,1830)
     1    ,RATIO(100)
      COMMON U,JSTOR,CTR,DIST,BLDSPD,SPACE,NBLADR,NBLADS,WAVE,RAD,KPRINT
     1   ,NPRINT,NDIST,KDIST,RATIO,J,J1,J2,J3,I11,DR,GAMMA,GAM1,SOVEL
     2    ,GAM11
      EQUIVALENCE (U,STORE)
*  J1 REFERS TO L CHARACTERISTIC
*  J2 REFERS TO R CHARACTERISTIC
*  J3 REFERS TO DIAGONAL POINT
*  J4 REFERS TO NEXT L CHARACTERISTIC POINT
*  J5 REFERS TO NEXT R CHARACTERISTIC POINT
      JSTOR(1,J)=J+I11
      JSTOR(2,J)=J1+I11
      NCOUNT=1
      JSTOR(4,J)=J2+I11
      IF(J3)1,1,3
    1 JSTOR(3,J)=0
      STORE(3,J) = (STORE(3,J1)+STORE(3,J2))/2.
      STORE(4,J) = (STORE(4,J1)+STORE(4,J2))/2.
      GOTO 5
    3 JSTOR(3,J)=J3+I11
      STORE (3,J) = STORE(3,J1)+STORE(3,J2)-STORE(3,J3)
      STORE(4,J)=STORE(4,J1)+STORE(4,J2)-STORE(4,J3)
    6 STORE(1,J)=STORE(1,J3)
      STORE(2,J)=STORE(2,J3)+2.*DR
      IF(JSTOR(2,J1))5,5,11
    5 C1=GAM11*DR*(STORE(3,J)/STORE(1,J)+STORE(3,J1)/STORE(1,J1))/2.
     1    +GAM1*STORE(3,J1)+STORE(4,J1)
      GO TO 13
   11 J4=JSTOR(2,J1)-I11
      IF(J4)5,5,12
   12 C1=GAM11*DR*(.416667*STORE(3,J)/STORE(1,J)+.666667*STORE(3,J1)
     1    /STORE(1,J1)-.083333*STORE(3,J4)/STORE(1,J4))+GAM1*STORE(3,J1)
     2    +STORE(4,J1)
   13 IF(JSTOR(4,J2))14,14,16
   14 C2=GAM11*DR*(STORE(3,J)/STORE(1,J)+STORE(3,J2)/STORE(1,J2))/2.
     1    +GAM11*STORE(3,J2)+STORE(4,J2)
      GO TO 15
   16 J5=JSTOR(4,J2)-I11
      IF(J5)14,14,17
   17 C2=GAM11*DR*(.416667*STORE(3,J)/STORE(1,J)+.666667*STORE(3,J2)
     1    /STORE(1,J2)-.083333*STORE(3,J5)/STORE(1,J5))+GAM11
     2    *STORE(3,J2)+STORE(4,J2)
   15 CALL DETER(C1,C2,GAM1,GAM11,1.,1.,CR,UR)
    7 IF(ABSF(CR-STORE(4,J))+ABSF(UR-STORE(3,J))-1.E-5)9,9,8
    8 STORE(4,J)=CR
      STORE(3,J)=UR
      NCOUNT=NCOUNT+1
```

```
      IF(NCOUNT-15)5,5,10
   10 CALL ERRORA
    9 RETURN
      END
CBILAG   BIVARIATE LINEAR INTERPOLATION, CYLINDRICAL WAVE INTERFERENCE
      SUBROUTINE BILAG(X,Y,Z)
      DIMENSION U(60,100),CTR(60),DIST(100),STORE(4,1830),JSTOR(4,1830)
     1    ,RATIO(100)
      COMMON U,JSTOR,CTR,DIST,BLDSPD,SPACE,NBLADR,NBLADS,WAVE,RAD,KPRINT
     1   ,NPRINT,NDIST,KDIST,RATIO,J,J1,J2,J3,I11,DR,GAMMA,GAM1,SDVEL
      EQUIVALENCE (U,STORE)
      I=1
      J=1
    1 IF(X-CTR(I+1))4,4,2
    2 I=I+1
      IF(I-59)1,3,3
    3 CALL ERROR
    4 IF(Y-RATIO(J+1))7,7,5
    5 J=J+1
      IF(J-NPRINT)4,6,6
    6 Z = U(I,J)+(X-CTR(I))/(CTR(I+1)-CTR(I))*(U(I+1,J)-U(I,J)
      GOTO 8
    7 DEN=(CTR(I+1)-CTR(I))*(DIST(J+1)-DIST(J))
      CLB=Y-DIST(J)
      CUB=DIST(J+1)-Y
      CLH=X-CTR(I)
      CRH=CTR(I+1)-X
      Z=(CUB*CRH*U(I,J)+CUB*CLH*U(I+1,J)+CLB*CRH*U(I,J+1)
     1    +CLB*CLH*U(I+1,J+1))/DEN
    8 RETURN
      END
```

APPENDIX V. ANALYTICAL INVESTIGATION OF THE RADIATION CHARACTERISTICS FROM A FAN FACE

The approach used is that of a piston with a varying particle velocity. The particle velocity was assumed to be a function of the radial position and the difference in the number of rotor and stator blades. If the number of rotor and stator blades is the same, the source is essentially a piston radiator, as all the rotor - stator excitations are in phase. When the number of rotor blades exceeds or is less than the number of stator blades, the pressure fluctuations are out of phase and the directivity pattern varies with an increase in the difference of rotor and stator blades, the wave length, frequency, and rotor dimensions. The basic equation for the derivation was the acoustic pressure at a point resulting from an excitation in a plane a distance r' away (reference 6).

Figure 63 is a schematic of the coordinate system used for the derivation.

$$dp = \frac{j\rho\omega}{2\pi r'} u_z e^{j\omega(t-r'/c)} ds \qquad (95)$$

where

ds = element of rotor surface area.

dp = acoustic pressure at point P.

ρ = density of medium.

ω = frequency of excitation ($\omega = N_r \times RPS$).

u_z = particle velocity.

t = time.

c = speed of sound in medium.

N_r = number of rotor blades.

RPS = revolutions per second of rotor.

The particle velocity may be assumed to have the form

$$u_z = U_o (r) e^{jn\psi} \qquad (96)$$

where

n = difference in the number of rotor and stator blades.

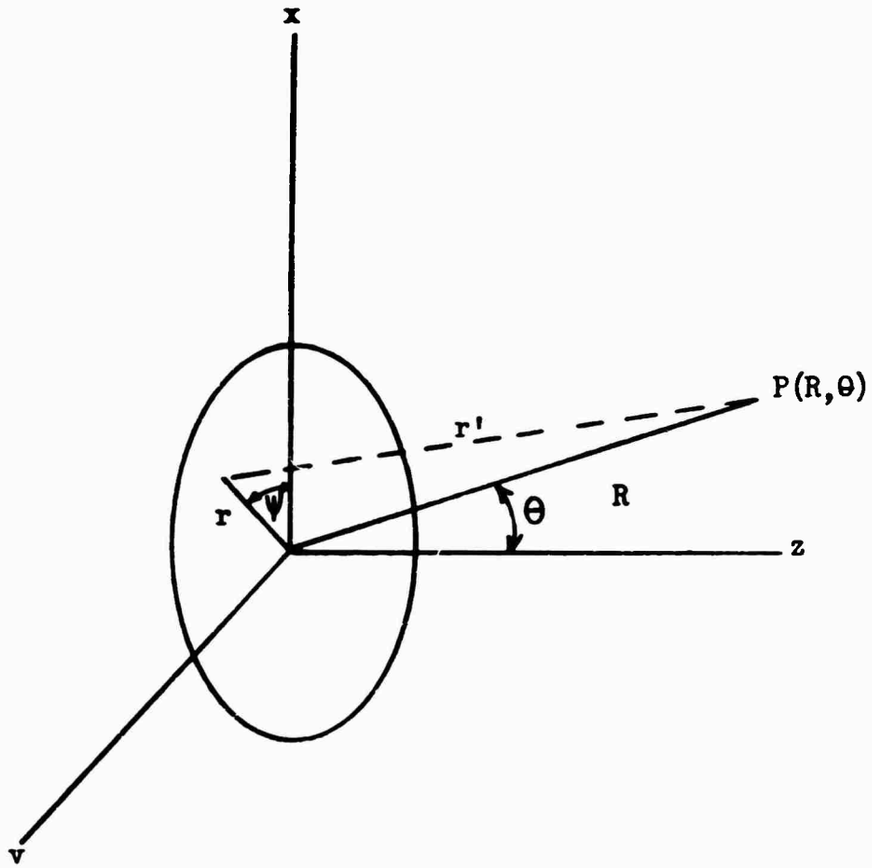

Figure 63: Schematic of Coordinate System.

Substituting (96) into (95),

$$dp = \frac{j\rho\omega\ U_o\ (r)}{2\pi r'}\ e^{j\left[\ n\psi + \omega\ (t - r'/c)\ \right]} rdrd\psi \qquad (97)$$

with

$$ds = rdrd\psi\ .$$

From Figure 63, the following may be determined:

$$r'^2 = (r\cos\psi)^2 + (R\sin\theta - r\sin\psi)^2 + (r\cos\theta)^2$$
$$= r^2 + R^2 - 2rR\sin\theta\sin\psi$$

$$r' = R\left(1 + \frac{r^2}{R_2} - 2\frac{r}{R}\sin\theta\sin\psi\right)^{1/2};$$

and if $\left(\frac{r}{R}\right)^2 \ll \frac{r}{R}$

$$r' = R\left(1 - 2\frac{r}{R}\sin\theta\sin\psi\right)^{1/2}$$

or

$$r' \quad R\left(1 - \frac{r}{R}\sin\theta\sin\psi\right)$$

$$r' \quad (R - r\sin\theta\sin\psi). \qquad (98)$$

Substituting equation (98) into (97),

$$dp \approx \frac{j\rho\omega\ U_o}{2\pi R}\ e^{j\quad (t - R/c)}\ e^{j\left(n\psi + \frac{\omega}{c}\ r\sin\ e\sin\psi\right)} rdrd\psi\ . \qquad (99)$$

Note that the last term of equation (98) was omitted in the denominator of equation (99), but retained in the exponential term. This was done by assuming that the term

$$\frac{j\rho\omega\ U_o}{2\pi\ r'}$$

oscillates about the value 1, which enables the term $r\sin\theta\ \sin\psi$ to be assumed negligible, while the exponential terms oscillate about a value of zero, which does not allow the term $r\sin\theta\ \sin\psi$ to be assumed negligible.

From "Tables of Functions" by Jahnke and Emde, equation (99) becomes

$$P = \frac{j\rho\omega}{R} e^{j\omega(t - R/c)} \int U_o J_n \left(\frac{\omega r}{c} \sin\theta\right) rdr \qquad (100)$$

from which

$$u = \frac{\omega}{Rc} \cos\omega (t - R/c) \int U_o(r) J_n \left(\frac{\omega r}{c} \sin\theta\right) rdr \qquad (101)$$

$$I = \frac{\rho\omega^2}{4R^2c} \left[\int U_o(r) J_n \left(\frac{\omega r}{c} \sin\theta\right) rdr\right]^2. \qquad (102)$$

Equations 100, 101, and 102 were programmed to provide an output of sound pressure level relative to an assumed reference pressure level as shown in the following FORTRAN source list.

FORTRAN SOURCE LIST FOR RADIATION FROM A ROTOR ANNULUS

```
*FANANNSD SOUND RADIATION FROM A ROTOR ANNULUS
      DIMENSION BITS(1),RAD(2,19),BESSEL(10,19),SDPAR(19),THETA(20)
     1    ,SDPRES(19)
      TABLE BITS(0-377777777777)
      IF ( SENSE LIGHT 1) 6,8
    8 RHO = .076475
      SDVEL = 1116.4
      DO 2 I = 1,38
    2 RAD(I) = BITS
      READ DIP RPM,BLADES,RAD,UO,SDVEL,RHO,BEATS
      IF ( SENSE LIGHT 1) 8,1
    1 ALBDA = SDVEL*9.54929/BLADES/RPM
      NRAD = LCOUNT(1,19,RAD,2)
      NRAD1 = (NRAD+1)/2
      SDREF = RHO*SDVEL/4.*RAD(2,NRAD1)**2/32.174/685.399
      REF = RAD(2,NRAD1)
      PREF = RHO*SDVEL/32.174*REF/2.08848E-3
      DO 3 I = 1,NRAD
      RAD(1,I) = RAD(1,I)/ALBDA
    3 RAD(2,I) = RAD(2,I)/REF
      THETA(1) = 0.
      SDPAR(1) = 0.
    9 NBEAT = BEATS
      NBLAD = BLADES
      DO 7 I = 1,19
      THETA(I+1) = THETA(I-1)+5.
      THET = SINF(THETA(I)*.0174532)
      DO 4 J = 1,NRAD
      CALL BESSL(1,RAD(1,J)*THET,NBEAT,NBEAT+5,BESSEL(1,J))
      IF(SENSE LIGHT 1 ) 6,4
    4 CONTINUE
      TRY1 = RAD(1,1)*RAD(2,1)*BESSEL(1,1)
      SDPRES(I) = 0.
      DO 5 J = 3,NRAD,2
      TRY2 = RAD(1,J-1)*RAD(2,J-1)*BESSEL(1,J-1)
      TRY3 = RAD(1,J)*RAD(2,J)*BESSEL(1,J)
      SDPRES(I)=SDPRES(I)+(RAD(1,J)-RAD(1,J-2))*(.166667*(TRY1+TRY3)+
     1    .666667*TRY2)
    5 TRY1 = TRY3
      SDPAR(I) =SDPRES(I)**2
      GOTO 7
    6 WRITE(3,1000)THETA(I),J,RAD(1,J),THET,NBLAD
    7 CONTINUE
      WRITE(3,1001)NBEAT,NBLAD,PREF,RPM,SDREF,ALBDA,RHO,REF,SDVEL,
     1    (RAD(1,J),RAD(2,J),THETA(J),SDPAR(J),SDPRES(J),J=1,19)
      GO TO 8
 1000 FORMAT
      SPACE
  BESSEL FUNCTION SUBROUTINE ENCOUNTERED AN ERROR AT THETA = -F3, J= -I,
X RAD(1,J)=    -E3, SINTHETA =  -F3, NBLADES = -I
```

```
      END OF FORMAT
 1001 FORMAT
      RESTORE
      SOUND RADIATION FROM A ROTOR BLADE ANNULUS
      SPACE
      NUMBER OF BEATS =       -I
      NUMBER OF BLADES    =    -I                                  REFERENCE PR
XESSURE    =     -1PG3  DYNES/CM2
      RPM                 =    -0PF0                               REFERENCE IN
XTENSITY   =     -1PG3  WATTS/CM2
      REFERENCE LENGTH    =    -0PF3 FT (2*PI*WAVE LENGTH)         AIR DENSITY
X          =      -F5  LBM/FT3
      REFERENCE VELOCITY =     -F3 FT/SEC                          SOUND VELOCI
XTY        =      -F1  FT/SEC
      SPACE
      RADIUS      PEAK VELOCITY              ANGLE FROM AXIS       SOUND I
XNTENSITY       SOUND PRESSURE
                REFERENCE VELOCITY                (DEGREES)       RATIO*(
XR/LBDA)SQ      RATIO*(R/LBDA)
       -0PF3           -F3                          -F0
X-1PG3                  -G3
      REPEAT 1
      END OF FORMAT
      END
```

```
*BESSL 00
C       BESSEL FUNCTION J(X) AND I(X)
C       BESSEL SUBROUTINE
C       CHANDLER MARCH - TIS 64TIP5
C       STEGUN AND ABRAMOWITZ, MTAC 60 P.252 - OCT 1957
        SUBROUTINE BESSL(ITYPE,X,NMIN,NMAX,BESJI)
C   ITYPE = 1 FOR  U(X)
C   ITYPE = 2 FOR  I(X)
C   STATEMENTS WITH 100 SERIES EFN JUMBERS DO NOT APPLY TO I(X)
     3  DIMENSION BESJI(10)
    10  XX = X
        MAXN=NMAX
         MINN=NMIN
        NDEL=MAXN-MINN
        IF(NDEL)11,14,14
    11  NTMP=MAXN
        MAXN=MINN
        MINN=NTMP
        NDEL=-NDEL
C   NDEL IS NUMBER OF ORDERS DESIRED
    14  NDEL=NDEL+1
        IF(XX)43,41,43
    41  DO 42 I=1,NDEL
    42  BESJI(I)=0.
        GO TO (44,40),ITYPE
    44  IF(NMIN)46,45,40
    45  BESJI(1)=1.
        GO TO 40
    46  IF(NMAX)40,47,48
    47  BESJI(NDEL)=1.
        GO TO 40
    48  N=1-NMIN
        BESJI(N)=1.
        GO TO 40
    43  NDEL1=NDEL
        GOTO(15,116),ITYPE
    15  C1 = -1.
        C2 = 2.
        GOTO 17
   116  C1 = 1.
        C2 = 1.
    17  K = (XMAXOF(MAXN,XFIXF(1.5*XX+.51))/2)*2+12
        FJP3 = 0.
        FJP2 = 1.E-11
C   SUMFJ ACCUMULATES TENTATIVE BESSEL FUNCTION VALUES
C   TO GET THE NORMALIZING FACTOR
        SUMFJ = 0.
        TWOX = 2./XX
        P = K+1
    18  FJP1 = TWOX*(P+1.)*FJP2+C1*FJP3
```

```
      ABFCN1 = ABSF(FJP1)
      IF(ABFCN1 - 1.E36)20,19,19
   19 SENSE LIGHT 1
      GOTO 40
   20 FJP0 = TWOX*P*FJP1+C1*FJP2
      ABFCN0= ABSF(FJP0)
      IF(ABFCN0-1.E36)21,19,19
   21 IF(ABFCN0+ABFCN1-1.E-30)22,23,23
   22 FJP0=0.
      FJP1 = 0.
   23 GOTO(25,24),ITYPE
   24 SUMFJ=SUMFJ+FJP1
   25 SUMFJ=SUMFJ+C2*FJP0
      IF(NDEL)32,32,51
 51   IF(K-MAXN)50,29,32
 50   IF(K+1-MAXN)32,27,32
C  THE FUNDAMENTAL RECURRENCE FORMULA
C  FOR J, JP(X) = 2*(P+1)/X*JP1(X)-JP2(X)
C  FOR I, IP(X) = 2*(P+1)/X*IP1(X)+IP2(X)
   27 BESJI(NDEL)=FJP1
      NDEL=NDEL-1
      MAXN=MAXN-1
      IF(K-NMIN)32,29,29
   29 BESJI(NDEL)=FJP0
      NDEL=NDEL-1
      MAXN=MAXN-1
      GOTO 32
C  THE SUM IN THE NORMALIZATION CONSTANT FOR J CONTAINS
C  ONLY EVEN K IN JK
   32 IF(K)34,34,33
   33 P=P-2.
      K=K-2
      FJP3=FJP1
      FJP2=FJP0
      GOTO 18
   34 SUMFJ=SUMFJ-FJP0
      GOTO(36,135),ITYPE
  135 SUMFJ=SUMFJ/EXPF(XX)
   36 DO 37 I=1,NDEL1
   37 BESJI(I)=BESJI(I)/SUMFJ
   40 RETURN
      END
```

APPENDIX VI. ABSORPTIVE SUPPRESSOR DESIGN CALCULATIONS

DESIGN PROCEDURE FOR ABSORPTIVE LOUVERS

A. Determine percent open area, number of louvers, axial length of louvers, and the frequency of the noise source.

B. Calculate l_y (louver spacing).

C. Calculate λ (wave length).

D. Consult reference 9, and read the db attenuation per length equal to l_y, Al_y, for the various values of l_y/λ for the design percent open area.

E. Multiply Al_y by $\frac{l_x}{l_y}$ to determine predicted noise reduction, Δdb.

F. Read F (flow resistance parameter) corresponding to design percent open area.

$$F = \frac{R_1 t}{\rho C}$$

Calculate R_1 and, with reference 9, select proper absorptive material.

SAMPLE CALCULATION

A. Assume: percent open area = 80
No. of louvers = 10
Axial length of louvers = 1 ft.
Frequency of Source: 1070 cps and harmonics

B. l_y = 2.04" (calculated)

C.

f (cps)	λ (ft)
1070	1.05
2140	.527
3210	.352
4280	.264
5350	.210

D.

l_y/λ	Al_y
.162	.3
.322	1.2
.483	1.9
.644	2.6
.81	3

E.

Al_y	A(Δ db)
.3	1.76
1.2	7.05
1.9	11
2.6	15.3
3	17.6

F. $F = .75$

$$F = \frac{R_1 t}{\rho C}$$

$t = 1/4" = .00635$ meters $\qquad \rho C = 406$ Mks Rayles for air

$R_1 = 4.8 \times 10^4$ Mks Rayles/m

From reference 9, select proper material for this R_1.